



Study Report

SR364 [2016]

B-RISK 2016 user guide and technical manual

Colleen Wade, Greg Baker, Kevin Frank,
Roger Harrison and Michael Spearpoint





1222 Moonshine Rd
RD1, Porirua 5381
Private Bag 50 908
Porirua 5240
New Zealand
branz.nz



**MINISTRY OF BUSINESS,
INNOVATION & EMPLOYMENT**
HĪKINA WHAKATUTUKI

The work reported here was jointly funded by BRANZ from the Building Research Levy and the Ministry of Business, Innovation and Employment.

Preface

This report has been prepared as a user and technical guide to the use of the B-RISK fire risk modelling software developed by BRANZ and the University of Canterbury. It is important that users are familiar with the underlying physics and assumptions in B-RISK in order to be able to critically evaluate results obtained.

BRANZ Ltd and the University of Canterbury take no responsibility for any loss or design resulting from the use of this program, whether proper or not. All responsibility lies with the end user, who shall decide on the validity of any results obtained using B-RISK and who shall exercise caution when applying the results to any particular situation.

Acknowledgements

The development of B-RISK was jointly funded by BRANZ from the Building Research Levy and the Ministry of Business, Innovation and Employment. Special thanks go to all those who worked on this project at various times and who made a valuable contribution.

Note

This report is intended for the users of the B-RISK fire risk model and applies to software version 2016.02.

B-RISK 2016 user guide and technical manual

BRANZ Study Report SR364

Authors

Colleen Wade, Greg Baker, Kevin Frank, Roger Harrison and Michael Spearpoint

Reference

Wade, C., Baker, G., Frank, K., Harrison, R. & Spearpoint, M. (2016). *B-RISK 2016 user guide and technical manual*. BRANZ Study Report SR364. Judgeford, New Zealand: BRANZ Ltd.

Abstract

This report provides B-RISK users with guidance on the use and application of the fire modelling software as well as describing the assumptions and underlying physics upon which the computer fire model is based. The software is intended for evaluating the performance and hazard associated with room fires.

Model output includes but is not limited to gas layer temperatures, pressure, room surface temperatures, layer height, visibility and fractional effective dose estimates. The option for probabilistic analysis based on repeated Monte Carlo simulations is also included.

This report is a revision of BRANZ Study Report SR282 (Wade et al., 2013).

Keywords

Building fires, fire growth, fire modeling, hazard assessment, smoke transport, fire engineering, zone models, Monte Carlo simulation, fire risk, B-RISK

Contents

| | |
|--|-----------|
| NOMENCLATURE | 1 |
| 1. INTRODUCTION | 6 |
| 2. COMPUTER REQUIREMENTS | 7 |
| 3. SETTING UP A PROJECT | 8 |
| 3.1 User mode..... | 8 |
| 3.2 Monte Carlo simulation | 10 |
| 3.3 Creating, saving or opening models and file/folder locations | 11 |
| 3.4 Project settings | 14 |
| 3.5 Assigning statistical distributions to input variables..... | 15 |
| 3.6 Building description | 17 |
| 3.6.1 Building geometry and room dimensions..... | 17 |
| 3.6.2 Adding horizontal flow (wall) vents..... | 19 |
| 3.6.3 Hold-open devices | 22 |
| 3.6.4 Displaying vents in Smokeview | 22 |
| 3.6.5 Adding vertical flow (ceiling) vents..... | 23 |
| 3.6.6 Adding mechanical ventilation fans..... | 25 |
| 3.7 Using Smokeview | 27 |
| 4. FIRE SPECIFICATION..... | 29 |
| 4.1 Managing fire items..... | 29 |
| 4.2 Item property data | 31 |
| 4.3 Design fire generator..... | 33 |
| 4.3.1 Room population methods..... | 33 |
| 4.3.2 Item-to-item fire spread..... | 34 |
| 4.4 Fire load energy density (FLED)..... | 38 |
| 4.5 Power law design fires..... | 38 |
| 5. MODEL SIMULATIONS..... | 40 |
| 5.1 Running simulations | 40 |
| 5.2 Displaying summary input and results from a single iteration | 41 |
| 5.3 Displaying graphical output from a single iteration | 42 |
| 5.4 Displaying time series output from multiple iterations..... | 43 |
| 5.5 Displaying probabilistic input from multiple iterations | 45 |
| 5.6 Displaying probabilistic output from multiple iterations | 47 |
| 5.7 Exporting data to an Excel spreadsheet..... | 49 |
| 6. TWO-ZONE MODEL..... | 50 |
| 6.1 Introduction..... | 50 |
| 6.2 Mass and energy balance..... | 50 |
| 6.3 Modelling rooms as a single zone..... | 51 |
| 6.4 Species generation | 52 |
| 6.5 Combustion chemistry | 53 |
| 6.6 Soot and smoke production..... | 56 |
| 6.7 Carbon monoxide production..... | 57 |
| 6.8 Burning rate enhancement..... | 58 |
| 6.9 Plume entrainment..... | 59 |

| | | |
|-----------|--|-----------|
| 6.9.1 | Heskestad strong plume | 60 |
| 6.9.2 | McCaffrey's correlations..... | 61 |
| 6.9.3 | Effect of fire location on plume entrainment..... | 62 |
| 6.9.4 | Effect of fire plume disturbances on plume entrainment..... | 63 |
| 6.10 | Wall vent flows | 63 |
| 6.10.1 | Natural vent flow | 63 |
| 6.10.2 | Near-vent mixing | 64 |
| 6.10.3 | Vent flow entrainment into adjacent spaces | 65 |
| 6.11 | Spill plumes | 66 |
| 6.11.1 | General..... | 66 |
| 6.11.2 | Adhered spill plumes..... | 66 |
| 6.11.3 | Balcony spill plumes..... | 69 |
| 6.12 | Natural vent flow through ceilings and floors | 70 |
| 6.13 | Oxygen-limited burning..... | 71 |
| 6.13.1 | Mass flow of oxygen needed for complete combustion | 71 |
| 6.13.2 | Mass flow of oxygen present in the plume | 71 |
| 6.13.3 | Oxygen concentration in the upper layer..... | 71 |
| 6.13.4 | Minimum oxygen concentration needed for combustion | 72 |
| 6.14 | Post-flashover burning..... | 72 |
| 6.14.1 | Flashover criteria | 72 |
| 6.14.2 | Ventilation limit and post-flashover behaviour | 73 |
| 6.14.3 | Post-flashover wood crib sub-model | 73 |
| 6.14.4 | Post-flashover plume entrainment..... | 74 |
| 6.14.5 | Equivalent fire resistance rating | 75 |
| 6.15 | Mechanical ventilation..... | 75 |
| 6.16 | Vent fires..... | 77 |
| 6.17 | Heat transfer | 77 |
| 6.17.1 | Radiation exchange model..... | 77 |
| 6.17.2 | Heat conduction model | 86 |
| 6.17.3 | Convective heat transfer coefficients | 87 |
| 6.18 | Numerical solution..... | 88 |
| 7. | LIFE HAZARD CALCULATIONS..... | 89 |
| 7.1 | Tenability settings | 89 |
| 7.2 | Visibility..... | 90 |
| 7.3 | Fractional effective dose – asphyxiant gases..... | 90 |
| 7.4 | Fractional effective dose – thermal effects..... | 93 |
| 7.5 | Egress path segments..... | 94 |
| 8. | SPRINKLERS AND THERMAL DETECTORS | 96 |
| 8.1 | General | 96 |
| 8.2 | Effect of sprinkler spray on fire-induced doorway flow | 98 |
| 8.3 | Sprinkler reliability..... | 99 |
| 8.4 | Probability of suppression or control | 99 |
| 8.5 | Effect of sprinkler spray on rate of heat release | 99 |
| 8.6 | Minimum number of sprinklers required for suppression or control | 100 |
| 8.7 | Ceiling jet algorithms..... | 101 |

| | | |
|------------|---|------------|
| 8.7.1 | Alpert’s correlations | 101 |
| 8.7.2 | JET algorithm | 102 |
| 8.8 | Sprinkler output | 102 |
| 9. | SMOKE DETECTORS..... | 104 |
| 9.1 | General | 104 |
| 9.2 | Smoke detection system reliability | 105 |
| 9.3 | Smoke detector response..... | 105 |
| 9.4 | Smoke detector output | 108 |
| 10. | GLASS FRACTURE..... | 109 |
| 11. | FIRE GROWTH ON SURFACE LININGS | 110 |
| 11.1 | General | 110 |
| 11.2 | Quintiere’s room-corner model | 111 |
| 11.3 | Characterising the burner..... | 111 |
| 11.4 | Ignition of the wall lining | 113 |
| 11.5 | Energy release rate – Method 1 | 113 |
| 11.6 | Energy release rate – Method 2..... | 115 |
| 11.7 | Determining the pyrolysis area | 115 |
| 11.8 | Upward flame spread..... | 117 |
| 11.9 | Independent ignition of the ceiling lining | 118 |
| 11.10 | Lateral and downward flame spread | 119 |
| 11.11 | Material property data | 119 |
| 11.11.1 | Method of Grenier and Janssens | 119 |
| 11.11.2 | Flux time product method..... | 123 |
| | REFERENCES | 124 |
| | APPENDIX A. FORMAT OF CONE DATA FILE | 131 |
| | APPENDIX B. LIST OF MODEL CONSTANTS | 134 |
| | APPENDIX C. TROUBLESHOOTING..... | 135 |

Figures

| | | |
|------------|--|----|
| Figure 1. | User mode selection. | 8 |
| Figure 2. | Intervals used with a Latin hypercube sample of size $n = 5$ in terms of the density function and cumulative distribution function for a normal random variable [extracted from (Wyss & Jorgensen, 1998)]. | 10 |
| Figure 3. | Base file name for naming project base file “basemodel_ <i>default.xml</i> ”. | 11 |
| Figure 4. | Project files and folder hierarchy..... | 12 |
| Figure 5. | Saving the base model..... | 12 |
| Figure 6. | Location of database files..... | 13 |
| Figure 7. | Change location of fire and materials database files. | 13 |
| Figure 8. | B-RISK Console screen..... | 14 |
| Figure 9. | Example of input variables with distribution option..... | 15 |
| Figure 10. | Example input screen for entering distributions..... | 15 |
| Figure 11. | Project description..... | 17 |
| Figure 12. | Building geometry. | 18 |
| Figure 13. | Rooms..... | 19 |

Figure 14. Room dimensions entry form..... 19

Figure 15. Horizontal flow or wall vents..... 20

Figure 16. Input form for wall vent properties..... 20

Figure 17. Input form for vent opening options..... 22

Figure 18. Vent positioning notation for Smokeview visualisation..... 23

Figure 19. Managing ceiling vents..... 24

Figure 20. Input form for ceiling vent properties. 24

Figure 21. Ceiling vent opening options..... 25

Figure 22. Mechanical ventilation..... 26

Figure 23. Input form for fan properties..... 26

Figure 24. Smokeview visualisation..... 28

Figure 25. Managing fire items..... 30

Figure 26. Fire object database..... 30

Figure 27. Item properties form..... 32

Figure 28. Plot of item rate of heat release versus time input..... 32

Figure 29. Populate room items..... 33

Figure 30. Ignite secondary items..... 35

Figure 31. Composite heat release rate in compartment..... 38

Figure 32. Power law design fire..... 39

Figure 33. Start simulation from console screen, 40

Figure 34. Stop simulation from console screen..... 40

Figure 35. Summary input and output for a single iteration..... 41

Figure 36. Graphical output for a single run..... 42

Figure 37. Example time series plot of upper layer temperature for multi-iteration
output..... 43

Figure 38. Example of upper percentile time series plot..... 44

Figure 39. Example histogram for sampled values of interior ambient temperature. ... 45

Figure 40. Example cumulative density function for sampled values of interior ambient
temperature..... 46

Figure 41. Example histogram for predicted output values of upper layer
temperature..... 47

Figure 42. Example cumulative density function for predicted output values of upper
layer temperature..... 48

Figure 43. Exporting multiple iteration data to excel..... 49

Figure 44. Schematic of a zone model [Extracted from (ISO, 2006a)]...... 50

Figure 45. Modelling room as a single zone..... 52

Figure 46. Additional combustion parameters..... 54

Figure 47. Soot yields..... 56

Figure 48. Carbon monoxide yields versus equivalence ratio [Adapted from (Gottuk et
al., 1992)]...... 58

Figure 49. Burning rate enhancement..... 58

Figure 50. Comparison of plume entrainment using the McCaffrey and Heskestad
correlations..... 62

Figure 51. Plume disturbance option..... 63

Figure 52. Adhered spill plume without soffit projection [Extracted from Harrison
(2009)]...... 67

Figure 53. Adhered spill plume with soffit projection.68

Figure 54. Balcony spill plume with balcony projection.....69

Figure 55. Post-flashover options.....72

Figure 56. Wood crib parameters.....74

Figure 57. A generic fan curve.....76

Figure 58. Geometry for determination of solid angles.....80

Figure 59. Schematic showing the surfaces considered in the configuration factor formulae.80

Figure 60. Solver and numerical settings.88

Figure 61. Tenability settings for hazard to life assessment.....89

Figure 62. Specifying FED egress path.95

Figure 63. Input form for managing sprinklers or heat detectors.96

Figure 64. Input form for entering sprinkler or heat detector properties.97

Figure 65. Room layout showing sprinkler locations (small hollow black squares indicate sprinkler location).98

Figure 66. Distribution for minimum number of sprinklers required to suppress or control the fire..... 100

Figure 67. Ceiling jet model selection..... 101

Figure 68. Input form for managing smoke detectors. 104

Figure 69. Input form for entering smoke detector properties. 105

Figure 70. Input form for vent – glass properties. 109

Figure 71. Flame spread settings. 110

Figure 72. Transformation of the heat release rate curve..... 114

Figure 73. Wall ignited – pyrolysis front has not reached the ceiling. 116

Figure 74. Wall ignited – pyrolysis front has reached the ceiling. 116

Figure 75. Correlation of ignition times for best-fit n..... 121

Figure 76. Correlation of ignition times for n=0.547. 122

Figure 77. Correlation of peak heat release rates. 122

Tables

Table 1. Summary of user mode settings.9

Table 2. Input parameters to which a statistical distribution can be assigned..... 16

Table 3. Radiative heat flux striking the k^{th} room surface.79

Table 4. Radiant heat absorbed by the upper layer.85

Table 5. Radiant heat absorbed by the lower layer.....85

Table 6. Surface coefficients.88

Table 7. RMVo and COHb incapacitation dose for different activity levels.91

Table 8. Default properties assigned to sprinklers and heat detectors following VM2. .97

Table 9. Summary of data from cone calorimeter tests. 121

Table 10. Constants used in B-RISK..... 134

Nomenclature

| | |
|--------------------|--|
| a | = gas absorption coefficient (m^{-1}) |
| A | = plume entrainment coefficient |
| A_f | = floor area of the room (m^2) |
| A_i | = area of surface i (m^2) |
| A_p | = pyrolysis area (m^2) |
| A_{p1} | = pyrolysis area on wall (m^2) |
| A_{pj1} | = pyrolysis area on wall in ceiling jet region (m^2) |
| A_{pc1} | = pyrolysis area on ceiling (m^2) |
| A_w | = wall area behind burner (m^2) |
| A_o | = initial pyrolysing area in ceiling (m^2) |
| Bi | = Biot Number |
| Bi_{int} | = Biot Number for the room interior surface |
| Bi_{ext} | = Biot Number for the room exterior surface |
| b_w | = side dimension of square burner (m) |
| c | = specific heat (J/kgK) |
| c_p | = specific heat of air (J/kgK) |
| C or C -factor | = sprinkler conduction factor (m/s) ^{1/2} |
| C_{soot} | = mass concentration of soot in the upper layer (kg soot/ m^3) |
| d_s | = depth of the smoke layer in the fire compartment (m) |
| D | = diameter of the fire (m) |
| D | = wood crib stick thickness (m) |
| D_i | = smoke optical density inside the detector (m^{-1}) |
| D_o | = smoke optical density outside the detector (m^{-1}) |
| F | = geometric configuration factor |
| F_{ij} | = geometric configuration factor for radiation emitted from surface i and intercepted by surface j |
| FED | = fractional effective dose |
| FTP | = flux time product ($[kW/m^2]^n s$) |
| F_o | = Fourier number |
| g | = gravitation constant (m/s^2) |
| h | = heat transfer coefficient (W/m^2K) |
| h_c | = convective heat transfer coefficient (W/m^2K) |
| h_c | = wood crib height (m) |
| h_v | = vent height (m) |
| h_{ig} | = total heat transfer coefficient from surface at ignition (W/m^2K) |
| \dot{h}_l | = enthalpy flow to the lower layer (kW) |
| \dot{h}_u | = enthalpy flow to the upper layer (kW) |
| k | = thermal conductivity (W/mK) |
| k | = extinction coefficient (m^{-1}) |

| | |
|------------------------|---|
| k_{avg} | = average extinction coefficient (m^{-1}) |
| k_m | = particle extinction cross-section (m^2/kg soot) |
| k_s | = effective absorption coefficient of soot |
| $k\rho c$ | = thermal inertia (W^2s/m^4K^2) |
| K | = flame area constant (m^2/kW) |
| l | = characteristic dimension (m) |
| L | = flame height (m) |
| L | = room plan length (m) |
| L_g | = heat of gasification (kJ/g) |
| L_o | = mean path length (m) |
| \dot{m}_d | = mass flow rate in vent mixing flow (kg/s) |
| \dot{m}_f | = mass loss rate of the fuel (kg/s) |
| \dot{m}_f'' | = mass loss rate of fuel per unit area (kg/s m^2) |
| \dot{m}_i | = mass flow rate of cool gases in through the vent (kg/s) |
| \dot{m}_o, \dot{m}_c | = mass flow rate of hot gases out through the vent (kg/s) |
| \dot{m}_p | = mass flow rate of air entrained into the plume (kg/s) |
| \dot{m}_s | = mass flow rate of at the spill edge of a balcony or soffit (kg/s) |
| M_l | = mass of the lower layer (kg) |
| M_u | = mass of the upper layer (kg) |
| MW_i | = molecular weight of species i |
| n | = flame length power |
| ppm | = parts per million |
| p | = horizontal flame projection distance (m) |
| p | = room perimeter (m) |
| P_a | = atmospheric pressure (kPa) |
| P | = pressure in the room at floor level relative to atmospheric (Pa) |
| P_i | = partial pressure of species i (kPa) |
| P_{ws} | = saturation pressure for water vapour (kPa) |
| Pr | = Prandtl number |
| \dot{q}'' | = heat flux per unit area (kW/ m^2) |
| \dot{q}_{cr}'' | = critical heat flux for ignition (kW/ m^2) |
| \dot{q}_e'' | = external heat flux incident on a surface (kW/ m^2) |
| \dot{q}_w'' | = net heat flux from the burner flame to a wall (kW/ m^2) |
| \dot{q}_f'' | = net heat flux from the flame impinging on ceiling (kW/ m^2) |
| \dot{q}_l | = net heat transfer to the lower gas layer (kW) |
| \dot{q}_{int}'' | = incident heat flux to surface due to gas layers and other surfaces (kW/ m^2) |
| \dot{q}_{net}'' | = net heat flux to a surface (kW/ m^2) |
| \dot{q}_{ff}'' | = heat flux ahead of the flame (kW/ m^2) |
| \dot{q}_{fl}'' | = heat flux received by a secondary target (kW/ m^2) |

| | |
|----------------------------|--|
| \dot{q}_r'' | = radiative component of heat flux (kW/m ²) |
| \dot{q}_u | = net heat transfer to the upper gas layer (kW) |
| \dot{q}_{f-k}'' | = heat flux striking the surface k due to a point source fire (kW) |
| $\dot{q}_{j-k}''^{i\ gas}$ | = heat flux striking the surface k due to emitting gas layer i (kW) |
| $\dot{Q}''(t)$ | = time-dependent heat release rate per unit area (kW/m ²) |
| \dot{Q}'' | = heat release rate per unit area (kW/m ²) |
| \dot{Q}_b | = heat release rate of the gas burner (kW) |
| \dot{Q}'_b | = heat release rate per unit length of the gas burner (kW) |
| \dot{Q}_c | = convective heat release from the fire (kW) |
| $\dot{Q}''_c(t)$ | = time-dependent heat release rate measured in cone calorimeter (kW/m ²) |
| \dot{Q}_f | = total heat release from the fire (kW) |
| $\dot{Q}''_{p,cone}$ | = peak rate of heat release measured in cone calorimeter test (kW/m ²) |
| \dot{Q}_p | = peak heat release (kW/m ²) |
| $\dot{Q}(t)$ | = heat release at time t (kW) |
| $\dot{Q}(t_{act})$ | = heat release rate at the time of sprinkler activation (kW) |
| $Q_{eq}(t)$ | = cumulative radiant energy per unit area at time t in a compartment fire (kJ/m ²) |
| $Q_{ISO}(t)$ | = cumulative radiant energy per unit area at time t in a standard fire resistance test (kJ/m ²) |
| r | = radial distance from the centre of the plume (m) radial distance (in plan view) from the centre of the burning object to the nearest part of a secondary item (m) |
| R | = universal gas constant (J/kmol/K) |
| RMV | = volume of air breathed (litres/min) |
| RTI | = response time index (m s) ^{1/2} |
| S | = wood crib stick spacing (m) |
| SA | = surface area of a flame volume (m ²) |
| t | = time (s) |
| t_{act} | = sprinkler activation time (s) |
| t_{ig} | = time to ignition in cone calorimeter (s) |
| t_h | = time for γ pyrolysis front to reach ceiling (s) |
| t_p | = dummy variable of integration |
| T | = temperature (K) |
| T_{cj} | = temperature of the ceiling jet (K) |
| T_{ig} | = surface temperature for ignition (K) |
| T_e | = temperature of detector/sprinkler link (K) |
| T_f | = flame temperature (K) |
| T_{fo} | = flashover temperature (K) |
| T_g | = gas temperature (K) |
| T_o | = initial surface temperature (K) |

| | |
|------------------|--|
| T_l | = temperature of the lower gas layer (K) |
| T_u | = temperature of the upper gas layer (K) |
| T_i | = temperature of the gas layer i (K) |
| T_{pm} | = temperature of node m at time p (K) |
| T_s | = surface temperature (K) |
| $T_{s,min}$ | = minimum surface temperature for spread (K) |
| T_∞ | = reference temperature of ambient air (K) |
| U_{cj} | = velocity of the ceiling jet (m/s) |
| V | = visibility in upper layer (m) |
| V_l | = volume of the lower layer (m ³) |
| V_u | = volume of the upper layer (m ³) |
| V_R | = volume of the room (m ³) |
| w | = vent width (m) |
| w_o | = width to which vent flow expands to (m) |
| \dot{w}'' | = water spray density (mm/s) |
| W | = room plan width (m) |
| W_s | = width of the compartment opening (m) |
| W_s | = humidity ratio of air at saturation |
| x_p | = pyrolysis front in lateral direction (m) |
| $x_{p,o}$ | = initial pyrolysis front in lateral direction (m) |
| X_f | = position of the flame front (m) |
| y_f | = flame length in upward direction (m) |
| y_p | = pyrolysis front in upward direction (m) |
| $y_{p,o}$ | = initial pyrolysis front in upward direction (m) |
| $Y_{i,l}$ | = mass fraction of species i in the lower layer |
| $Y_{i,u}$ | = mass fraction of species i in the upper layer |
| $Y_{i,\infty}$ | = mass fraction of species i in ambient air |
| Y_{soot} | = mass fraction of soot in the upper layer |
| z_p | = pyrolysis front in downward direction from ceiling jet (m) |
| z_s | = entrainment height from top of the compartment opening to the underside of the smoke layer (m) |
| Z | = height of the smoke layer from the base of the fire (m) |
| Z_o | = virtual origin (m) |
| Z_n | = height of the neutral plane (m) |
| %COHb | = concentration of carboxyhemoglobin in the blood (%) |
| α | = thermal diffusivity (m ² /s) |
| α | = fire growth rate coefficient (kW s ⁻² or kW s ⁻³ m ⁻¹) |
| α_t | = total absorptance of gas-soot mixture |
| α_{j-k}^i | = absorptivity of gas layer i for a path between surfaces j and k |
| ε | = emissivity |
| ε_t | = total emissivity of gas-soot mixture |

| | |
|--------------------|--|
| ρ | = density (kg/m ³) |
| $\delta_{k,j}$ | = Kronecker delta function |
| γ | = c_p/c_v |
| ρ_l | = density of the lower layer (kg/m ³) |
| ρ_u | = density of the upper layer (kg/m ³) |
| λ_r | = radiative fraction of energy loss by radiation from the flame/plume |
| $\lambda_{r,vc}$ | = radiant loss fraction under ventilation-controlled conditions |
| v_p | = surface regression rate for wood (m/s) |
| Φ | = flame spread parameter (kW ² /m ³) |
| Φ_e | = global equivalence ratio |
| Φ_{RH} | = relative humidity |
| ω_{f-k} | = solid angle between surface ^k and a point source fire |
| σ | = Stefan-Boltzmann constant (= 5.67 × 10 ⁻⁸ W/m ² K ⁴) |
| τ | = time constant for the detector (s) |
| τ | = time to ignition (s) |
| τ_t | = radiation transmission factor |
| τ_w | = time to ignition of the wall lining (s) |
| τ_{j-k}^i | = transmissivity of gas layer ⁱ for a path between surfaces ^j and ^k |
| ψ_i | = yield of species ⁱ from the pyrolysing fuel (kg species ⁱ /kg fuel) |
| ψ_{soot} | = yield of soot from the pyrolysing fuel (kg soot/kg fuel) |
| ΔA_p | = incremental change in pyrolysis area (m ²) |
| Δt | = time step (s) |
| ΔH_c | = heat of combustion (kJ/g) |
| $\Delta H_{ch,vc}$ | = chemical heat of combustion under ventilation-controlled conditions (kJ/g) |
| $\Delta H_{ch,wv}$ | = chemical heat of combustion under well ventilated conditions (kJ/g) |
| Δx | = incremental surface thickness for heat conduction calculation (m) |

1. Introduction

B-RISK is a fire simulation model and software program comprising a fire risk simulator for generating probability distributions for relevant model outputs, given that statistical distributions to key input parameters are assigned. Central to B-RISK is an underlying deterministic fire zone model previously developed and known as BRANZFIRE (Wade, 1996; Wade & Barnett, 1997; Wade, 2000). B-RISK has included and extended the physics of the core BRANZFIRE model and provides the user with a new tool for better understanding of the uncertainty and risk associated with fires in building enclosures.

The B-RISK model may be used for both single deterministic runs for predictions of smoke spread within enclosures as well as for multiple iterations of a scenario. The latter is useful for the purpose of sensitivity analysis or for producing probabilistic descriptors of fire risk under defined conditions.

This report is a revision of BRANZ Study Report SR282 (Wade et al., 2013) and applies to B-RISK software version 2016.02.

2. Computer requirements

B-RISK has been written in Microsoft Visual Basic 2008 using the VB.NET framework to run on any computer using a Microsoft Windows XP or later operating system.

B-RISK can be downloaded by visiting www.b-risk.com.

Smokeview software version 6.0.x or 6.1.x (Forney, 2012) can be used for visualisation of B-RISK models but must be installed separately. It can be downloaded from <https://bintray.com/nist-fire-research/releases/SMV>.

See Appendix C for troubleshooting tips.

3. Setting up a project

3.1 User mode

There are two user modes available within B-RISK located under the FILE menu command (see Figure 1).

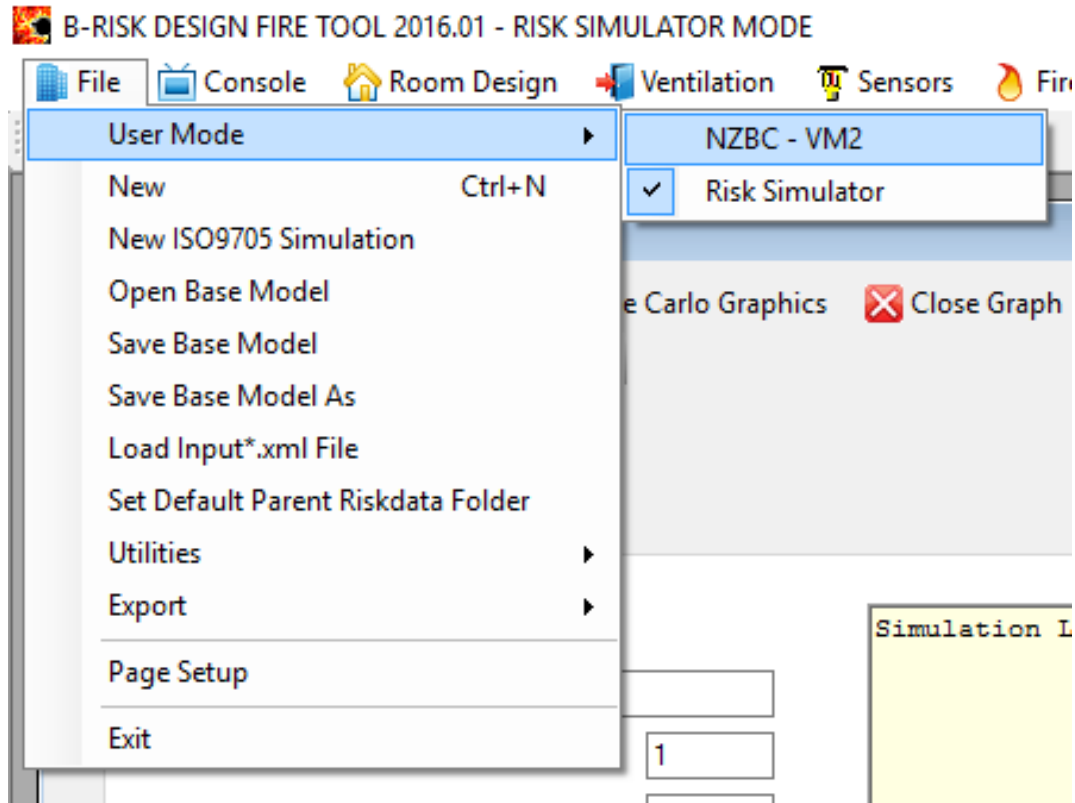


Figure 1. User mode selection.

NZBC - VM2 mode refers to a mode of operation designed to support the Verification Method (MBIE, 2014) for fire safety design for compliance with the New Zealand Building Code. C/VM2 provides specific input values for the design fire as well as a number of modelling rules to be applied when using computer fire models. Selecting VM2 mode in the software will enable/disable certain features and capabilities within the software (see Table 1) and change certain default input values to be in accordance with C/VM2. While some input values become preset using this mode, the user is still responsible for reviewing all input for correctness and compliance with C/VM2.

RISK SIMULATOR mode provides access to all publicly available features in the software including the design fire generator for populating rooms with contents and the item-to-item fire spread routines.

A summary of the relevant settings and sub-model availability for the two user modes is given in Table 1.

Table 1. Summary of user mode settings.

| | C/VM2 mode | Risk Simulator mode |
|--|---|--|
| FED asphyxiant gas calculation | Option 2 – FED(CO) C/VM2 based on ISO 13571 See section 7.3 | Option 1 – FED(CO/CO ₂ /HCN) or Option 2 – FED(CO) C/VM2 can be selected |
| FED thermal calculation | Follows ISO 13571 See section 7.4 | Follows ISO 13571 See section 7.4 |
| Design fire rate of heat release | Power law design fires with initial defaults See section 4.5 for details | Power law design fires or user-specified |
| Sprinkler system response | Probability of suppression = 0 (control mode) Sprinkler cooling coefficient = 1 Sprinkler radial distance as specified, option to calculate based on location of sprinkler is disabled | All options available See also section 8 |
| Smoke detector response | Detector response based on optical density outside the detector housing See section 9 | Detector response can be based on optical density inside or outside the detector housing |
| Combustion parameters – fuel type | Use VM2 fuel type with: Flame emission coefficient = 1.0 (1/m) Fuel formula = CH ₂ O _{0.5} No HCN generation CO ₂ yield = 1.5 g/g H ₂ O yield = 0.82 g/g CO yield = 0.04 g/g pre-flashover CO yield = 0.4 g/g post-flashover Soot yield = 0.07 g/g pre-flashover Soot yield = 0.14 g/g post-flashover Also see sections 6.6 and 6.7 | Choice of available fuels or user defined |
| Flashover criterion | Upper layer temp = 500°C | Choice of criteria |
| Ventilation limit and post-flashover behaviour | See section 6.14.2 | |
| Design fire generator, room population | ✘ | ✓ |
| Enhanced burning option | ✘ | ✓ |
| Item-to-item ignition and fire spread to secondary targets | ✘ | ✓ |
| Post-flashover wood crib model | ✘ | ✓ |
| Flame spread model | ✘ | ✓ |

3.2 Monte Carlo simulation

B-RISK allows the user to carry out a single-run deterministic analysis for a specific building with fixed input values. It also allows the user to carry out multiple runs where selected input parameters can be described with a statistical distribution (see section 3.5), which is randomly sampled to obtain the input value for each successive iteration.

A stratified sampling method similar to Latin hypercube sampling (Vose, 2000) is employed over Monte Carlo sampling, as being a more efficient technique. However, unlike Latin hypercube sampling, each input parameter is sampled independently. The method can be briefly summarised as follows:

- A cumulative density function $F(x)$ corresponding to the probability distribution $f(x)$ for an input parameter is split into n intervals of equal probability, where n is the number of iterations to be performed.
- For the first iteration, one of the intervals is randomly selected, and within that interval, a value of $F(x)$ is randomly sampled.
- The value of $x = G(F(x))$ is calculated for that value of $F(x)$.
- The process is then repeated for the next and subsequent iterations, with a new interval sampled each time, except that each interval is only sampled once and, once sampled, is marked so as not to be selected again.
- The method is repeated for each input parameter.

Figure 2 illustrates, as an example, the intervals used for a normal random variable using five iterations.

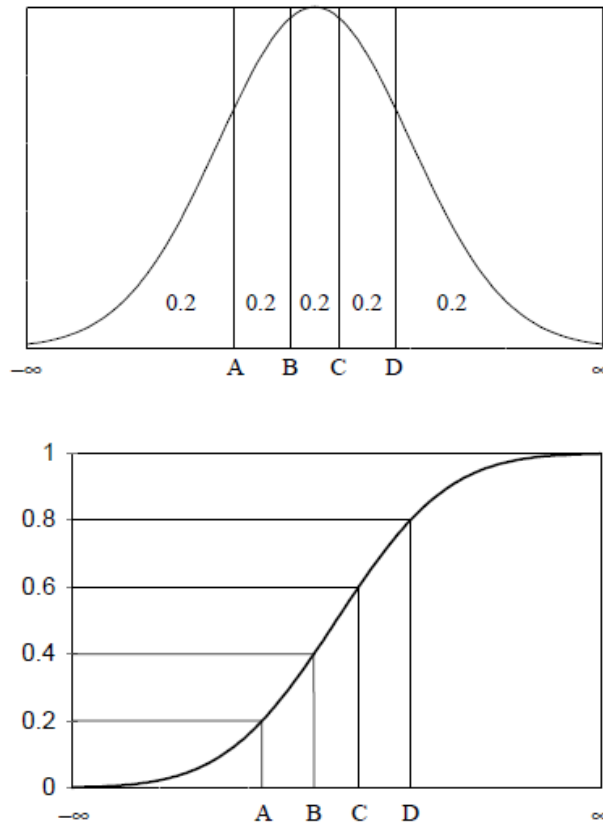


Figure 2. Intervals used with a Latin hypercube sample of size $n = 5$ in terms of the density function and cumulative distribution function for a normal random variable [extracted from (Wyss & Jorgensen, 1998)].

3.3 Creating, saving or opening models and file/folder locations

Each simulation project is stored in a separate folder or directory. The project subfolder will be automatically created when a project is saved and will be given the base file name appended with the suffix "basemodel_", for example, C:\Users\userxyz\Documents\B-RISK\riskdata\basemodel_default.

Project folders are located beneath the riskdata folder, i.e. "...riskdata\myproject". The user can change the default riskdata parent folder location from the FILE menu. The currently selected default location of the riskdata folder and the current project folder are displayed beneath the output log screen. Projects can be run from other locations, but a prompt will ask the user if they wish to copy the project to the riskdata folder.

The main project file will be saved in the same folder and given the name "basemodel_default.xml", where the text in italics is that entered as the base file name in the B-RISK Console screen by the user as shown in Figure 3 below.

The basemodel_default.xml file can also be modified in a text editor.

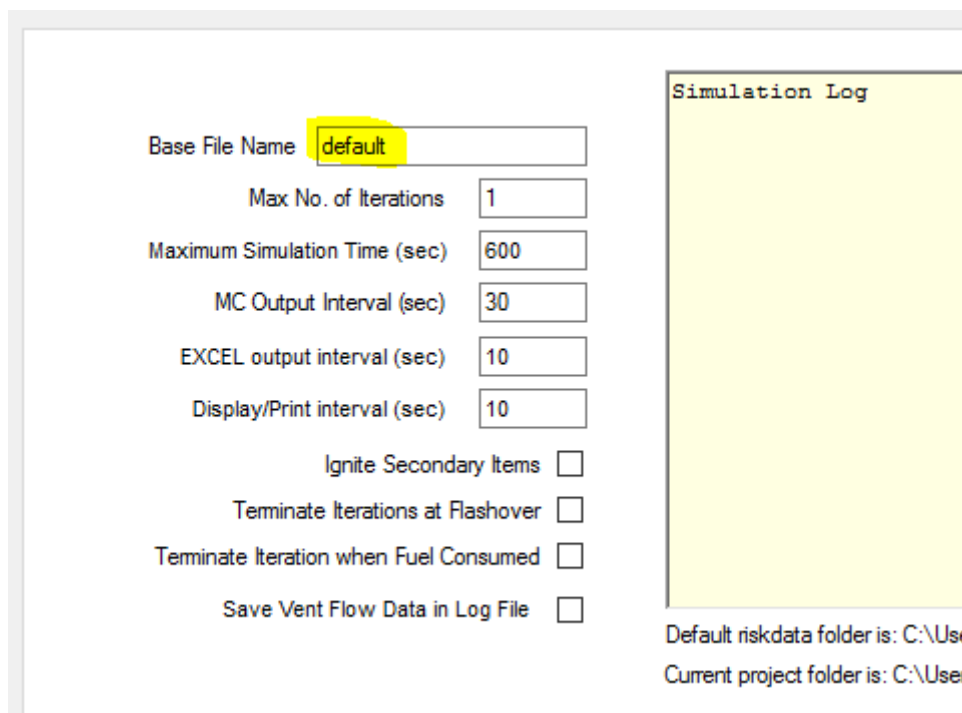


Figure 3. Base file name for naming project base file "basemodel_default.xml".

There are eight additional files created in the project folder called "distributions.xml", "rooms.xml", "vents.xml", "cvents.xml", "items.xml", "fans.xml", "smokedetects.xml" and "sprinklers.xml" as shown in Figure 4. These files contain input data required for the simulation and must be present. After running a simulation, various additional input and output files will also be created and stored in the same project folder.

| This PC > Documents > B-RISK > riskdata > basemodel_default | | | |
|---|--------------------|--------------|------|
| Name | Date modified | Type | Size |
| vents.xml | 21/01/2016 3:13 PM | XML Document | 5 KB |
| sprinklers.xml | 20/02/2015 4:09 PM | XML Document | 1 KB |
| smokedets.xml | 20/02/2015 4:09 PM | XML Document | 1 KB |
| rooms.xml | 20/02/2015 4:09 PM | XML Document | 2 KB |
| items.xml | 21/01/2016 3:12 PM | XML Document | 3 KB |
| fans.xml | 20/02/2015 4:08 PM | XML Document | 1 KB |
| distributions.xml | 18/01/2016 5:19 PM | XML Document | 6 KB |
| cvents.xml | 29/07/2015 4:35 PM | XML Document | 1 KB |
| basemodel_default.xml | 1/08/2015 11:46 AM | XML Document | 6 KB |
| basemodel_default.smv | 18/01/2016 2:53 PM | SMV File | 1 KB |

Figure 4. Project files and folder hierarchy.

A project or model is saved by using the FILE, SAVE BASE MODEL AS menu item (see Figure 5) or the SAVE icon on the toolbar. The folder and file name is automatically assigned using the base file name entered in the Console screen.

The FILE, SAVE BASE MODEL AS menu item allows the user to save the project folder in another location chosen by the user.

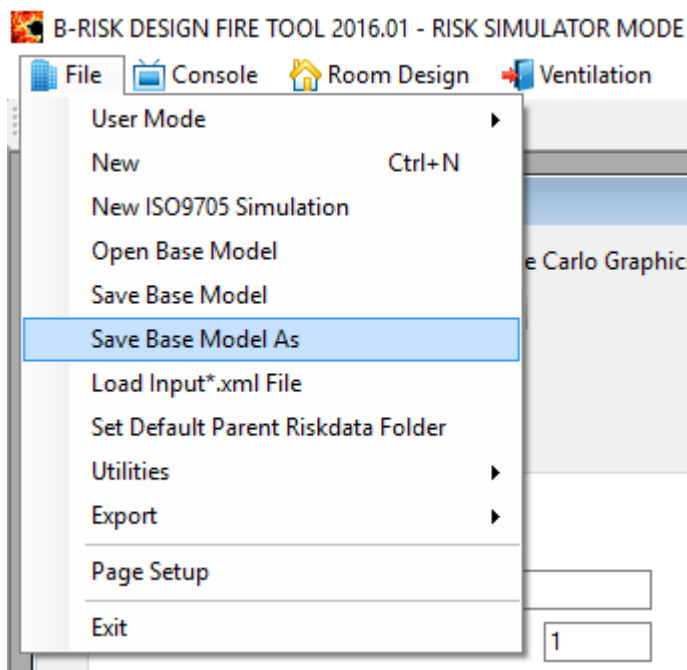


Figure 5. Saving the base model.

Similarly, a project or model can be opened using the FILE, OPEN BASE MODEL menu item.

After a simulation has been run, a single input file from that simulation can be loaded using the FILE, LOAD INPUT*.XML FILE menu item. This enables results to be shown and plotted for that simulation.

A new project using room dimensions, materials, gas burner and ventilation opening as per the ISO 9705 standard room test specification can be loaded from a template by using the FILE, NEW ISO9705 SIMULATION menu item.

The FILE, NEW menu item can be used to reload the original data for the default case. The data is stored and copied from files stored in the C:\Program Files (x86)\BRANZ\ folder location.

The fire and thermal databases are found in the dbases folder under the application folder, and these are copied to the user's documents folder for new projects as shown in Figure 6. This allows the user to customise these database files without losing the original default files.

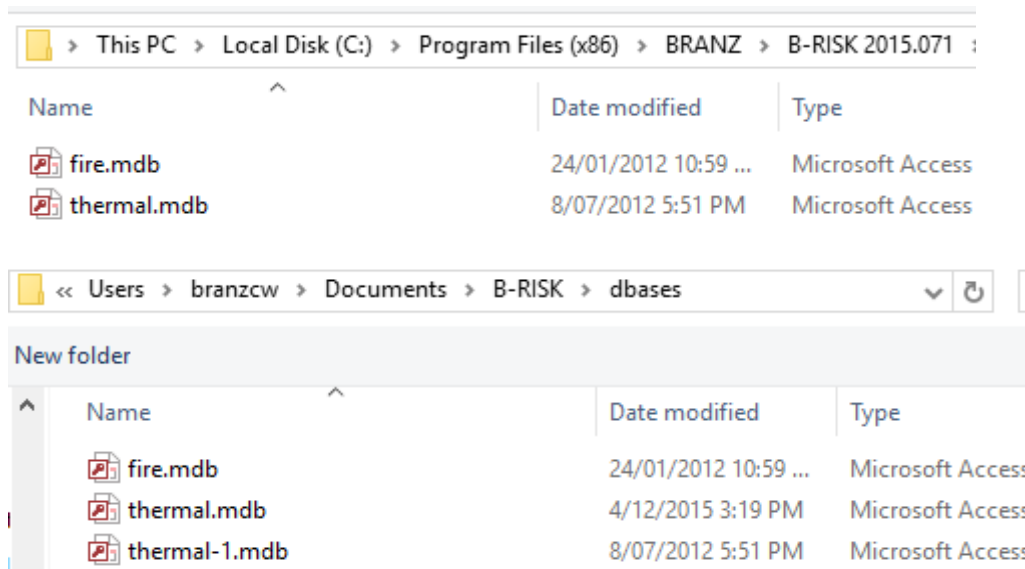


Figure 6. Location of database files.

The user is also able to load database files stored in alternative locations using the FILE, UTILITIES menu item (see Figure 7).

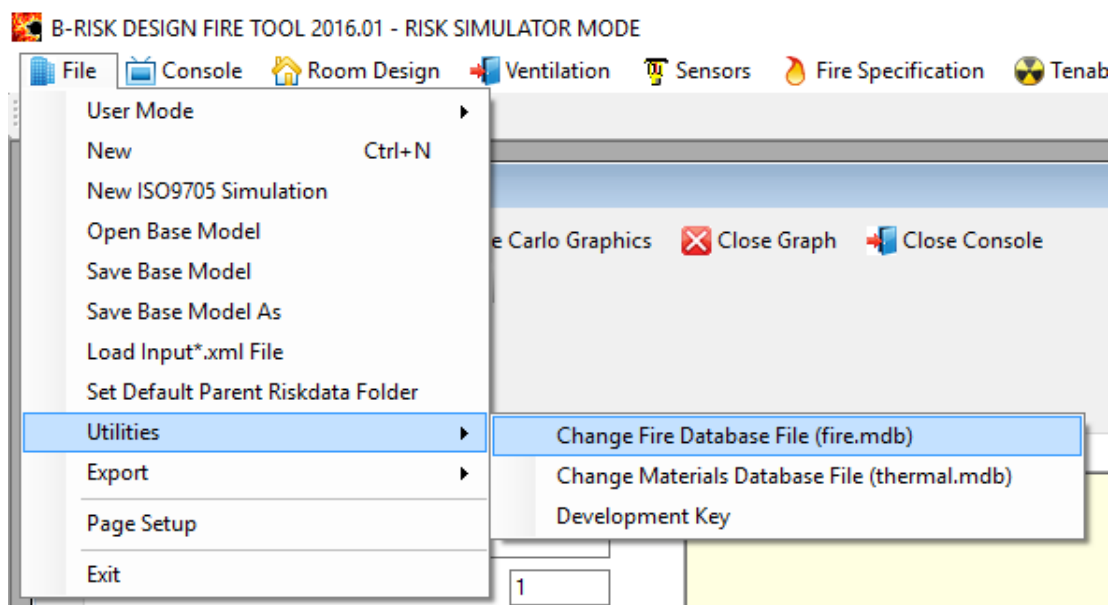


Figure 7. Change location of fire and materials database files.

3.4 Project settings

The B-RISK Console screen (see Figure 8) allows the user to specify the following parameters:

- MAX NO. OF ITERATIONS – the number of repeated simulations to run with sampling of specified input parameters with distributions as specified by the user.
- MAXIMUM SIMULATION TIME (SEC).
- MC OUTPUT INTERVAL (SEC) – the data interval used for saving/plotting output (e.g. time series plots, histograms) from multiple iterations. In some cases, data storage requirements may require this to be a larger value than the time step used within each iteration. Cannot be less than the solver time step.
- EXCEL OUTPUT INTERVAL (SEC) – the data interval used for exporting data to an Excel spreadsheet. Cannot be less than the solver time step.
- DISPLAY/PRINT INTERVAL (SEC) – the data interval used for displaying output using the VIEW, VIEW RESULTS menu item. Cannot be less than the solver time step.
- IGNITE SECONDARY ITEMS (checked/unchecked) – allows item-to-item fire spread to be modelled where multiple items have been located within the fire room (see section 4.3.2).
- TERMINATE ITERATIONS AT FLASHOVER (checked/unchecked) – each iteration is terminated when the flashover criterion is given under the MISC SETTINGS, POSTFLASHOVER BEHAVIOUR menu item. This provides a quick option to terminate iterations where the user is only interested in pre-flashover behaviours.
- SAVE VENT FLOW DATA IN LOG FILE (checked/unchecked) – this option provides the user with access to detailed information about the magnitude and direction of vent mass flow for each wall vent or ceiling vent. These can be inspected for a completed simulation using the VIEW, VIEW WALL VENT FLOW DATA and VIEW, VIEW CEILING VENT FLOW DATA menu items respectively.

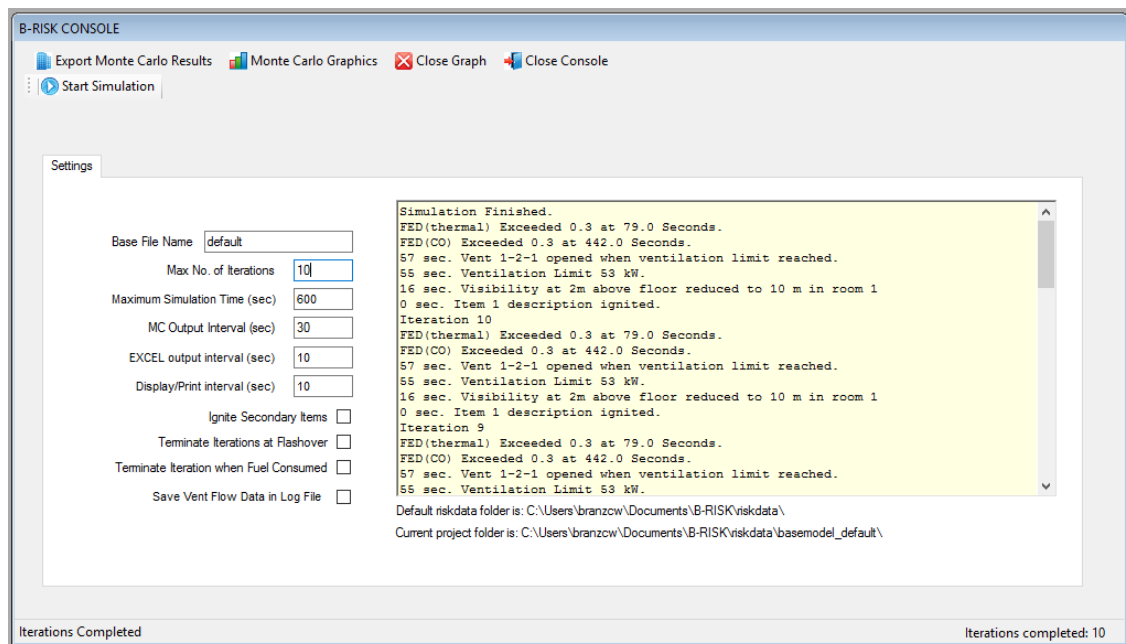


Figure 8. B-RISK Console screen.

The Console screen includes an area for displaying a running log or commentary on events and warnings as each iteration progresses. A right-clicked mouse button allows the log contents to be saved to a rich text file or copied to the windows clipboard.

3.5 Assigning statistical distributions to input variables

A selected number of input parameters can optionally be assigned a statistical distribution for sampling from for each iteration as described in section 3.2. The distributions currently available and the parameters required (in brackets) are:

- uniform (lower bound, upper bound)
- triangular (lower bound, mode, upper bound)
- normal (mean, variance, lower bound, upper bound)
- lognormal (mean, variance).

When a distribution is available to be assigned to a given variable, a DISTRIBUTION command button will be shown adjacent to the input variable, as shown for the ambient conditions in Figure 9. The input screen for describing individual distributions is shown in Figure 10.

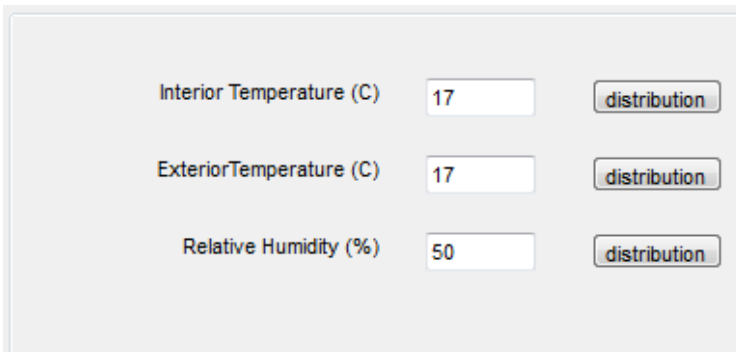


Figure 9. Example of input variables with distribution option.

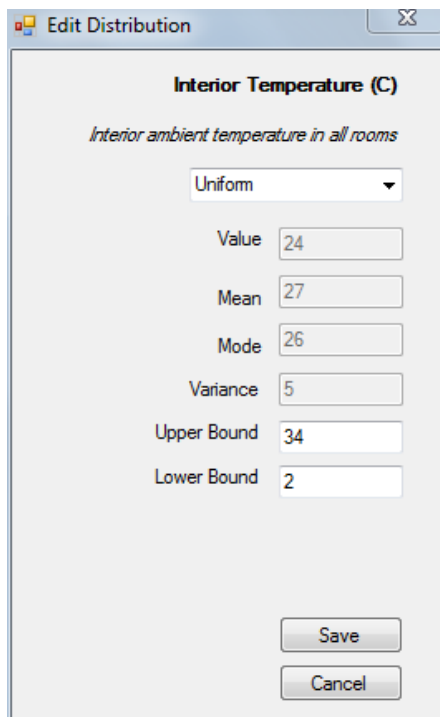


Figure 10. Example input screen for entering distributions.

Table 2 lists the input parameters to which a statistical distribution can be assigned. All inputs are treated as independent variables.

Table 2. Input parameters to which a statistical distribution can be assigned.

| | | |
|----------------------------------|--|--|
| Ambient conditions | Interior temperature | °C |
| | Exterior temperature | °C |
| | Relative humidity | % |
| Wood crib post-flashover model | Fuel heat of combustion | MJ/kg |
| CO/soot (manual input) | CO pre-flashover yield | g/g |
| | Soot pre-flashover yield | g/g |
| Rooms | Room length | m |
| | Room width | m |
| Wall vents (each vent) | Vent width | m |
| | Vent height | m |
| | Probability vent is initially closed | - |
| | Hold-open device reliability | - |
| Ceiling vents (each vent) | Vent area | m ² |
| Sprinkler system | Sprinkler system reliability | - |
| | Probability of suppression | - |
| | Sprinkler cooling coefficient | - |
| | Number of sprinklers required for suppression (discrete distribution only) | - |
| Sprinkler head (each head) | RTI | (m s) ^{1/2} |
| | Activation temperature | °C |
| | C-factor | (m/s) ^{1/2} |
| | Water spray density | mm/min |
| | Radial distance (plume centre to sprinkler head) | m |
| | Distance below ceiling | m |
| Smoke detection system | System reliability | - |
| Smoke detectors (each detector) | Optical density at alarm | 1/m |
| | Radial distance (plume centre to smoke detector) | m |
| | Distance below ceiling | m |
| | Characteristic length | m |
| Mechanical ventilation system | System reliability | - |
| Fans (each fan) | Fan flow rate | m ³ /s |
| | Pressure limit | Pa |
| | Start time | s |
| | Fan reliability | - |
| Fuel | Fire load energy density | MJ/m ² |
| Power law design fire | Growth rate coefficient (alpha) | kWs ⁻² or kWs ⁻³ m ⁻¹ |
| | Peak rate of heat release | kW |
| Fuel item properties (each item) | Heat of combustion | kJ/g |
| | Soot yield | g/g |
| | CO ₂ yield | g/g |
| | Latent heat of gasification | kJ/g |
| | Radiant loss fraction | - |
| | Heat release rate per unit area | kW/m ² |

3.6 Building description

3.6.1 Building geometry and room dimensions

A description and project identification can be added to printouts by specifying details using the MISC SETTINGS, DESCRIBE PROJECT menu item as shown in Figure 11.

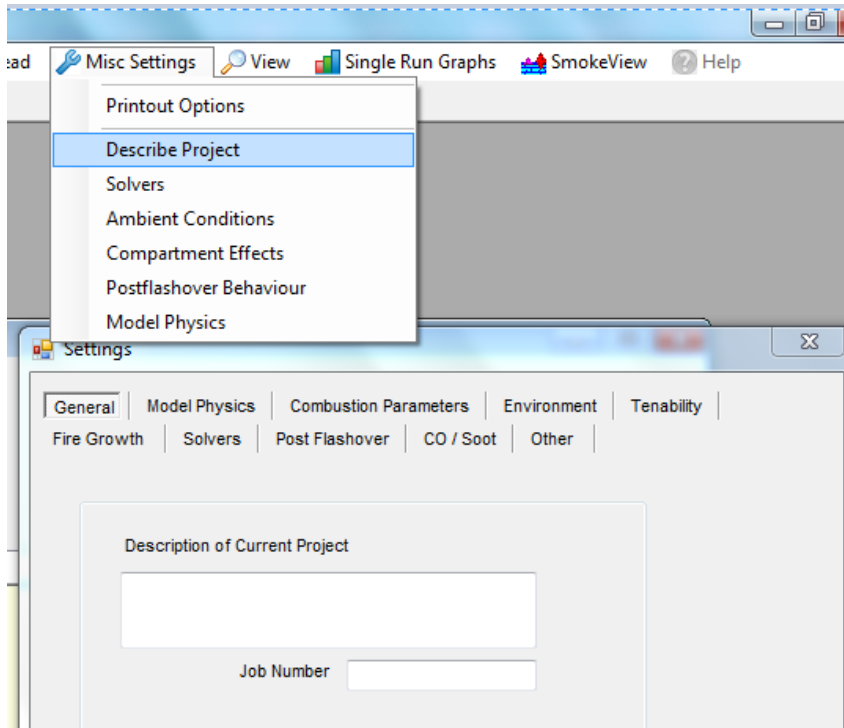


Figure 11. Project description.

Room enclosures must be represented as rectangular volumes with a defined length, width and height as shown in Figure 12.

Where the floor area (A_f) and room perimeter (P) of a non-rectilinear room of volume (V_R) are known, this should be converted to an equivalent rectilinear room as described here. In order to better represent the heat transfer by conserving both room volume and surface area, it is recommended that the length (L), width (W) and height (H) of an equivalent rectilinear volume is determined by:

$$L = \frac{\frac{P}{2} + \sqrt{\left(\frac{P}{2}\right)^2 - 4A_f}}{2} \quad (1)$$

$$W = \frac{A_f}{L} \quad (2)$$

$$H = \frac{V_R}{A_f} \quad (3)$$

The X and Y coordinate system is associated with the length and width dimensions respectively.

A room can be offset from the coordinate origin by specifying the absolute X position and absolute Y position as shown in Figure 12. These horizontal offset parameters are only used to correctly display the building geometry using the Smokeview software (Forney, 2012). They do not affect any calculations made by the fire model, and therefore it is not essential to include them.

The floor elevation of a room is specified relative to an arbitrary datum level set at or lower than the floor level of the lowest room in the model.

When locating a vent within a wall, the specific wall segment in a room is identified using a face property, where the face is one of the following: "front, right, rear or left" as shown in Figure 12.

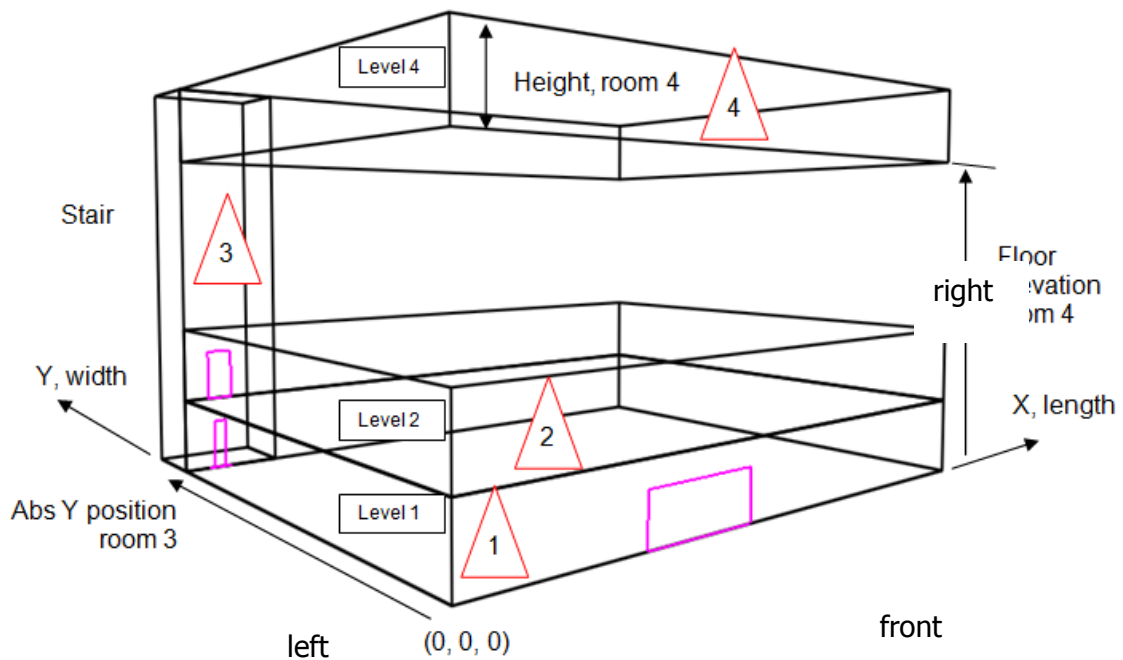


Figure 12. Building geometry.

Rooms are managed from the ROOM DESIGN, ROOMS menu as shown in Figure 13. Rooms can be added, edited, copied or removed from the project. The entry form for setting dimensions of a room is shown in Figure 14.

A sloping ceiling can be defined by specifying different values for the MINIMUM HEIGHT and MAXIMUM HEIGHT parameters. The change in cross-sectional area over the height of the enclosure will be taken into account when determining the volume of the smoke layer and the height of the smoke layer above the floor. The fire plume is assumed to be located beneath the highest part of the ceiling. Activation time of sprinklers and detectors will also be determined using the MAXIMUM HEIGHT parameter.

The sloping ceiling will not be portrayed in Smokeview visualisations where the enclosure height will be represented by the MAXIMUM HEIGHT parameter and a flat ceiling.

More complicated roof shapes that change in cross-section over their height should be represented as flat roof enclosures using equations (1)–(3), but the layer height and concentrations may not be accurate over the upper part of the enclosure where the cross-sectional area changes. Therefore, in those cases, the simplified geometry is only valid where occupants are not located at upper levels within the enclosure.

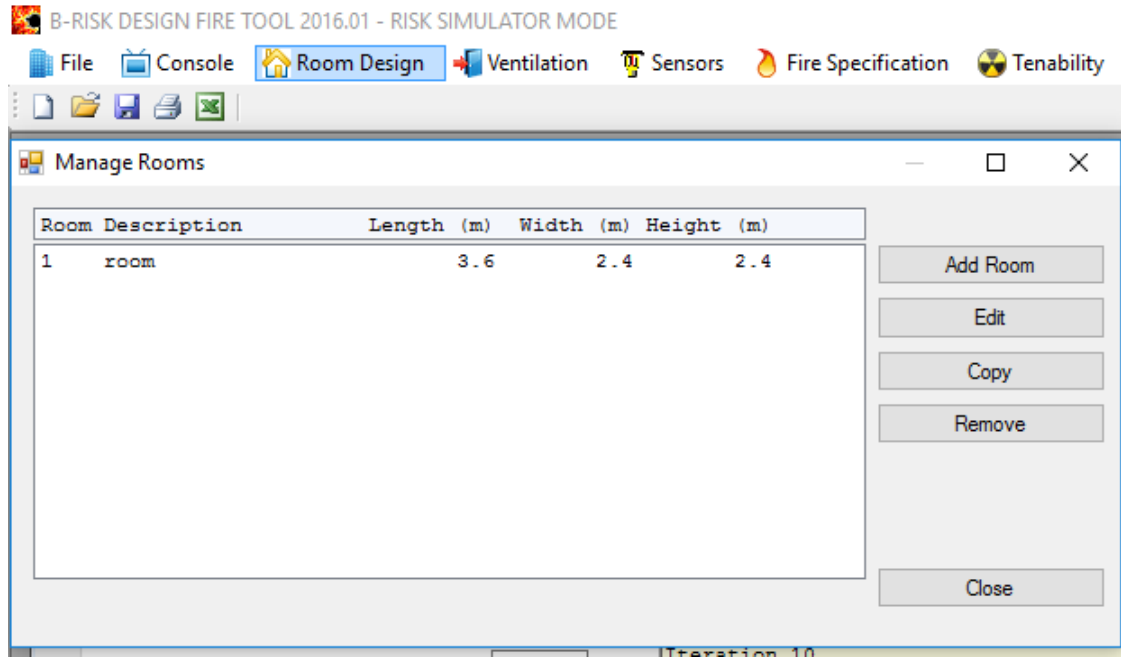


Figure 13. Rooms.

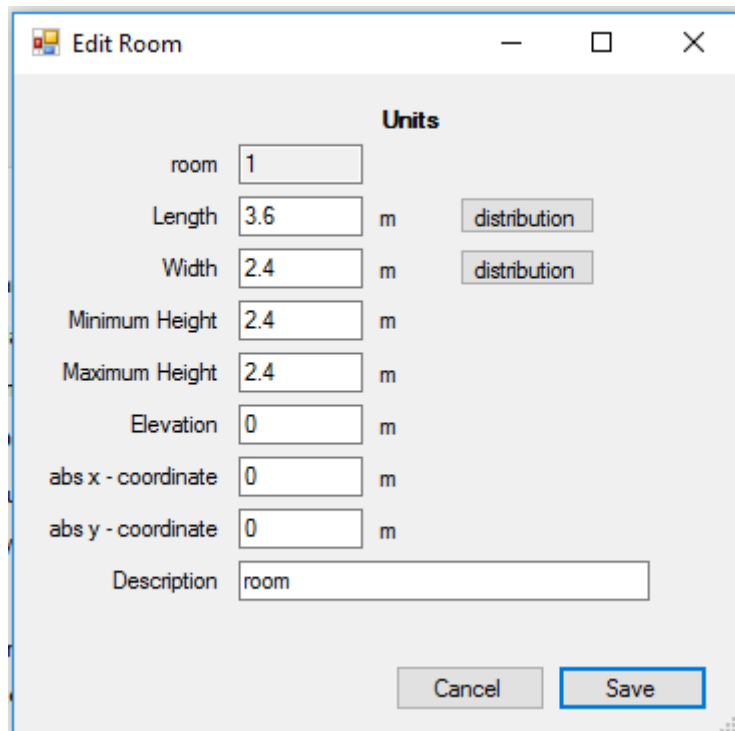


Figure 14. Room dimensions entry form

3.6.2 Adding horizontal flow (wall) vents

Horizontal flow or wall vents such as doors and windows are managed from the VENTILATION, WALL VENTS menu as shown in Figure 15. Wall vents can be added, edited, copied or removed from the project. The entry form for setting properties of a wall vent is shown in Figure 16.

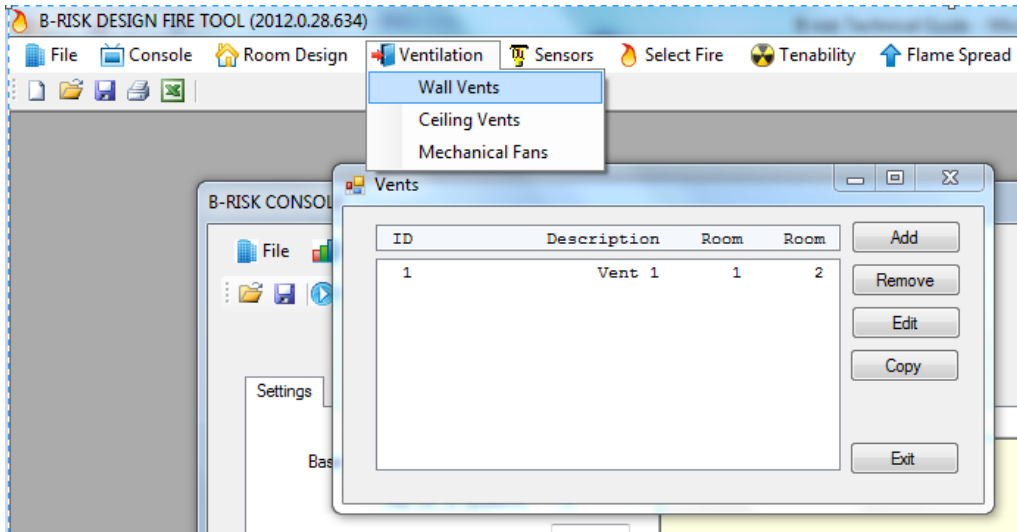


Figure 15. Horizontal flow or wall vents.

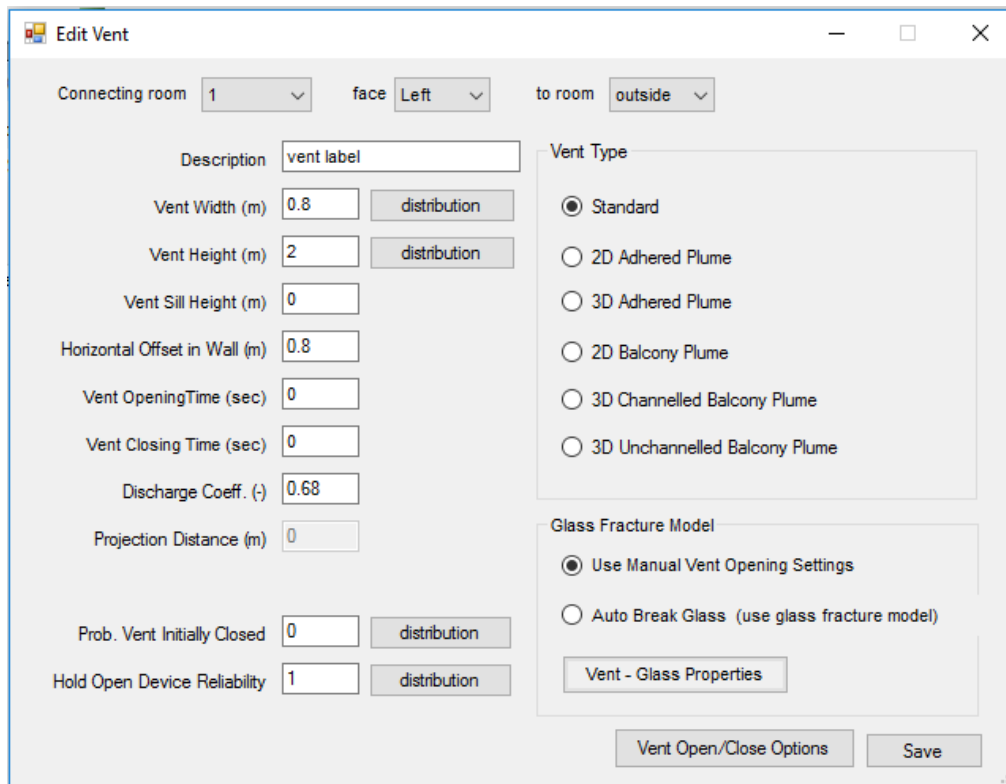


Figure 16. Input form for wall vent properties.

Vents placed within walls are considered to be rectangular, with height, width and the sill height (above floor level of the first connecting room) defined. The face property refers to the first room using the notation shown in Figure 12. The vent offset property is used as described in section 3.6.4.

The basis for the wall vent flow calculations is described later in section 6.10.1.

The discharge (or flow) coefficient is typically in the range 0.6–0.7 for square-edged rectangular openings with a default value of 0.68. The user is responsible for entering an appropriate value if the vent is not a square-edged rectangular opening. In cases where the top of the vent is flush with the ceiling, a value of 1.0 is recommended.

The vent type determines the entrainment sub-model used to calculate the mass flow entrained into the hot gases leaving through the vent opening and rising to the ceiling in an attached room. Vent type can be adhered or balcony spill plumes (see section 6.11) or a standard vent (see section 6.10.3). For flows from a room to an outside space, the vent type will therefore have no effect as the entrainment occurs outside the building. The basis for calculating mass flow and entrainment into adhered plumes and balcony spill plumes is given in sections 6.11.2 and 6.11.3 respectively.

A distribution (uniform, triangular, normal, lognormal) may be optionally assigned to the following inputs:

- Vent width.
- Vent height.
- Probability of the vent initial state being closed.

Vents are considered to be initially open except in the following situations:

- When a non-zero value for the vent opening time is entered, in which case, the vent is initially closed, opens at the vent opening time and closes at the vent closing time.
- When the vent is set to open at flashover, when the ventilation limit is reached or when a detector responds. These options are set using the vent opening options form (see Figure 17).
- When the AUTO BREAK GLASS option is selected, the vent is assumed to be initially closed and fully glazed. A glass fracture and fallout sub-model is used to determine the time for the vent to be opened. The glass properties can be specified using the VENT - GLASS PROPERTIES button (see Figure 16). The basis for modelling fracture of window glass is given in section 10.
- When the value entered for the probability the vent is initially closed is non-zero. In this case, a uniformly distributed random number between 0 and 1 will be sampled for each run, and if this sampled value is greater than the probability value entered, the initial state of the vent will be open. Conversely, if the sampled value is less than the probability value entered, the initial state of the vent will be closed. This is achieved by setting the discharge coefficient to zero. Note that, if using this option causes the initial state of the vent to be closed, using the vent opening options will not subsequently open the vent.

The opening (and closing of vents) is not instantaneous but is assumed to occur over a 2-second period with a linear change occurring in the width of the vent from fully closed to fully open (and vice versa).

Wall vents may be set to open automatically based on specified conditions or triggers reached during the simulation. These include at flashover, upon reaching the ventilation limit, upon reaching a minimum fire size or upon activation of a smoke/heat detector or sprinkler. The options are shown in Figure 17. To use any of the options on this screen requires ENABLE AUTOMATIC OPENING OPTIONS FOR THIS VENT to be checked. The vent also needs to connect to the room of fire origin to automatically open using the flashover, ventilation-limit or fire size triggers.

The opening of the vent can be delayed following the trigger event by entering a desired time period in the text input box. The duration of the vent remaining open can also be specified by entering a desired time period in the appropriate text box.

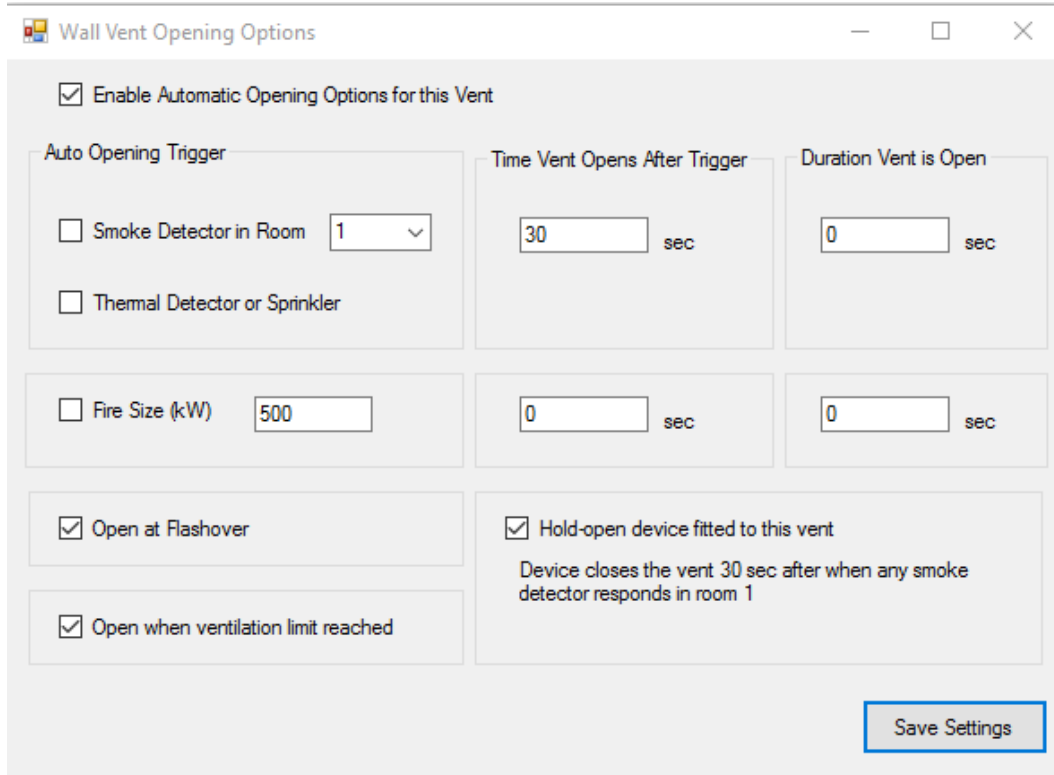


Figure 17. Input form for vent opening options.

Allowance for compartment leakage is not included in B-RISK. The user is required to represent any leakage through the compartment boundaries by adding vents. It is not recommended that B-RISK be used to model fully sealed compartments.

3.6.3 Hold-open devices

A hold-open device can be associated with a vent (usually a door that will be held open under normal use conditions but is to be kept closed under fire conditions) by checking the relevant checkbox in the WALL VENT OPENING OPTIONS screen (see Figure 17). The hold-open device will release and automatically close the opening following the activation of a smoke detector in the room selected under AUTO OPENING TRIGGER. If a hold-open device is to be assigned to a vent, the option to also open the vent using a smoke detector should not be checked at the same time. If a smoke detector delay time is entered, it will be used to delay the activation of the hold-open device (i.e. to allow for a notification time).

A reliability value in the range 0–1 (or distribution if desired) applying to the hold-open device can be specified as shown in Figure 16. For each iteration, the reliability parameter (sampled from the assigned distribution if applicable) is compared to a uniformly selected random number between 0 and 1, and if the value is greater than the random number, the hold-open device is deemed ineffective and is assumed to not operate, otherwise the device operates as intended.

3.6.4 Displaying vents in Smokeview

This section describes the notation for positioning wall vents to display correctly in Smokeview. The “Face” and “Offset” settings are used only for visualisation purposes, and they do not affect the fire model vent flow calculations. See section 3.7 for further details on using Smokeview with B-RISK.

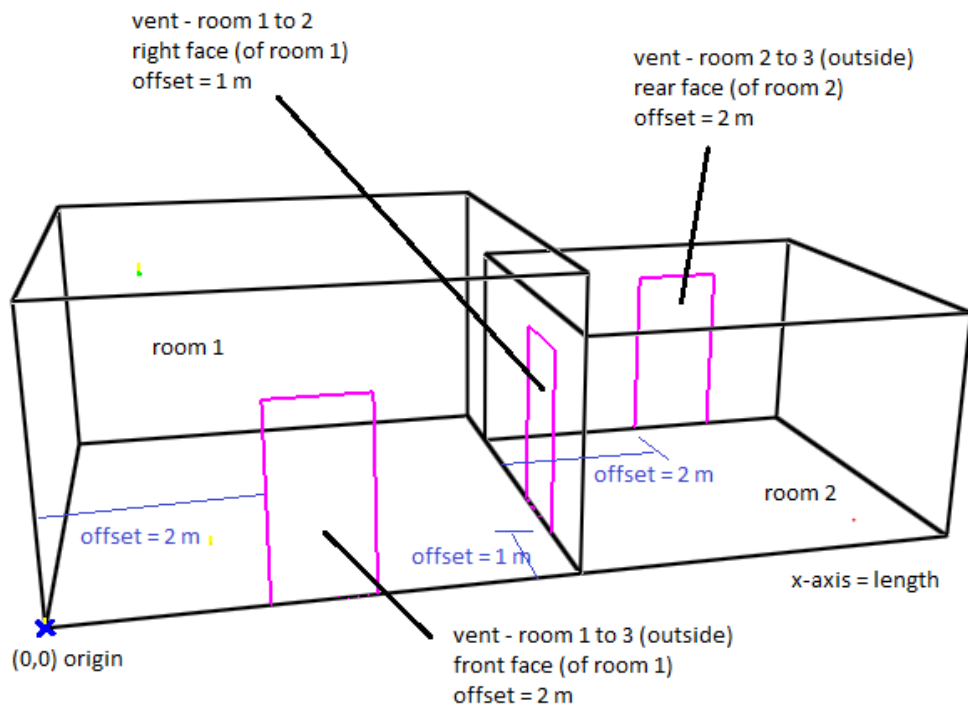


Figure 18. Vent positioning notation for Smokeview visualisation.

3.6.5 Adding vertical flow (ceiling) vents

Vertical flow (ceiling) vents are managed from the VENTILATION, CEILING VENTS menu as shown in Figure 19. Ceiling vents can be added, edited, copied or removed from the project. The entry form for setting properties of a ceiling vent is shown in Figure 20.

For each vent, the lower room and upper rooms must be selected from the drop-down boxes and the area of the vent entered. The ceiling vent area can be assigned a distribution.

A discharge coefficient for the ceiling vent can be entered by the user (default is 0.6).

Ceiling vents may be set to open automatically based on specified conditions or triggers reached during the simulation. These include at flashover, upon reaching the ventilation limit, upon reaching a minimum fire size or upon activation of a smoke/heat detector or sprinkler. The options are shown in Figure 21. To use any of the options on this screen requires ENABLE AUTOMATIC OPENING OPTIONS FOR THIS VENT to be checked. The vent also needs to connect to the room of fire origin to automatically open using the flashover, ventilation-limit or fire size triggers.

The basis for the ceiling vent flow calculations is described in section 6.12.

Ceiling vents are shown as being centrally located in the ceiling and are shown as square in shape when using Smokeview for visualisation purposes (see section 3.7).

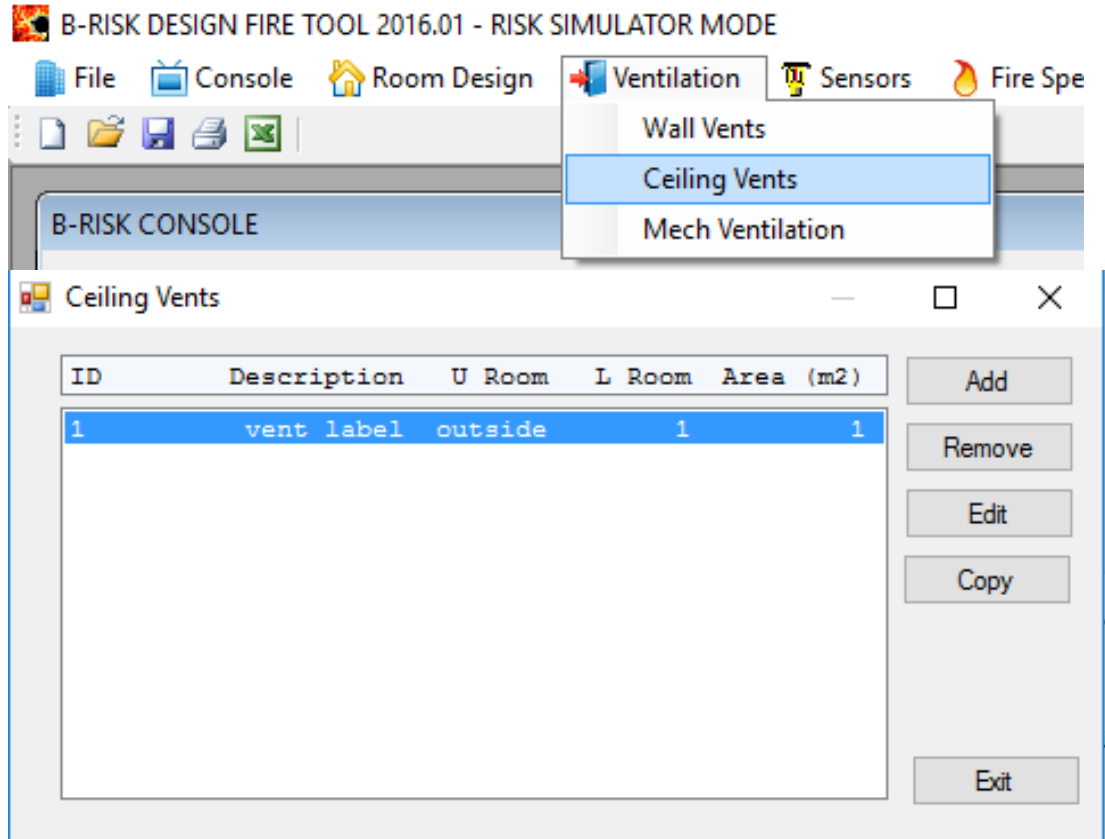


Figure 19. Managing ceiling vents.

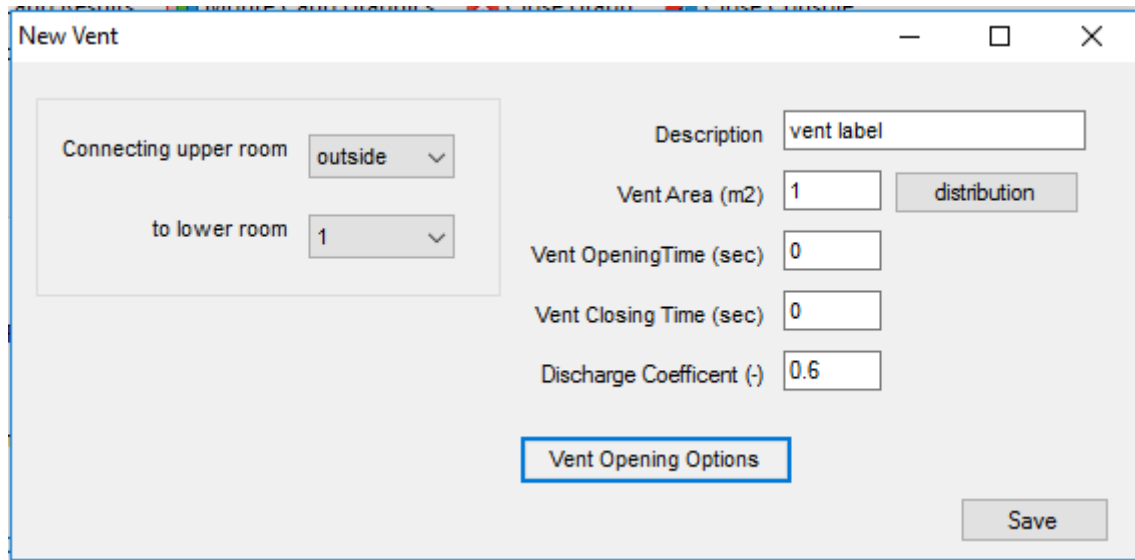


Figure 20. Input form for ceiling vent properties.

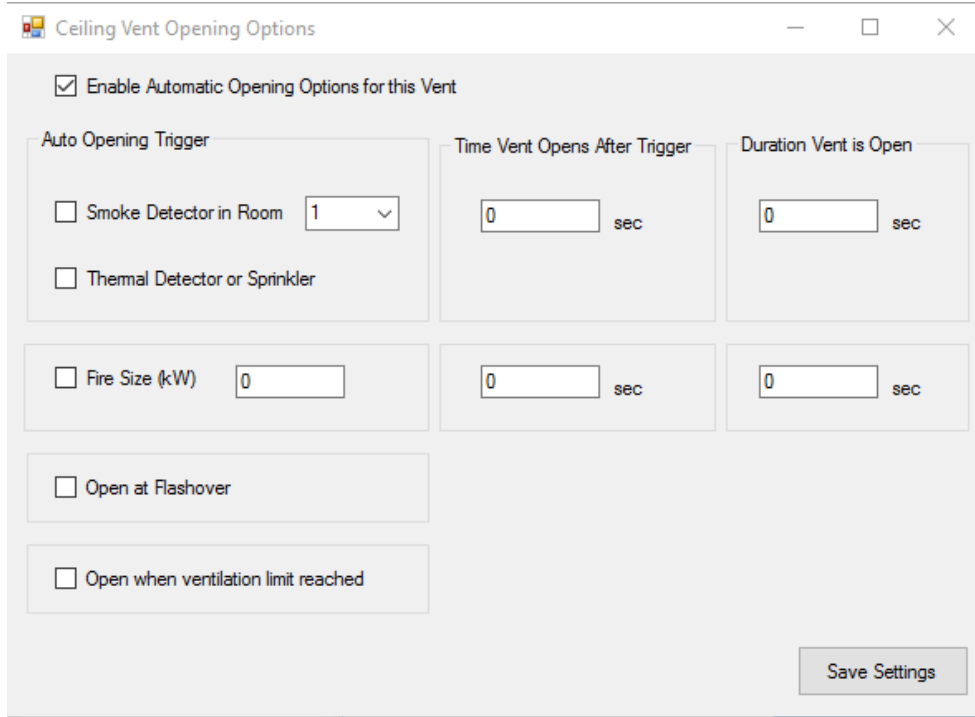


Figure 21. Ceiling vent opening options.

3.6.6 Adding mechanical ventilation fans

Mechanical ventilation using fans is managed from the VENTILATION, MECH VENTILATION menu as shown in Figure 22. Fans can be added, edited, copied or removed from the project.

The mechanical ventilation system can be assigned a reliability value in the 0 to 1 range or a distribution. This influences the overall system operation and could be used to represent the probability of a fault that would disable all fans in the system. To model a perfectly reliable system, this value should be set to 1.0.

For each iteration, the reliability parameter (sampled from the assigned distribution if applicable) is compared to a uniformly selected random number between 0 and 1, and if the value is greater than the random number, the mechanical ventilation system is deemed ineffective and is assumed to not operate, otherwise the system operates as intended.

The entry form for setting properties of an individual fan is shown in Figure 23.

Fans can be set to either extract from or supply to the designated room at the nominated flow rate and elevation or height specified.

In addition to the system reliability value above, a reliability value or distribution can also be assigned to an individual fan.

A fan can be activated at a set start time (manual) or be automatically started following the operation of a local smoke detector located in the same room as the fan or by a smoke detector in the room of fire origin.

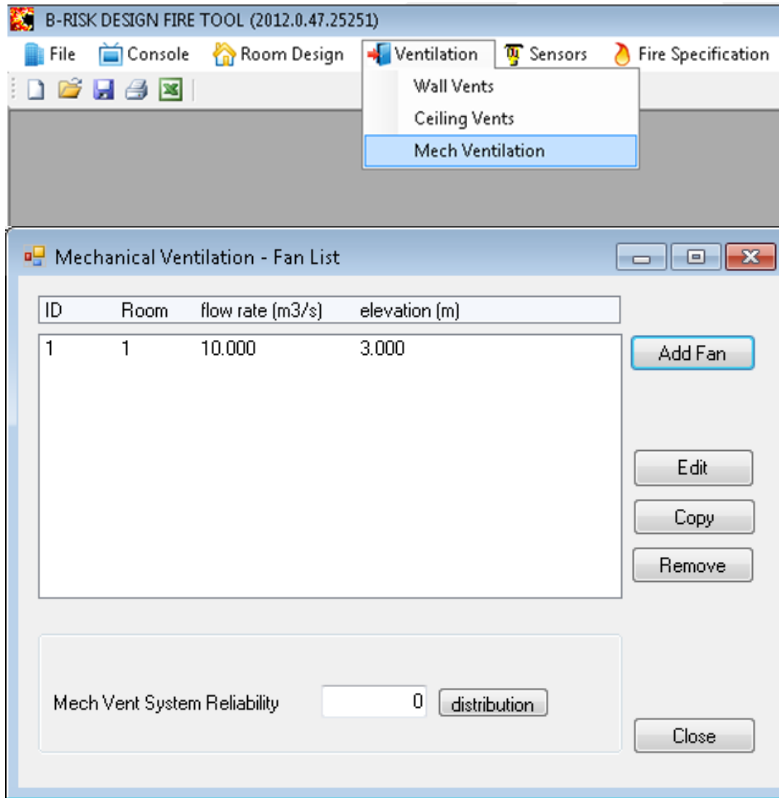


Figure 22. Mechanical ventilation.

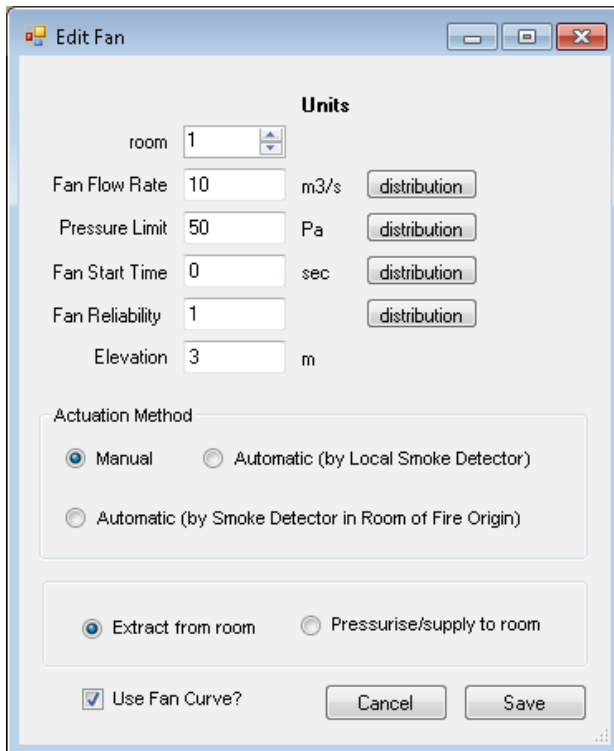


Figure 23. Input form for fan properties.

A fan curve, which specifies the relationship between the flow rate and the cross-fan pressure difference (as described in section 6.15), can optionally be used.

The file called "fans.xml" contains the details about each fan and what distributions, if any, have been assigned.

This file will be found in the relevant project folder under the "Riskdata" directory (e.g. C:\Users\...\Documents\B-RISK\riskdata\basemodel_default\fans.xml).

The input files (inputxxx.xml) created by B-RISK contain the fan data for each iteration including the sampled system reliability value and whether the mechanical ventilation system is operational (True) or not (False). These are contained within the <fans></fans> xml element.

Where parameters have previously been assigned distributions, these files contain the sampled values for each iteration.

Individual fans also are assigned a reliability value or distribution, and their operational status is also given (True/False) within each <fan></fan> xml element.

```
- <fans operational_status="False" sys_reliability="0.5000">
  - <fan id="1" room="2">
    <flow_rate>10</flow_rate>
    <start_time>1</start_time>
    <fan_reliability>1</fan_reliability>
    <pressure_limit>50</pressure_limit>
    <elevation>48</elevation>
    <extract>False</extract>
    <manual>2</manual>
    <fan_curve>True</fan_curve>
    <operational_status>True</operational_status>
  </fan>
</fans>
```

3.7 Using Smokeview

Smokeview (Forney, 2012) is a software tool designed to visualise numerical calculations generated by fire models. Smokeview and associated documentation may be downloaded from the website <https://bintray.com/nist-fire-research/releases/SMV>. B-RISK requires Smokeview Version 6.0.x or 6.1.x to be separately installed on the user's computer. It is not included as part of the B-RISK installation.

Smokeview can be used to view the model geometry including wall and ceiling vents and can visualise temperature and smoke concentration predictions in B-RISK using the SMOKEVIEW menu item as shown in Figure 24.

The model geometry details are stored in a file called "basemodel_default.smv" (where the text in italics is that entered as the base file name in the B-RISK Console screen), which is read by Smokeview to display the model. When running a simulation, B-RISK creates a .csv file called "basemodel_default_zone.csv" containing output from the model simulation that is available for use by Smokeview. This is created in the project folder.

Users should be aware that the vent flow data displayed by Smokeview is not accurate, as it is not read from B-RISK output and does not account for any change in the open/close status of vents.

Readers are referred to the Smokeview documentation (Forney, 2012) for further details on using this software.

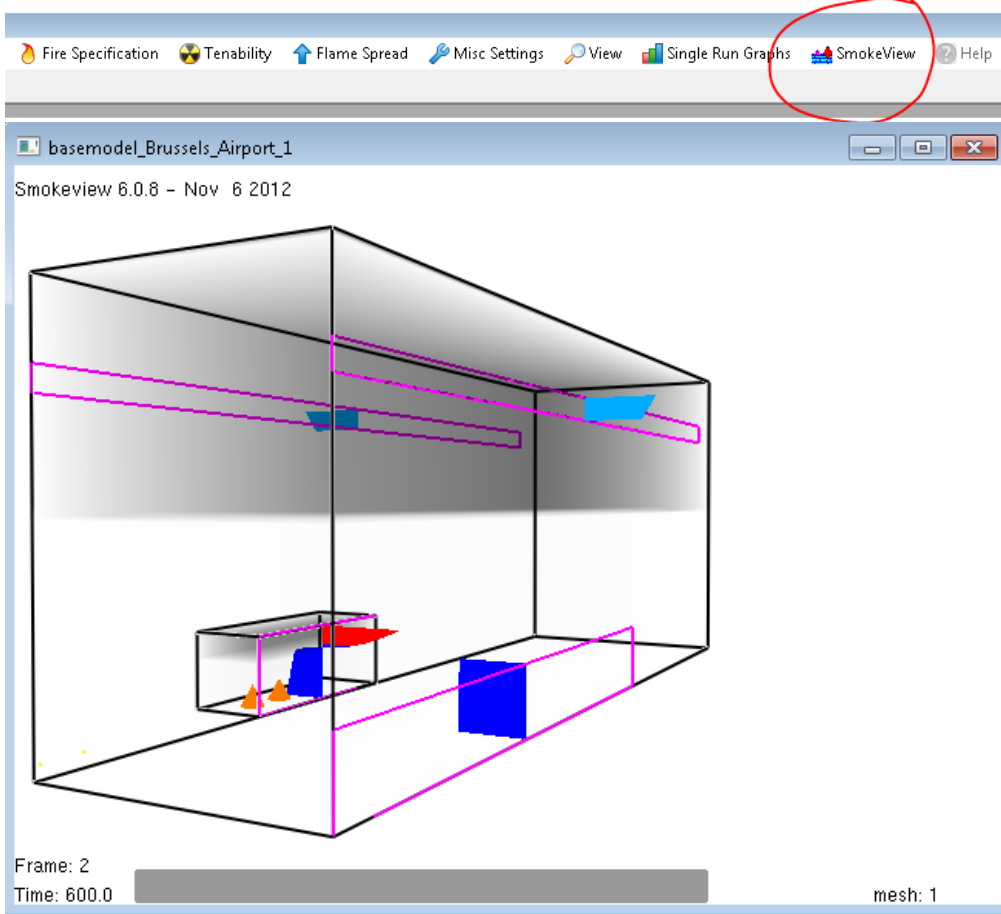


Figure 24. Smokeview visualisation.

4. Fire specification

4.1 Managing fire items

Fire items can be specified and managed from the FIRE SPECIFICATION, SELECT FIRE menu as shown in Figure 25. Fire items can be added, edited, copied or removed using this screen. All fire items are located within the room of fire origin.

The room of fire origin (fire room) is selected from the drop-down list as shown in Figure 25.

Fire items can also be imported from a local fire objects database by using the IMPORT button. An item can be selected from the list of items in the database and imported to the current project by clicking on the SEND TO ITEM LIST menu item shown in Figure 26.

Currently, only a limited number of the item properties are stored in the database, and additional property information will need to be introduced by the user after adding the item to the current project.

Where multiple items exist, the first item ignited can either be selected by highlighting it and clicking on the FIRST IGNITE button (the word IGNITE will appear to the right of the item name), or the first item can be randomly selected for each iteration by clicking on the RANDOM IGNITE button.

The layout of items within the fire room can be viewed by clicking on the ROOM POPULATE button with additional information and options described in section 4.2.

If the USE POWER LAW DESIGN FIRE option is checked, only one item will show in the item list (and be used in the simulation) and item-to-item spread cannot be modelled.

The growth rate coefficient α , peak rate of heat release and storage height (if applicable) can be specified as described in section 4.5 using the SETTINGS button.

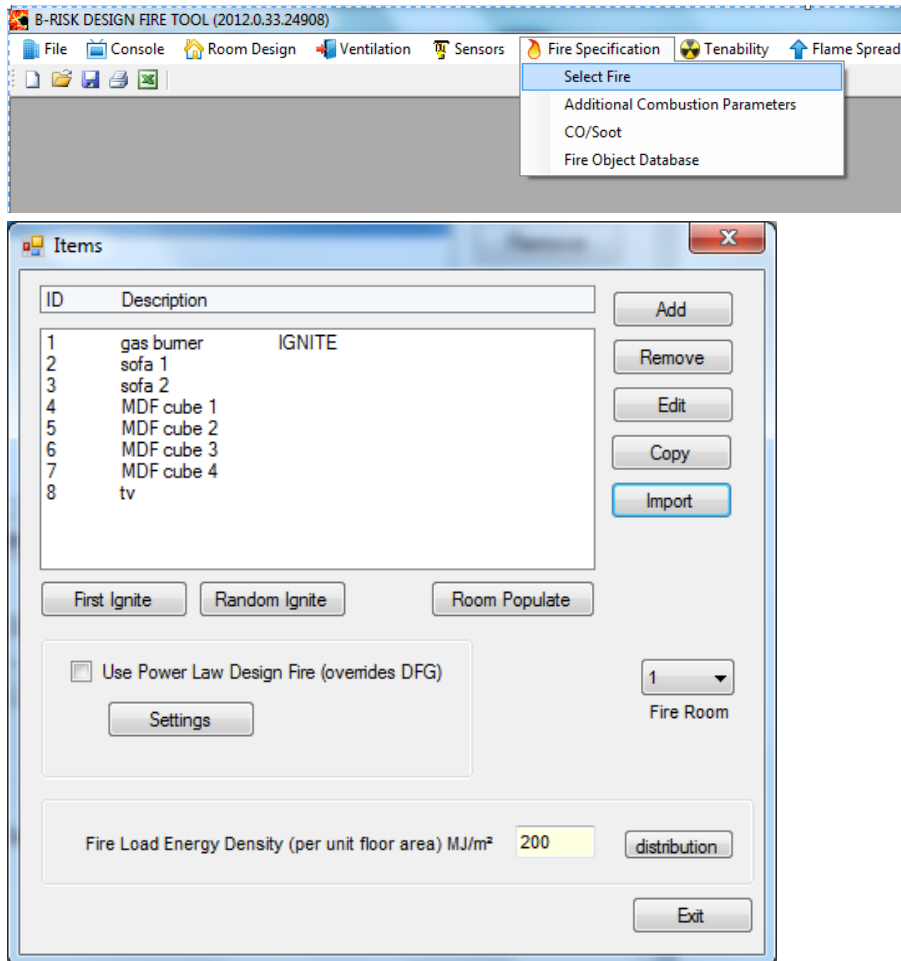


Figure 25. Managing fire items.

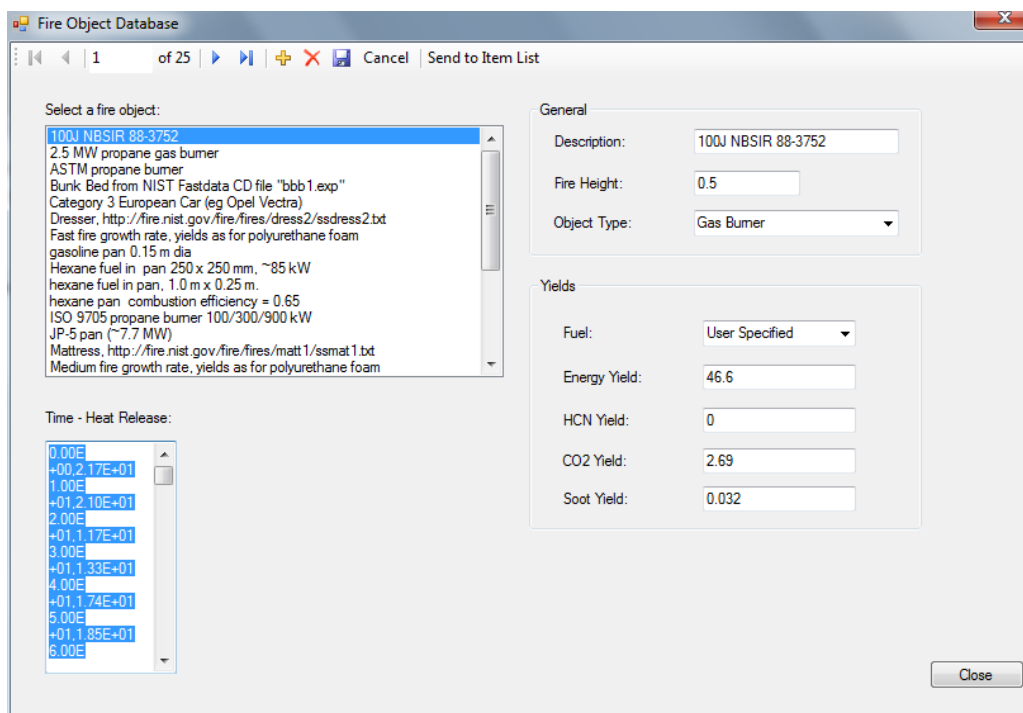


Figure 26. Fire object database.

4.2 Item property data

The screen describing the detailed properties of each fuel item is shown in Figure 27.

The LENGTH, WIDTH and HEIGHT properties refer to the rectilinear dimensions of the item.

ELEVATION refers to the height of the base of the item above floor level. B-RISK will assume that burning and entrainment will occur at and above this elevation. For the purposes of determining auto-ignition of the top surface of an item, the top surface is assumed to be located at the level $ELEVATION + HEIGHT$.

X-COORD and Y-COORD locate the item in the room and are used in the item-to-item fire spread model (see section 4.3.2) but also to determine which plume entrainment correlation is used (i.e. wall, corner or centre – see section 6.9.3).

If any part of the item is located within one grid interval of a wall or corner, the wall or corner location will be used for the plume entrainment, otherwise a centre location will be assumed.

COMBUSTIBLE MASS of the item can either be entered directly by the user, or the MASS CALC button can be used to calculate a mass based on the area under the rate of heat release curve divided by the heat of combustion. The combustible mass is used when auto-populating the room with items (see section 4.3.1) to calculate the total fire load and fire load energy density in the room.

MAX NUMBER PERMITTED IN ROOM and PROB NEAR WALL are both used in the design fire generator as described in section 4.3.1.

HEAT OF COMBUSTION, SOOT YIELD, CO₂ YIELD and RADIANT LOSS FRACTION are used by the zone model engine as described elsewhere. LATENT HEAT OF GASIFICATION is required if the burning rate enhancement sub-model is used (see section 6.8).

A characteristic mass burning rate is determined either using the CONSTANT A and CONSTANT B properties or by entering a value for HRR PER UNIT AREA. If a value is entered for the latter, it will be used in preference to any values assigned to the CONSTANT A and CONSTANT B properties. The characteristic mass burning rate is used by the burning rate enhancement sub-model and in the Heskestad plume entrainment sub-model in the calculation of the virtual source location. Further explanation of these inputs is given in section 6.8 and section 6.9.1 respectively.

HEAT RELEASE RATE data for the item is entered as pairs of values corresponding to the time (s) and heat release rate (kW) separated by a comma. The data can be plotted as shown in Figure 28 using the PLOT button.

An option to include a wind effect or disturbance increasing the rate of entrainment in the fire plume is also available and is further described in section 6.9.4. For most applications, the UNDISTURBED PLUME option should be used. However, if B-RISK is used for designing a smoke management system using spill plume vent types, the DISTURBED PLUME option is recommended (see section 6.9.4).

Edit Item

Short Description: User Label:

Detailed Description:

Type:

| Geometry | Units | Type |
|-------------------------------|---------|--|
| Length | 0.8 m | |
| Width | 0.6 m | |
| Height | 0.5 m | |
| Elevation | 0.4 m | |
| x-coord (left edge of item) | 1.9 m | |
| y-coord (bottom edge of item) | 0 m | |
| Combustible Mass | 3.72 kg | <input type="button" value="Mass Calc"/> |
| Max Number Permitted in Room | 1 | |
| Prob Near Wall | 0 - | |

Wind Effects

Undisturbed Plume

Disturbed Plume

Heat Release Rate

Time (s), HRR (kW)

| |
|------------|
| 0,34.9162 |
| 3,38.9672 |
| 6,42.9976 |
| 9,47.2032 |
| 12,51.0112 |
| 15,52.1171 |
| 18,50.9959 |
| 21,52.5048 |
| 24,55.738 |
| 27,55.5966 |
| 30,55.5743 |
| 33,54.5598 |
| 36,53.5409 |
| 39,57.6118 |
| 42,62.1867 |
| 45,64.6043 |
| 48,66.6126 |
| 51,70.8329 |
| 54,75.5216 |

Chemistry

| | | |
|-----------------------------|------------------------|---|
| Heat of Combustion | 29.2 kJ/g | <input type="button" value="distribution"/> |
| Soot Yield | 0.07 g/g | <input type="button" value="distribution"/> |
| CO ₂ Yield | 1.92 g/g | <input type="button" value="distribution"/> |
| Latent Heat of Gasification | 1.22 kJ/g | <input type="button" value="distribution"/> |
| Radiant Loss Fraction | 0.5 - | <input type="button" value="distribution"/> |
| Constant A | 0 mdot="= A qdote" + B | |
| Constant B | 0 mdot="= A qdote" + B | |
| HRR per unit area | 500 kW/m ² | <input type="button" value="distribution"/> |

Ignition of Vertical Surface by Source Items

| | |
|---------------|--|
| FTP limit | 812 kW ^s ⁿ /m ² |
| FTP index, n | 1.67 |
| Critical Flux | 8.5 kW/m ² |

Ignition of Horizontal Surface by Upper Layer

| | |
|---------------|---|
| FTP limit | 5759 kW ^s ⁿ /m ² |
| FTP index, n | 1.96 |
| Critical Flux | 28.2 kW/m ² |

Figure 27. Item properties form.

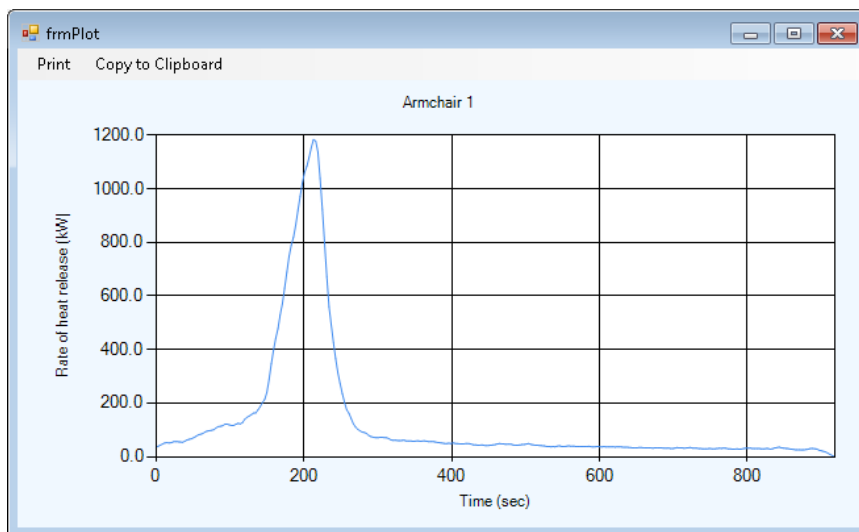


Figure 28. Plot of item rate of heat release versus time input.

4.3 Design fire generator

4.3.1 Room population methods

Fire items can be either placed in the room location specified under the item properties or they can be randomly located for each iteration by selecting either the MANUAL POSITIONING OF ITEMS or AUTO POPULATE ITEMS for the population method as shown in Figure 29.

GRID SIZE determines the number of potential locations for items to be positioned. A typical value might be in the order of 0.5–2% of the room length. If too small a value is used, the time required to complete the population process can be excessively long.

The VENT CLEARANCE entry causes a rectangular area immediately in front of a vent, defined by the width of the vent and the value entered, to be unavailable for locating items.

The SHOW VECTORS checkbox displays a vector connecting the centre of the first item ignited to the nearest vertical surface of each of the other items and displays the distance. This is the distance used in the point source radiation calculation in the item-to-item fire spread model.

The SHOW SPRINKLERS checkbox displays the plan location of sprinklers in the room.

The SHOW ITEM LABELS option allows the user to display either the item user label or a numeric ID number assigned to the item.

After a simulation has been run, this screen can also be used to display the room layout for each iteration by using the RECALL LAYOUT BY ITERATION up-down box. Ignition times for secondary target items will also be displayed here.

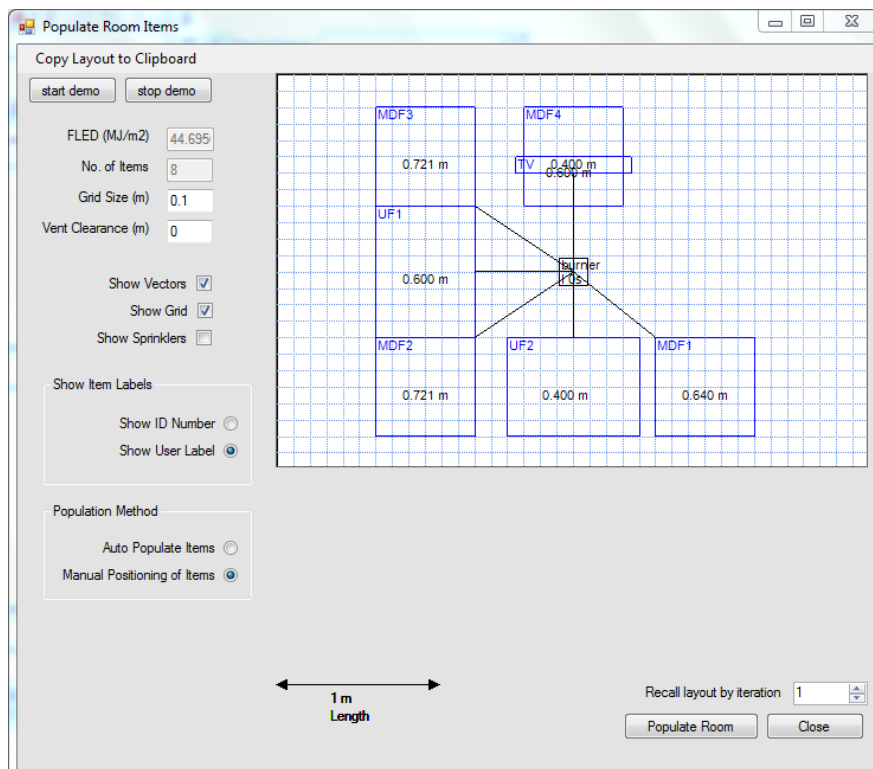


Figure 29. Populate room items.

The following procedure is used for locating items within the room for each iteration when the AUTO POPULATE ITEMS option is selected.

1. The room is overlaid with a rectangular grid of spacing given by the value entered for the GRID SIZE. The grid points (intersections) denote possible locations for the centre point of a rectangular-shaped item.
2. The locations of any openings in the walls of the room are noted and a vent clearance zone identified, of depth given by the value entered for the VENT CLEARANCE, in front of each the vent. Items are not permitted to be located within a vent clearance zone.
3. The FLED (fire load energy density) variable is randomly sampled (where a distribution has been assigned) and multiplied by the floor area of the room to determine the total fire load in the room in MJ.
4. Items in the room are randomly sampled from the list of items (see Figure 25). The first item randomly selected is taken as the item first ignited (unless the user has selected another item as the first ignited) while subsequent items are the secondary targets.
5. Each item selected has associated properties (including length, width and how many of that item can be placed in the room). Items are sequentially added to the room, keeping track of the sum of the fire load from all items, until the total fire load for the room is reached and no further items are added. The fire load for each individual item is given by multiplying the item mass by its heat of combustion.
6. An item can be oriented in one of two directions in the room – either the length dimension or the width dimension is aligned parallel to the y-axis of the room grid.
7. A subset of possible grid points is determined, on which each item is able to be centrally located. Grid points located within a distance of half of the width or length of the item to the adjacent wall surface are excluded from the subset, since the item will not fit if centred at those locations. Grid points within a distance of half of the length dimension of the item to the vent clearance zones are also excluded.
8. While assembling the subset of grid points, an effective cumulative probability density value, which is based on whether the major axis (taken as the length dimension) of an item is located close to a wall or not, is calculated. This is used to translate the probability distribution over the two-dimensional room floor area into a one-dimensional integer problem.
9. An integer is randomly chosen between 0 and the maximum value calculated for the effective cumulative probability density value by:
 - a. using a changeable seed for the inbuilt random number generator
 - b. scaling the range of the inbuilt random number generator to span 0 to the maximum number calculated
 - c. truncating the decimals.
10. To select the item centre location and orientation, the randomly generated integer is compared to the effective cumulative probability density values. The effective cumulative probability density value that is just greater than the random value is the one of interest.
11. The steps are repeated for the next item.

When locating items within the room using the MANUAL POSITIONING OF ITEMS option, each item is positioning using the X-COORD and Y-COORD item properties.

4.3.2 Item-to-item fire spread

To activate the secondary ignition module, the user must select the IGNITE SECONDARY ITEMS checkbox on the Console as shown in Figure 30 prior to starting the simulation.

The item-to-item fire spread model was developed by Baker et al. (Baker, Fleury et al., 2011; Baker, Spearpoint et al., 2011a).

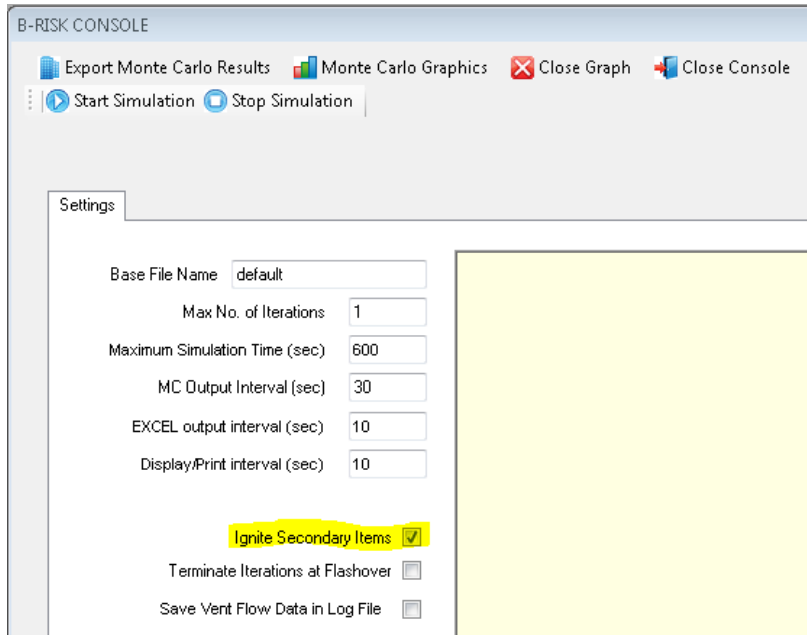


Figure 30. Ignite secondary items.

The first item sampled from the items database using the AUTO POPULATE ITEMS option becomes the item first ignited, unless otherwise specified. Remaining items in the room become secondary items or targets.

The secondary ignition module of the design fire generator (DFG) models items as rectilinear prisms having the length, width and height dimensions specified in the EDIT ITEM dialogue box, shown in Figure 27.

The ignition of secondary items is based on the radiation that is received by the secondary item, which occurs in one of two ways.

Radiation from the flames of burning items is modelled using the point source model (Modak, 1977) represented mathematically as:

$$\dot{q}_{fl}'' = \frac{\dot{Q}\lambda_r}{4\pi r^2} \quad (4)$$

Where \dot{q}_{fl}'' (kW/m²) is the heat flux received by the secondary target (where the incident flux is assumed to be received normal to the surface), \dot{Q} (kW) is the heat output, λ_r is the radiative fraction respectively from the burning object and r (m) is the radial distance (in plan view) from the centre of the burning object (point source) to the nearest part of the secondary item. To calculate r , each side of the target object is divided into 10 equal intervals, the distance between the point source and the dividing points on each side of the target is calculated and the nearest distance is determined. Where multiple items are burning, \dot{q}_{fl}'' is the sum of heat flux on the secondary target from all burning items.

In addition to flame radiation, the DFG concurrently calculates radiation from the underside of the hot upper layer, which is treated as a planar, uniform, isothermal

“surface”. The surface is also assumed to be both “diffuse”, i.e. the intensity of the emitted radiation is uniform in all directions and “grey”, i.e. the emitted radiation is independent of wavelength (Tien, Lee & Stretton, 2008). The heat flux from the hot upper layer, q_U'' (kW/m²), to the top surface of the object is therefore calculated as:

$$q_U'' = \epsilon_U \sigma T_U^4 F \quad (5)$$

Where σ (kW/K⁴m²) is the Stefan-Boltzmann constant, T_U (K) is the temperature of the hot upper layer as calculated by B-RISK for every time step in the simulation and F is the configuration factor. The DFG assumes that the secondary object is located at the centre of the compartment and computes F as (Tien, Lee & Stretton, 2008):

$$F = \frac{2}{\pi} \left[\frac{A}{\sqrt{1+A^2}} \tan^{-1} \frac{B}{\sqrt{1+A^2}} + \frac{B}{\sqrt{1+B^2}} \tan^{-1} \frac{A}{\sqrt{1+B^2}} \right] \quad (6)$$

Where $A = \frac{X}{2z(t)}$ and $B = \frac{Y}{2z(t)}$, and X and Y (m) are the length and width of the compartment respectively and $z(t)$ (m) is the height from the top of the secondary object to the underside of the hot upper layer as a function of time. In many instances, the secondary object will not be located at the centre of the compartment, giving a different value for F , but the former approach gives the maximum value and is hence conservative. In the calculation procedure in the DFG, when the upper layer reaches the top of the secondary object, the value of F becomes unity. The remaining parameter in equation (5) is the emissivity of the soot-gas mixture comprising the upper layer, ϵ_U , which is calculated by the DFG as (Tien, Lee & Stretton, 2008):

$$\epsilon_U = 1 - e^{-kL} + \epsilon_g e^{-kL} \quad (7)$$

In equation (7), the term $1 - e^{-kL}$ accounts for the emissivity of the soot in the upper layer, while the term $\epsilon_g e^{-kL}$ represents the emissivity of the upper layer gases. In the B-RISK model, it is assumed that only water vapour and carbon dioxide contribute to the gas emissivity, ϵ_g . The exponent k (1/m) is the extinction coefficient of the upper layer, which, neglecting the scattering coefficient, equates to the absorption coefficient of the upper layer (Tien, Lee & Stretton, 2008). In B-RISK, the extinction coefficient is calculated as the mass concentration of soot in the upper layer (kg soot/m³) multiplied by the particle extinction cross-section (m²/kg soot).

The other exponent in equation (7) is the mean beam length, L (m). Tien et al. indicate that the mean beam length can be used to calculate the radiation from an arbitrary gas volume to its bounding surfaces and “represents the equivalent radius of hemispherical gas body such that it radiates a flux to the centre of its base equal to the average flux radiated to the boundary surface by the actual volume of gas” (Tien, Lee & Stretton, 2008). In the B-RISK model, the upper layer is assumed to be optically thick, so therefore the mean beam length, L (m), is approximated as $L = CL_0$, where C is a correction factor that has the value 0.9 for many geometries and L_0 (m) is the actual geometric mean beam length of the upper layer. The geometric mean beam length is approximated as $L_0 = \frac{4V_U}{A_U}$, where V_U (m³) is the volume of the upper layer and A_U (m²) is the area bounded by the upper layer. Combining these parameters together, the mean beam length is defined as:

$$L = \frac{3.6V_U}{A_U} \quad (8)$$

The DFG checks the two radiation mechanisms represented by equation (4) and equation (5) concurrently. The first case is likely to dominate where secondary objects are relatively close to burning items, and point source model radiation is assumed to be received by the closest vertical surface of a secondary object. Target ignition properties are defined for this case as previously shown in Figure 27 as IGNITION OF VERTICAL SURFACE BY SOURCE ITEMS.

The second case is likely to dominate for more remote items, where radiation from the underside of the hot upper layer is received by the top surface of the secondary object. Target ignition properties are defined for this case as previously shown in Figure 27 as IGNITION OF HORIZONTAL SURFACE BY THE UPPER LAYER.

The methodology that the DFG uses to determine when secondary items ignite is based on the Flux-Time Product (FTP) procedure. Each item in the database has a FTP dataset for both the vertical surface and the horizontal surface cases, consisting of a *FTP* value ($[\text{kW}/\text{m}^2]^n \text{ s}$), a critical incident flux \dot{q}_{cr}'' (kW/m^2) and an FTP index n (must be in the range 1–2). These three parameters are determined experimentally in an ignition apparatus such as the cone calorimeter (Baker, Spearpoint et al., 2011b). For every time step in the modelling process of the DFG where the incident radiation \dot{q}_i'' (kW/m^2) exceeds \dot{q}_{cr}'' , the *FTP* accumulates until the threshold value is exceeded, at which point, ignition is deemed to have occurred, as represented in equation (9):

$$FTP = \sum_{i=1}^m (\dot{q}_i'' - \dot{q}_{cr}'')^n \Delta t_i \quad (9)$$

In equation (9), \dot{q}_i'' is the incident radiation at the i^{th} time increment Δt_i (s) and consists of either \dot{q}_{fl}'' from equation (4) for the item-to-item ignition case or \dot{q}_U'' from equation (5) for the hot layer ignition situation. The FTP parameters selected for input may be determined under either piloted or auto-ignition scenarios, and one or other may be considered more appropriate for a given scenario depending on which is the most likely mode of ignition.

Each fuel object in the item database has its own heat release rate (HRR) – generally free-burning – and once the first item ignites, the total heat release rate within the compartment is that of the first object, until secondary objects are ignited either by radiation directly from the initial burning object or by radiation from the hot upper layer. As soon as other items in the compartment ignite, the HRR of the secondary items are added to the combined HRR of the other burning items, i.e. the total HRR for the compartment is the sum of the HRRs of the individual items – this approach is the same as the FREEBURN procedure within the MAKEFIRE module of FPETOOL (Deal, 1995). As such, possible enhancement of the HRR of individual items (due to the ignition source for the subsequently ignited objects varying from that applicable to the experimental HRR data) is not modelled by the DFG. However, this enhancement can be included using the sub-model described in section 6.8.

Subject to applicable fuel and ventilation conditions, the total compartment HRR continues to grow in this fashion during the initial fuel-controlled phase, up to the stage where the fire becomes ventilation controlled. Figure 31 shows an example of a cumulative total compartment HRR generated in this fashion by the DFG, with

ventilation-limited burning occurring and compared to the curve for the HRR of individual items being added together, regardless of the impact of the ventilation on the HRR.

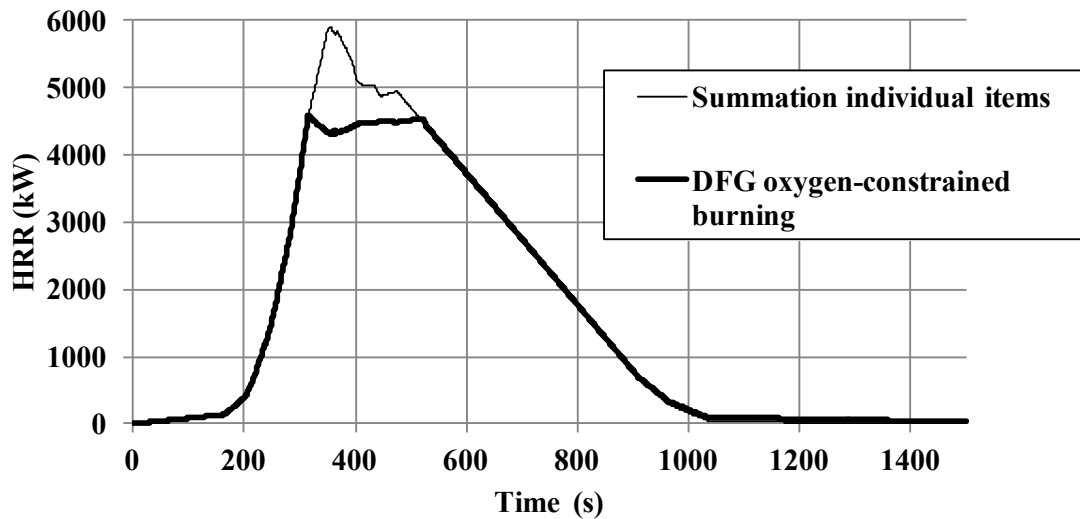


Figure 31. Composite heat release rate in compartment.

4.4 Fire load energy density (FLED)

The fire load energy density value in MJ per room floor area (m²) controls the maximum fire load within the fire room. When the DFG is used to randomly populate the fire room with items, this value will determine the total number of items added to the room.

In the case of a power law fire, the FLED is used to determine the duration of burning with the mass loss and heat release rate set to zero when all the fuel has been consumed.

Distributions can be assigned to the value of fire load energy density.

4.5 Power law design fires

Two types of automatically generated power law design fires are provided as specified for use by C/VM2 (MBIE, 2014) and can be selected as shown in Figure 32. They are:

$$\dot{Q}_f = \alpha t^2 \quad (10)$$

$$\dot{Q}_f = \alpha t^3 H_{st} \quad (11)$$

Where the total rate of heat release (in kW) is \dot{Q}_f and α is the fire growth rate coefficient (in kW s⁻² or kW s⁻³ m⁻¹), t is time from ignition and H_{st} is the storage height (in m).

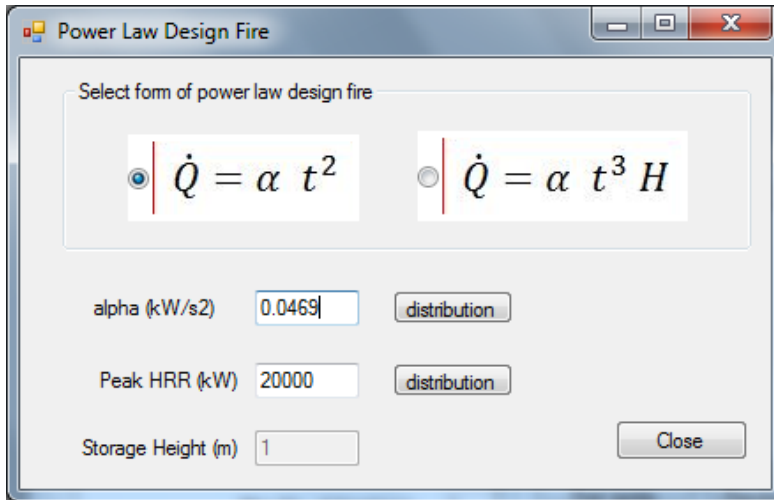


Figure 32. Power law design fire.

5. Model simulations

5.1 Running simulations

Once input parameters have been set by the user, the simulation is started by clicking on the START SIMULATION menu item from the B-RISK Console screen as shown in Figure 33.

Repeat iterations will be run sequentially according to the maximum number of iterations specified. A commentary for each iteration will be posted to the log screen as the simulation proceeds.

When the simulation is in progress, the user can terminate the simulation at any time using the STOP SIMULATION menu item on the Console screen as shown in Figure 34.

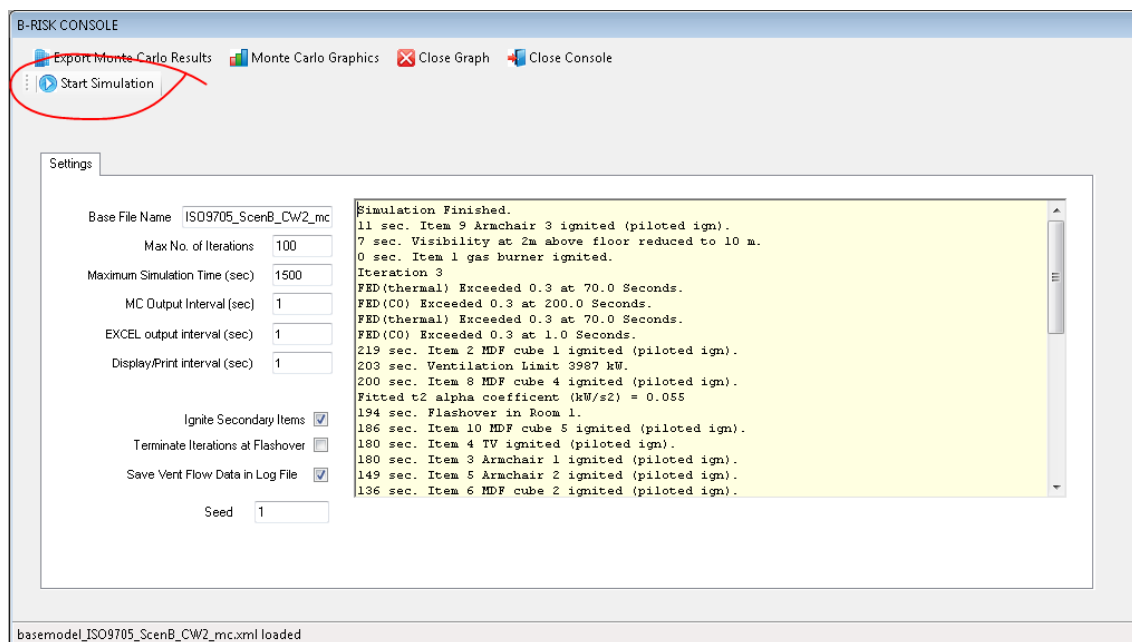


Figure 33. Start simulation from console screen,

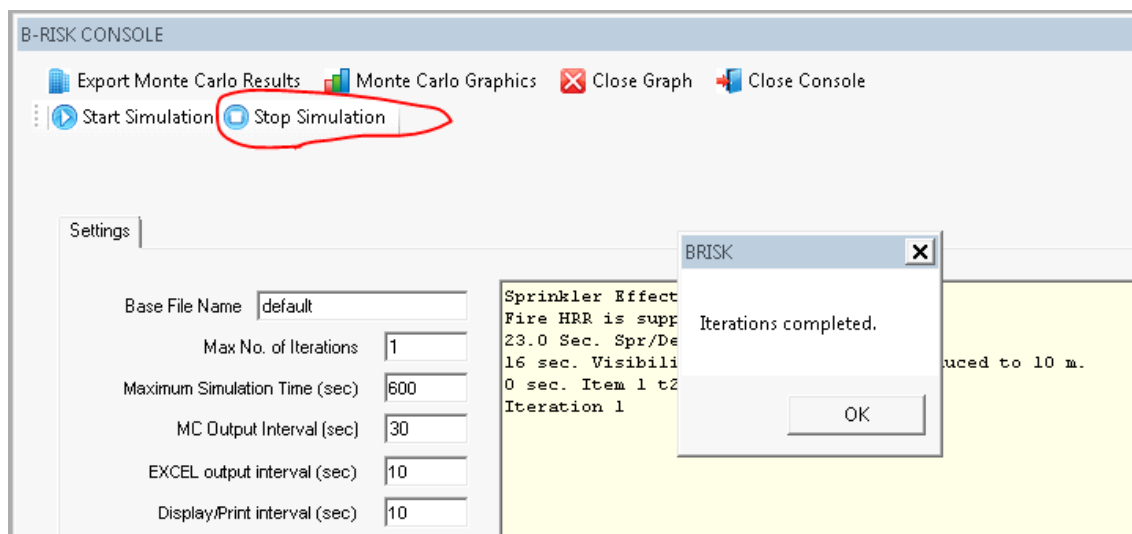


Figure 34. Stop simulation from console screen.

5.2 Displaying summary input and results from a single iteration

After running the simulation, a summary of input and output from the last iteration is displayed using the VIEW, VIEW RESULTS menu item as shown in Figure 35. A summary of the input only can be displayed using the VIEW, VIEW INPUT menu item. The user selects the output variables to be displayed from the SELECT VARIABLES menu item.

Output will be listed at time intervals given by the DISPLAY/PRINT INTERVAL as shown in Figure 38.

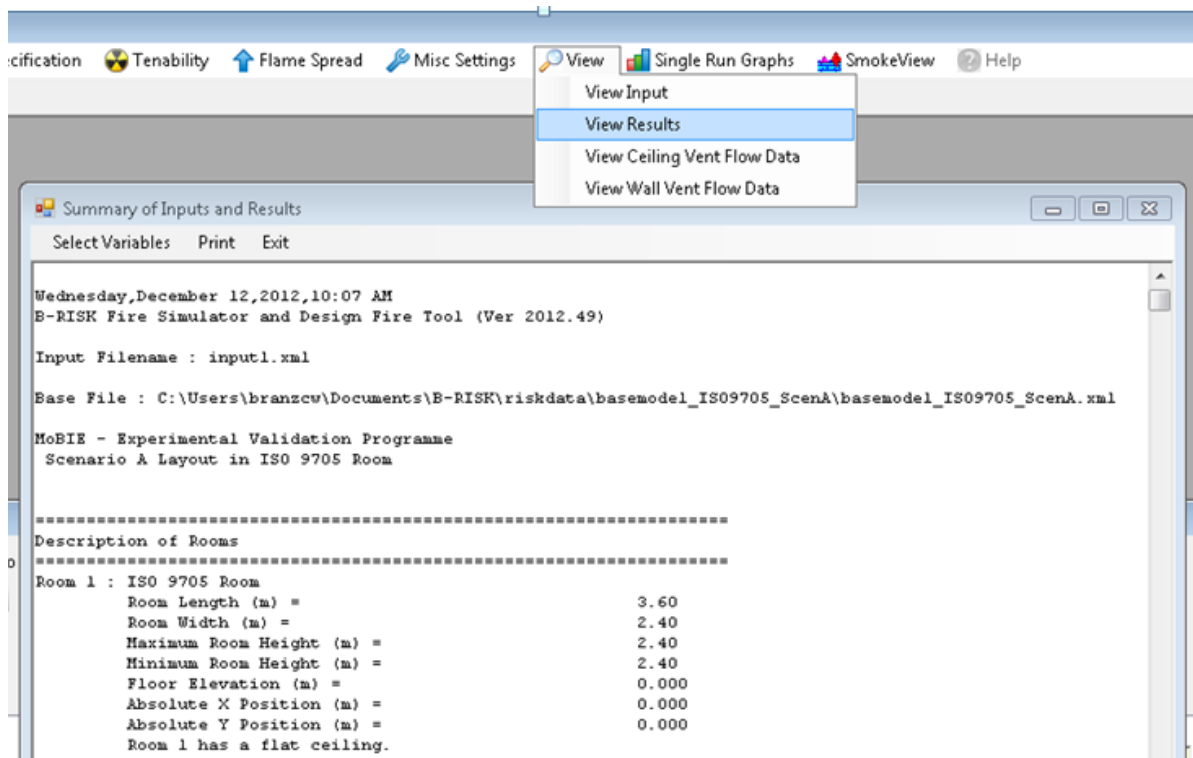


Figure 35. Summary input and output for a single iteration.

Results from a previously run iteration can be loaded using the FILE, LOAD INPUT*.XML file menu item.

5.3 Displaying graphical output from a single iteration

Graphical output from the most recently run iteration or from a previously loaded iteration can be viewed using the SINGLE RUN GRAPHS menu item as shown in Figure 36.

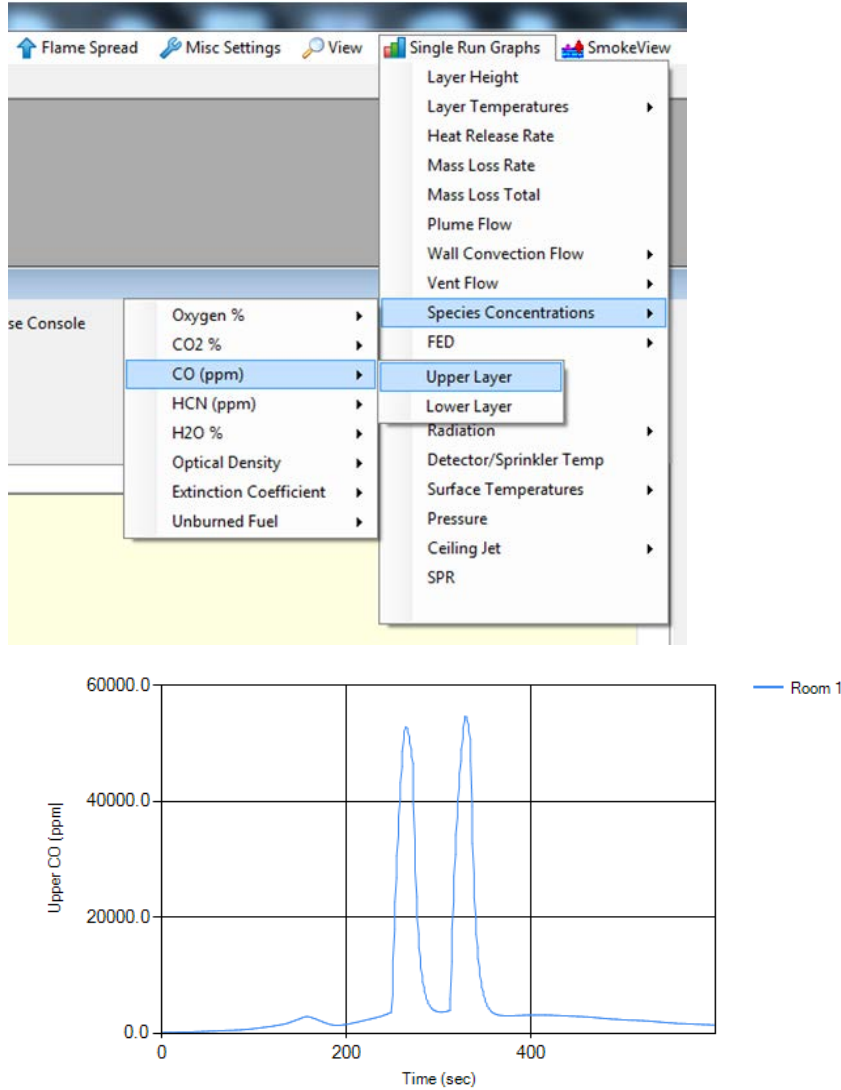


Figure 36. Graphical output for a single run.

5.4 Displaying time series output from multiple iterations

Time series plots of selected output can be displayed where the output for all simulations can be displayed on a single graph. Time series plots are accessed by using the MONTE CARLO GRAPHICS, TIME-SERIES PLOT menu item on the Console screen as shown for UPPER LAYER TEMPERATURE in Figure 37.

Available time series plots include UPPER LAYER TEMPERATURE, LOWER LAYER TEMPERATURE, LAYER HEIGHT, FED GASES, FED THERMAL, VISIBILITY, HEAT RELEASE RATE and NO. OF SPRINKLERS ACTIVATED.

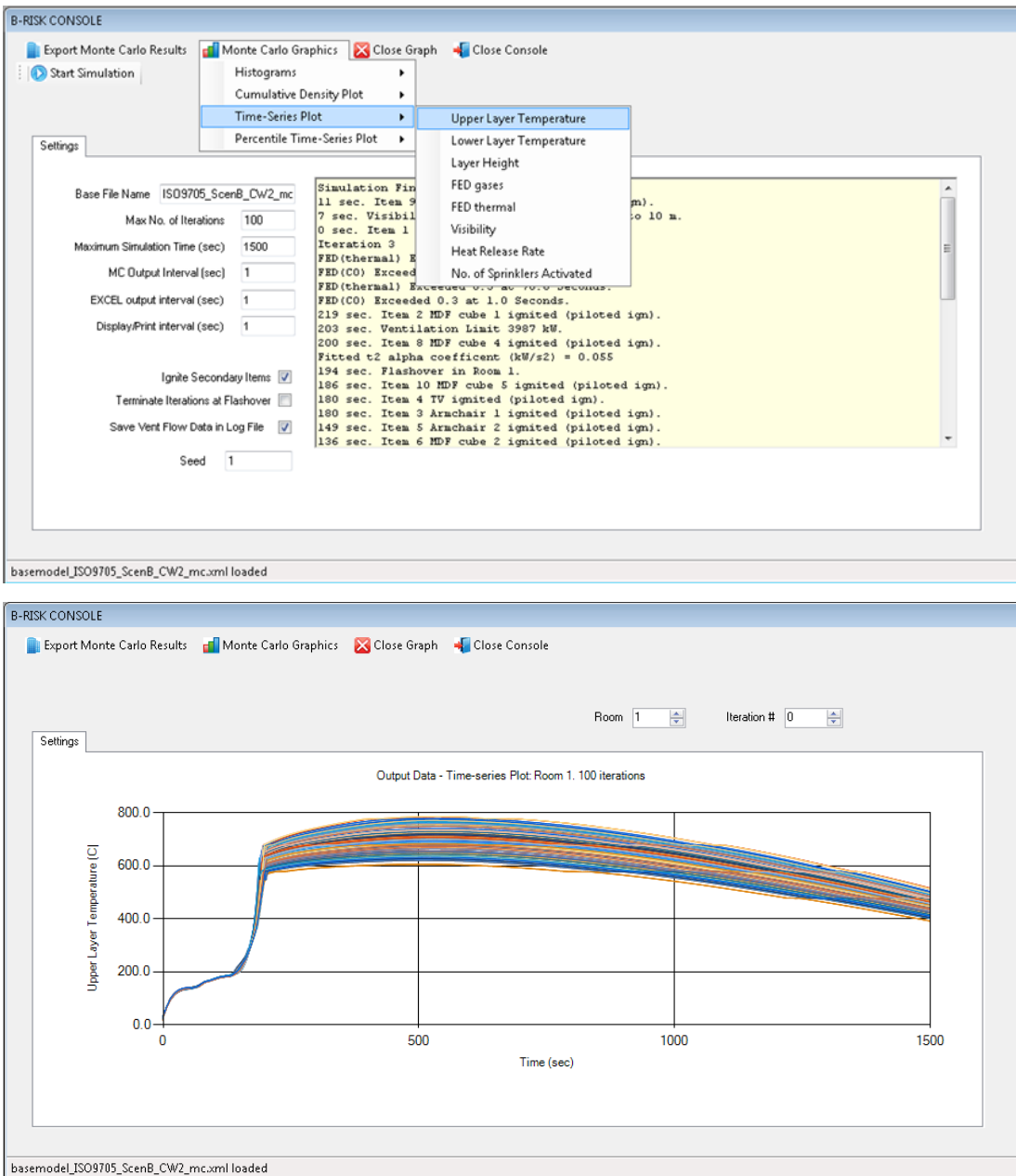


Figure 37. Example time series plot of upper layer temperature for multi-iteration output.

The room to display can be selected from the ROOM up-down box above the graph, and individual iterations can be displayed using the ITERATION # up-down box. Iteration 0 displays all iterations.

A percentile time series plot can be generated using the MONTE CARLO GRAPHICS, PERCENTILE TIME-SERIES PLOT menu item on the Console screen. This constructs an output curve using the upper x-percentile value at each time step. An example is shown in Figure 38 for the upper 50th percentile upper layer temperature.

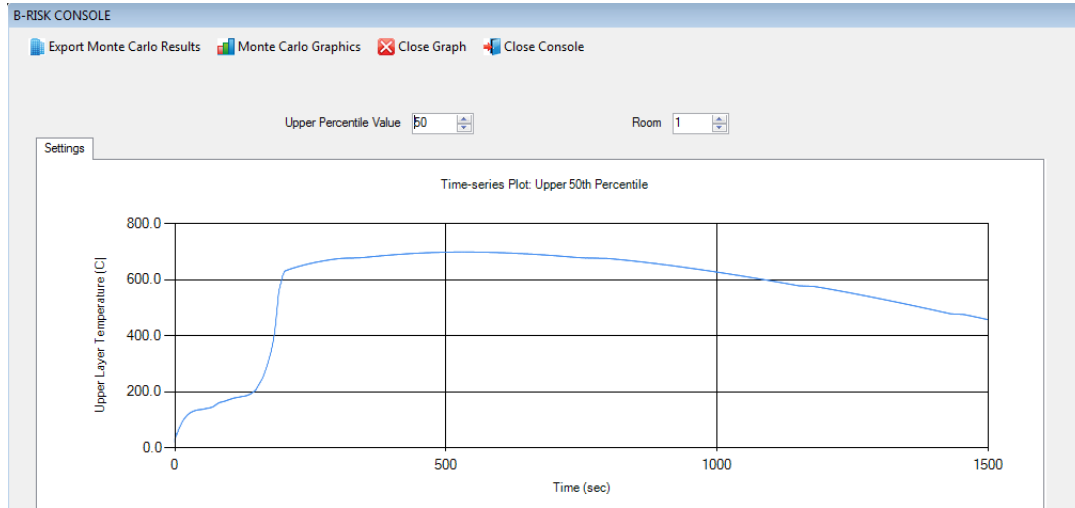


Figure 38. Example of upper percentile time series plot.

5.5 Displaying probabilistic input from multiple iterations

Histograms for the sampled input for selected parameters can be displayed using the MONTE CARLO GRAPHICS, HISTOGRAMS, INPUTS menu item on the Console screen as shown in Figure 39. The number of histogram bins can be modified by using the # BINS up-down box.

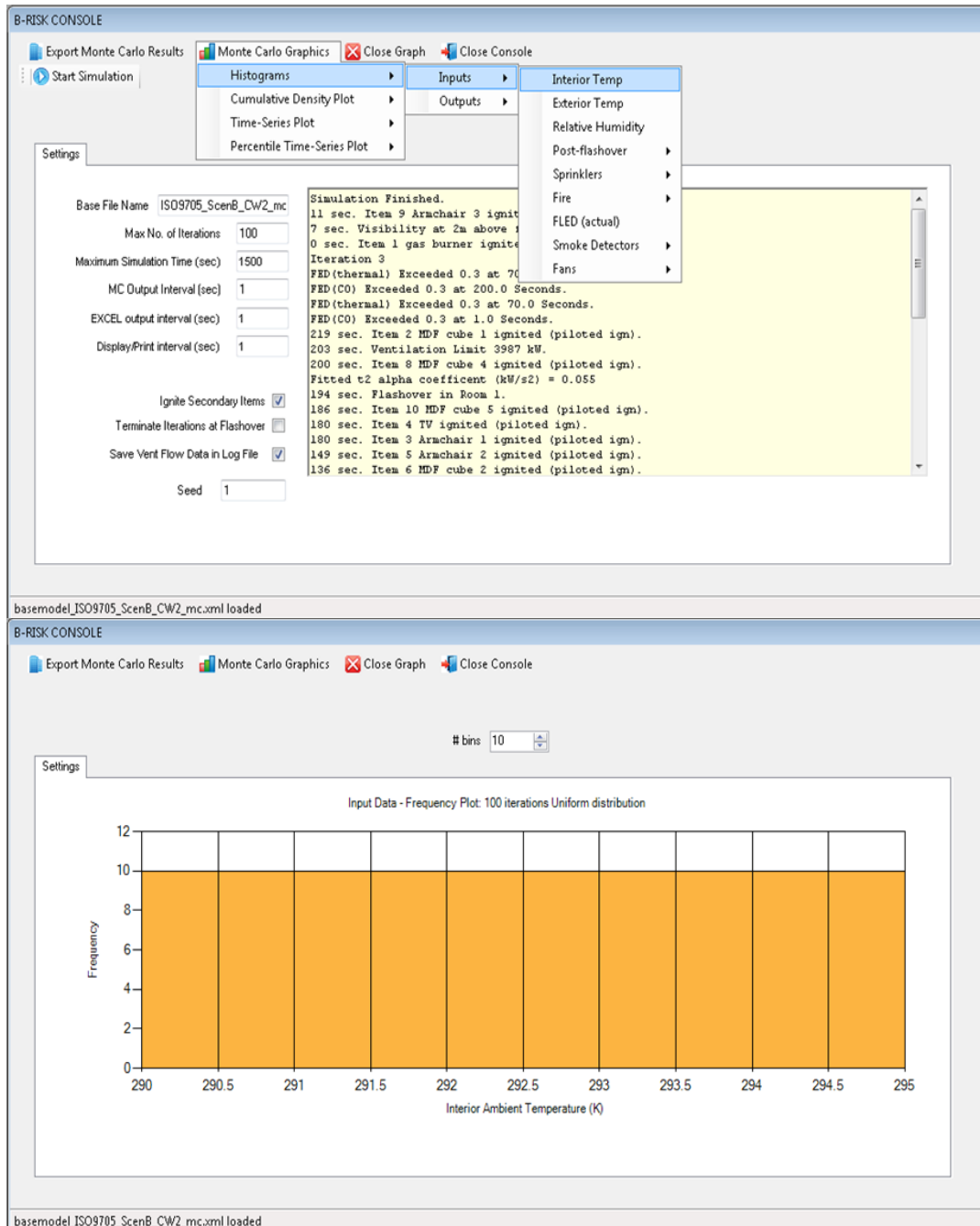


Figure 39. Example histogram for sampled values of interior ambient temperature.

Cumulative density functions for the sampled input for selected parameters can be displayed using the MONTE CARLO GRAPHICS, CUMULATIVE DENSITY PLOT, INPUTS menu item on the Console screen as shown in Figure 40.

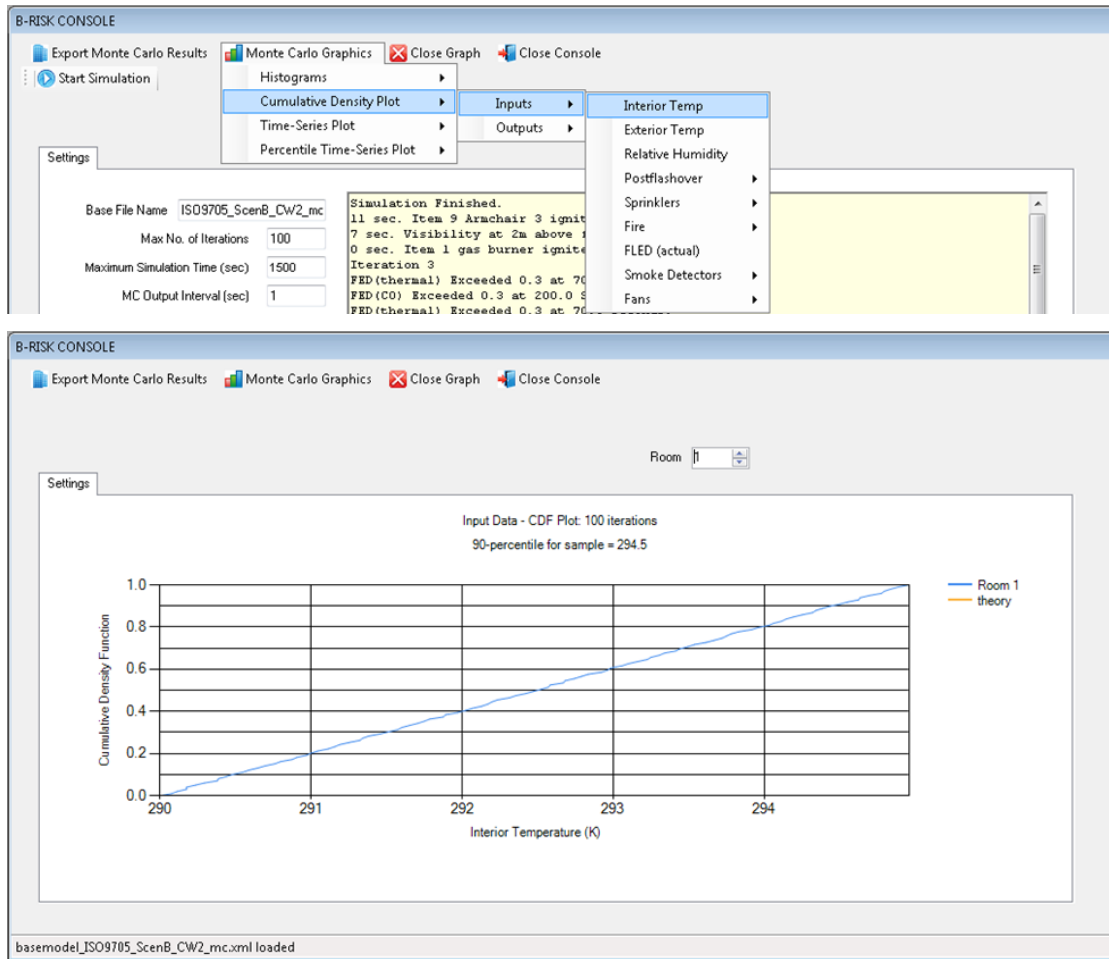


Figure 40. Example cumulative density function for sampled values of interior ambient temperature.

5.6 Displaying probabilistic output from multiple iterations

Histograms for selected output parameters can be displayed using the MONTE CARLO GRAPHICS, HISTOGRAMS, OUTPUTS menu item on the Console screen as shown in Figure 41. These histograms display output data at a specified time selected by the user from the TIME up-down box. The number of histogram bins can be modified by the user using the # BINS up-down box.

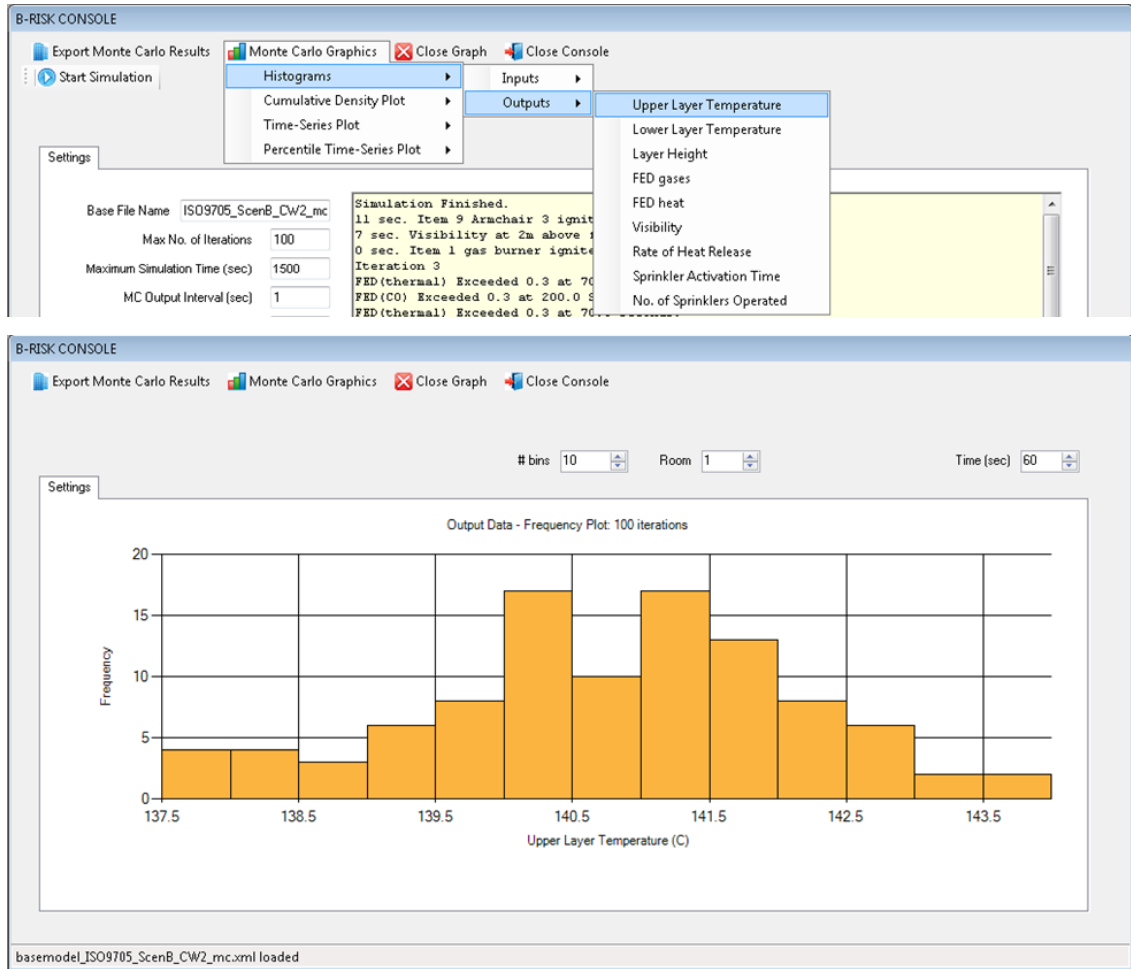


Figure 41. Example histogram for predicted output values of upper layer temperature.

Cumulative density functions for selected output parameters can be displayed using the MONTE CARLO GRAPHICS, CUMULATIVE DENSITY PLOT, OUTPUTS menu item on the Console screen as shown in Figure 42. These cumulative density functions display output data at a specified time selected by the user from the TIME up-down box.

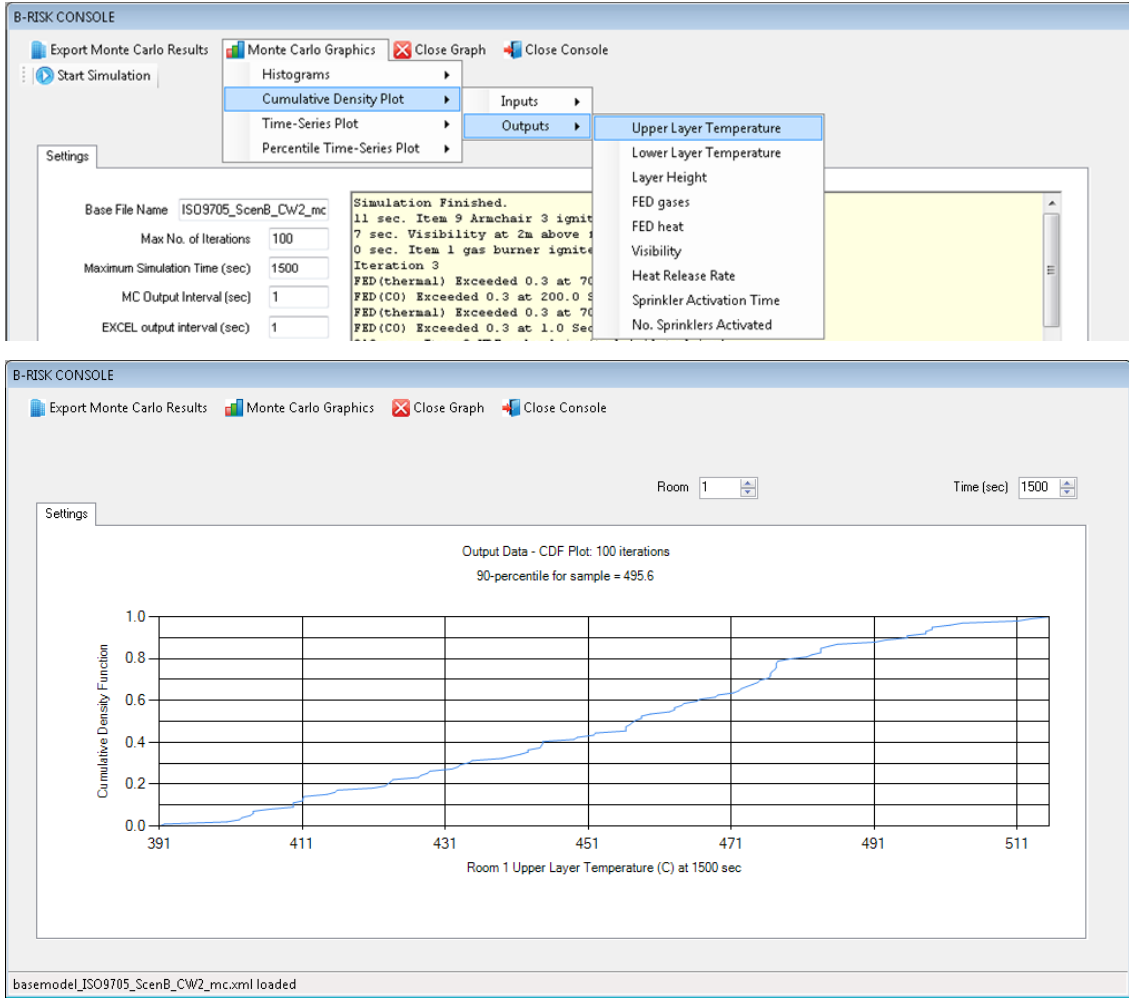


Figure 42. Example cumulative density function for predicted output values of upper layer temperature.

5.7 Exporting data to an Excel spreadsheet

Output from multiple iterations can be exported to an Excel spreadsheet using the EXPORT MONTE CARLO RESULTS, EXPORT OUTPUT TO EXCEL, EXPORT ALL from the B-RISK Console. The user will be asked for the room number, start iteration and end iteration for the data to be exported. Each iteration will be saved in a separate Excel worksheet.

Alternatively, selected output parameters can be exported as shown in Figure 43. For the listed output parameter, data for each iteration will be put in a separate column on the same worksheet.

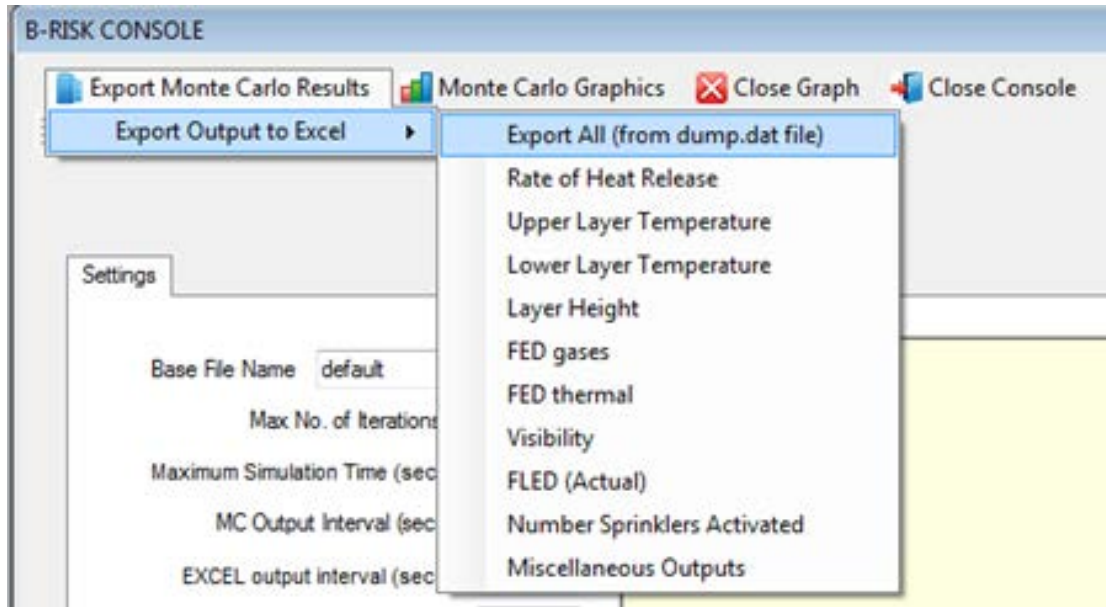


Figure 43. Exporting multiple iteration data to excel

6. Two-zone model

6.1 Introduction

The fire zone model is developed using principles of mass and energy conservation to predict various phenomena associated with room fires. The zone model essentially consists of two homogeneous zones – a hot upper layer and a relatively cool lower layer. The fire plume is treated as the mechanism by which the combustion products from the fire and entrained air are transported from the lower layer to the upper layer. The model allows up to 10 interconnected rooms. A schematic of a fire zone model showing the mass and heat flows for an enclosure is shown in Figure 44.

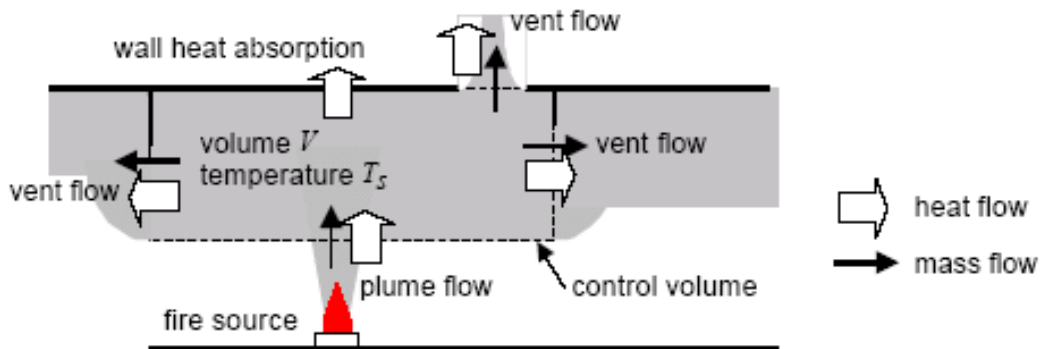


Figure 44. Schematic of a zone model [Extracted from (ISO, 2006a)].

6.2 Mass and energy balance

Conservation of mass and energy leads to a set of first-order differential equations that allow the upper layer volume, upper and lower layer temperatures and the pressure equation to be solved.

The form of the equations is as given by Peacock et al. (1993) for the CFAST model.

The equation for the pressure in the room is:

$$\frac{dP}{dt} = \frac{\gamma - 1}{V_R} (\dot{h}_L + \dot{h}_U) \quad (12)$$

The pressure is nominally that at the elevation of the floor and is relative to the atmospheric pressure at a nominated reference elevation. The offset pressure is used to avoid unnecessary loss of significant digits when solving vent flow equations, where the pressure differences across the vent are very small.

The equation for the volume of the upper layer is:

$$\frac{dV_U}{dt} = \frac{1}{\gamma P} \left[(\gamma - 1) \dot{h}_U - V_U \frac{dP}{dt} \right] \quad (13)$$

The lower layer volume is the difference between the room volume (a constant) and the upper layer volume. The height of the smoke layer interface above the floor for a room of uniform area and flat ceiling is then given by:

$$z = \frac{V_R - V_u}{A_f} \quad (14)$$

The ceiling can be specified as flat or sloping. In the latter case, the geometry of the upper volume is taken into account by the model when solving for the position of the layer interface height.

The equation for the temperature of the upper layer is:

$$\frac{dT_u}{dt} = \frac{1}{c_p \rho_u V_u} \left[(\dot{h}_u - c_p \dot{M}_u T_u) + V_u \frac{dP}{dt} \right] \quad (15)$$

The equation for the temperature of the lower layer is:

$$\frac{dT_l}{dt} = \frac{1}{c_p \rho_l V_l} \left[(\dot{h}_l - c_p \dot{M}_l T_l) + V_l \frac{dP}{dt} \right] \quad (16)$$

The convective enthalpy of the fire \dot{Q}_f includes that from the burner/source, the burning wall lining and the ceiling lining. In the case of a room-corner fire, the fire is represented by a single fire plume. The description of the mass flow in the plume is given in section 6.9.

The equations for the rate of change of mass in the upper and lower layers are given by:

$$\frac{dM_u}{dt} = \dot{m}_p + \dot{m}_f - \dot{m}_d - \dot{m}_o \quad (17)$$

$$\frac{dM_l}{dt} = \dot{m}_i + \dot{m}_d - \dot{m}_p \quad (18)$$

The mass from the fuel includes the burner/source, wall and ceiling linings involved in the fire. A vent shear mixing flow from the upper layer to the lower layer is represented by \dot{m}_d (see section 6.10.2). In the model, \dot{m}_d , \dot{m}_i and \dot{m}_o are provided by the vent flow algorithm (see section 6.10.1) as a single term representing the net flow to/from the upper/lower layer due to all vent flows. There may also be an additional mass flow term where mechanical ventilation (extract to/from a room from/to an exterior space) is specified (see section 6.15). This is not shown in the above equations.

6.3 Modelling rooms as a single zone

Users are provided with the option to model rooms as a single zone rather than two zones provided the room is not the room of fire origin. This can be useful for shafts or other rooms remote from the fire where mixing or smoke-logging effects may mean that a two-zone representation is less likely or less pronounced. This is used in situations where the stratification does not occur. Examples are elevators, shafts, complex stairwells and compartments far from the fire (Peacock et al., 2005). The single-zone option should be considered when the compartment height to width (or length) ratio exceeds about 5.

The single-zone behaviour is implemented by forcing the smoke layer to be 0.1 m above floor level. The remainder of the differential equation set described in section 6.2 are solved as before.

The user can assign the single-zone option to a room using the MISC SETTINGS, MODEL PHYSICS menu item as shown in Figure 45.

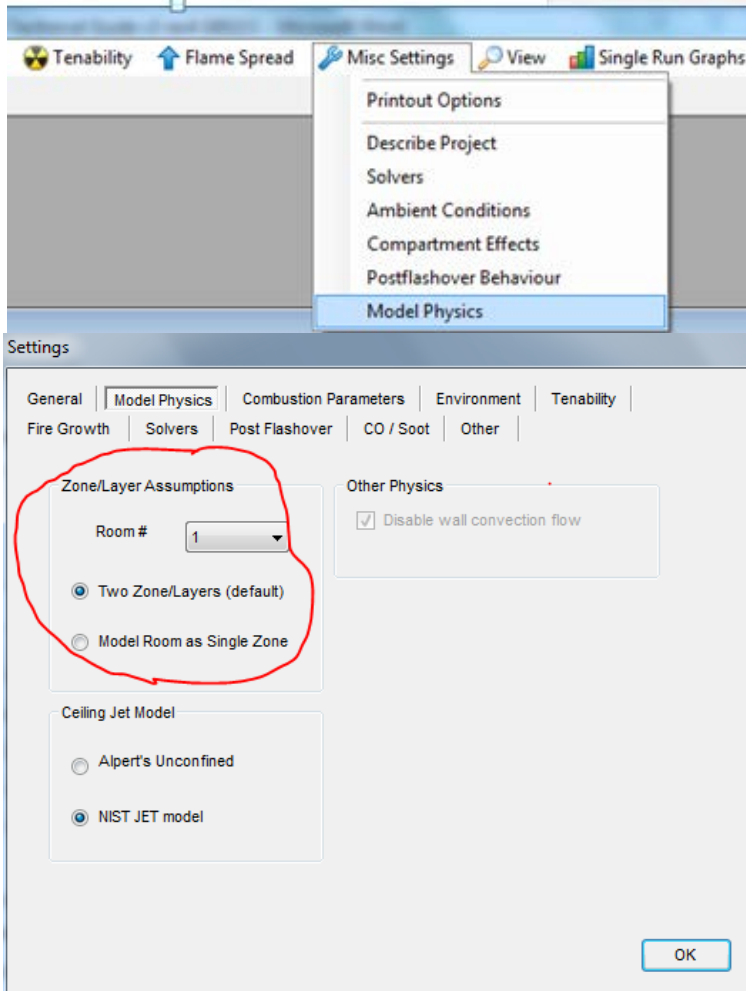


Figure 45. Modelling room as a single zone.

6.4 Species generation

The conservation equation for species in the upper layer is:

$$\frac{dY_{i,u}}{dt} = \frac{1}{M_u} [\dot{m}_p(Y_{i,l} - Y_{i,u}) + \dot{m}_f(\psi_i - Y_{i,u})] \quad (19)$$

The conservation equation for species in the lower layer is:

$$\frac{dY_{i,l}}{dt} = \frac{1}{M_l} [\dot{m}_i(Y_{i,\infty} - Y_{i,l}) + \dot{m}_d(Y_{i,u} - Y_{i,l})] \quad (20)$$

M_u and M_l are obtained from applying the ideal gas law such that $M_i = MW_i PV_i / (RT_i)$.

Where subscript i represents the upper or lower layer and MW_i is the average molecular weight of the layer based on the gas composition of the layer and R is the universal gas constant.

Species tracked in the model are soot, CO, CO₂, HCN, water vapour, unburned fuel and O₂. The mass fractions of soot, HCN and CO initially present in the room are considered to be negligible, while the initial mass fraction of O₂ is equal to 0.231 (ambient) and of CO₂ equal to 0.0005. Unburned fuel is only “produced” under a ventilation-limited burning regime.

The mass fraction of water vapour, Y_{H_2O} , initially present in the room is determined from the known relative humidity and ambient temperature as follows (Karlekar, 1983):

$$Y_{H_2O} = \frac{0.622 \Phi_{RH} W_s}{W_s + 0.622 - \Phi_{RH} W_s} \quad (21)$$

Where Φ_{RH} is the relative humidity, W_s is the humidity ratio at saturation and 0.622 is the ratio between the molecular weights of water vapour and air. The humidity ratio at saturation (Karlekar, 1983) is given by:

$$W_s = \frac{0.622 P_{ws}}{P_a - P_{ws}} \quad (22)$$

Where P_{ws} is the saturation pressure for water vapour corresponding to the ambient temperature and is determined from steam tables (Rogers & Mayhew, 1992) and P_a is atmospheric pressure.

For a room-corner fire, the species generated by objects/burner, wall linings and ceiling linings are separately accounted for and summed.

6.5 Combustion chemistry

The user specifies the composition of the fuel by number of atoms of C, H, O and N in a fuel molecule using the FIRE SPECIFICATION, ADDITIONAL COMBUSTION PARAMETERS menu item. A material can be selected from the FUEL TYPE drop-down list, and appropriate values will populate the relevant fields. Alternatively, a USER DEFINED material can be selected in the FUEL TYPE drop-down list and desired values entered into the relevant fields as shown in Figure 46.

The molecular weight of the fuel is then calculated using the respective atomic weights as required.

Production of hydrogen cyanide (HCN) can be included in the general combustion equation by checking the CALCULATE HCN BASED ON COMBUSTION option shown in Figure 46. The soot constants shown in Figure 46 are discussed in section 6.6. The flame emission coefficient is only used with the glass fracture model discussed in section 10.

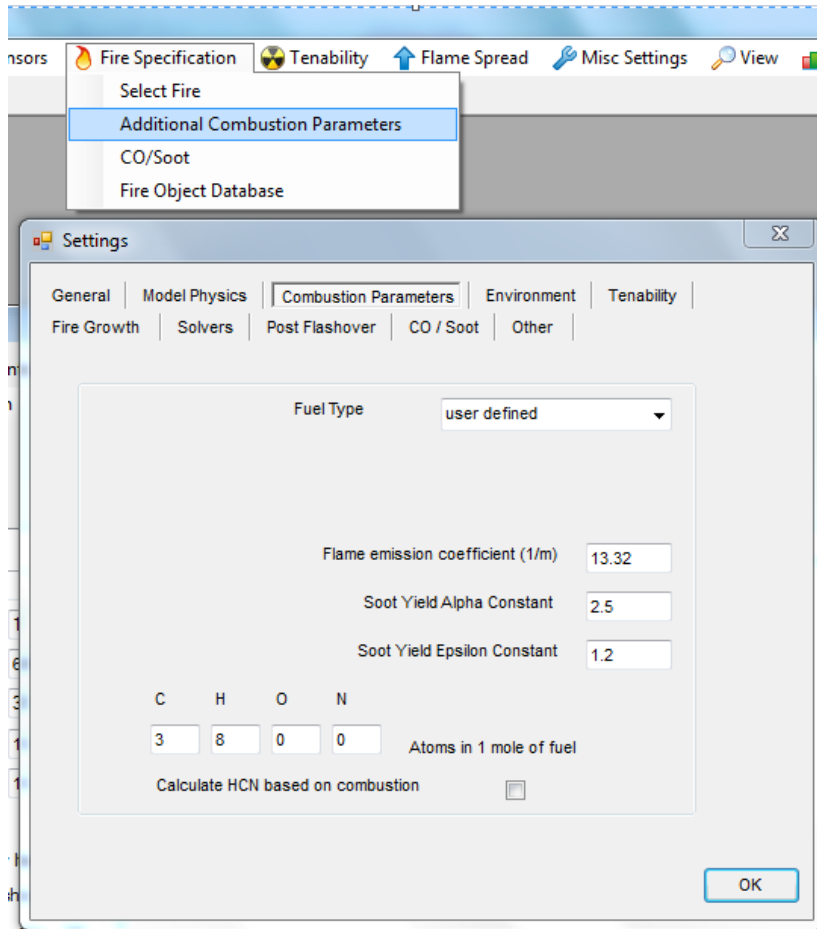
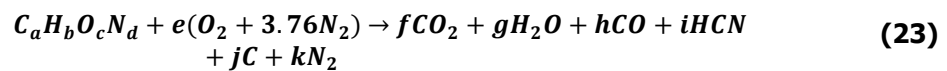


Figure 46. Additional combustion parameters.

Following the methodology outlined by Ierardi (n.d.), the general combustion equation is given by:



a, b, c and d are known values, while f, h and j are derived from the specified species yields for carbon dioxide, carbon monoxide and soot respectively, such that:

$$\eta_{\text{product}} = \frac{Y_{\text{product}} MW_{\text{fuel}}}{\eta_{\text{fuel}} MW_{\text{product}}} \quad (24)$$

For a balanced equation, the following algebraic expressions apply:

$$a = f + h + i + j \quad (25)$$

$$b = 2g + i \quad (26)$$

$$c + 2e = 2f + g + h \quad (27)$$

$$d + 7.52e = i + 2k \quad (28)$$

Solving the equations simultaneously for the unknown variables gives:

$$i = a - f - h - j \quad (29)$$

$$g = (b - i)/2 \quad (30)$$

$$e = (2f + g + h - c)/2 \quad (31)$$

$$k = (d + 7.52e - i)/2 \quad (32)$$

Therefore, the yields of HCN and H₂O products are:

$$Y_{\text{HCN}} = \frac{i \text{MW}_{\text{HCN}}}{\text{MW}_{\text{fuel}}} \quad (33)$$

$$Y_{\text{H}_2\text{O}} = \frac{g \text{MW}_{\text{H}_2\text{O}}}{\text{MW}_{\text{fuel}}} \quad (34)$$

For fires that are under-ventilated, the yields of CO₂ and H₂O are reduced depending on the calculated plume global equivalence ratio. The global equivalence ratio (Pitts, 1994) is calculated as follows:

$$\phi_e = \frac{\Delta H_c \dot{m}_f}{\Delta H_{O_2} Y_{O_2,i} \dot{m}_p} \quad (35)$$

Where ΔH_{O_2} is taken to be a constant (13.1 MJ/kg).

When the global (plume) equivalence ratio (ϕ_e) for the fire compartment is greater than 1 (under-ventilated fire), the yields are given by:

$$Y_{\text{CO}_2,vc} = \frac{Y_{\text{CO}_2,wv}}{\phi} \quad (36)$$

$$Y_{\text{H}_2\text{O},vc} = \frac{Y_{\text{H}_2\text{O},wv}}{\phi} \quad (37)$$

The subscripts wv and vc are for “well ventilated” and “ventilation controlled” respectively. In addition, adjustments are made to the specified fuel heat of combustion and the radiant loss fraction depending on the degree of under ventilation. Using the correlations provided by Tewarson et al. (Tewarson, Jiang & Morikawa, 1993; Tewarson, 2002), the heat of combustion and radiant loss fraction are reduced as the global equivalence ratio increases according to:

$$\frac{\Delta H_{ch,vc}}{\Delta H_{ch,wv}} = 1 - \frac{0.97}{\exp((\phi/2.15)^{-1.2})} \quad (38)$$

$$\frac{\Delta H_{con,vc}}{\Delta H_{con,wv}} = 1 - \frac{1.0}{\exp((\phi/1.38)^{-2.8})} \quad (39)$$

Since the radiant loss fraction is the converse of the convective fraction, rearranging the above equations gives the following expression for radiant loss fraction under ventilation-controlled conditions.

$$\lambda_{r,vc} = 1 - \left[\frac{(1 - \lambda_{r,wv}) \left(1 - \frac{1.0}{\exp((\phi/1.38)^{-2.8})} \right)}{\left(1 - \frac{0.97}{\exp((\phi/2.15)^{-1.2})} \right)} \right] \quad (40)$$

6.6 Soot and smoke production

There are two options available for specifying soot yields using the FIRE SPECIFICATION, CO/SOOT yield file menu item as shown in Figure 47.

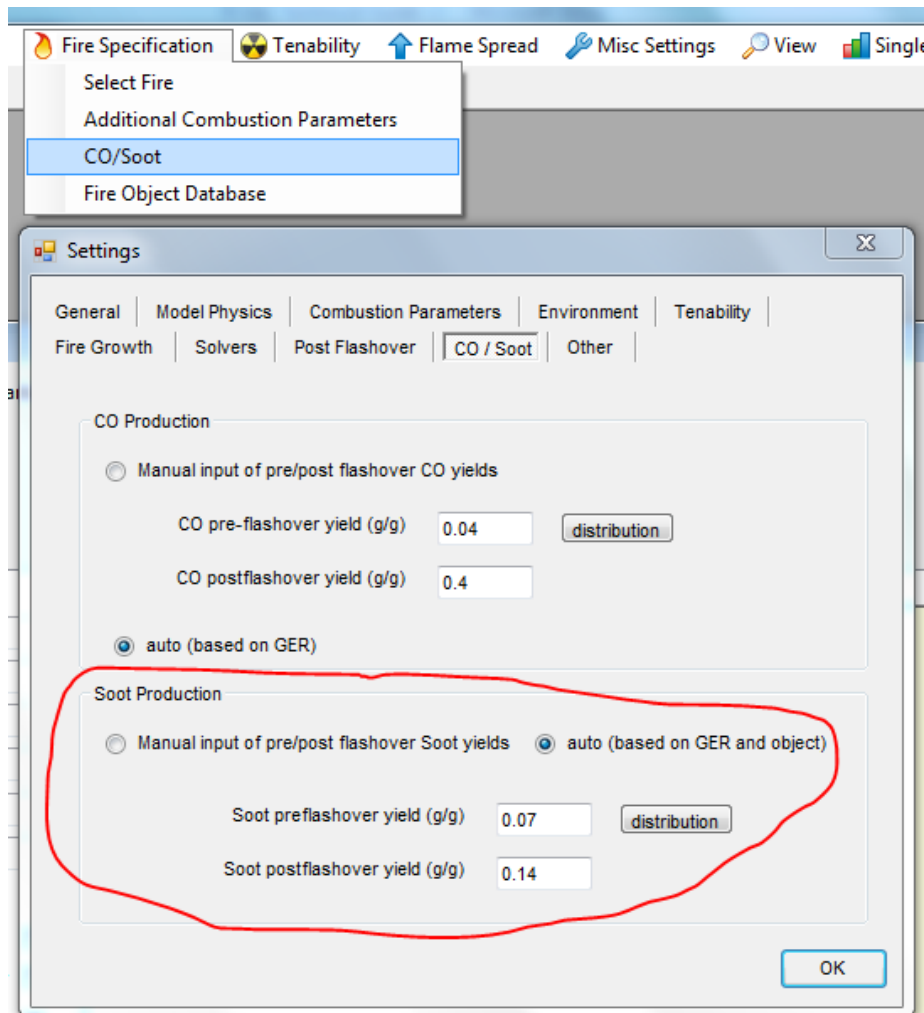


Figure 47. Soot yields.

Option 1: Auto (based on GER and object)

The well ventilated (pre-flashover) soot yield (in g/g) is specified for each burning item, and the following correlation developed by Tewarson et al. (Tewarson, Jiang & Morikawa, 1993; Tewarson, 2002) is used for the dependence of the soot yield on the global equivalence ratio where $\phi_{s,vc}$ is the soot yield under ventilation-controlled

conditions, $\varphi_{s,wv}$ is the soot yield under well ventilated conditions, ϕ is the global equivalence ratio and α and ζ are constants dependent on the fuel.

$$\frac{\varphi_{s,vc}}{\varphi_{s,wv}} = 1 + \frac{\alpha}{\exp(2.5\phi^{-\zeta})} \quad (41)$$

The soot yield alpha constant α and soot yield epsilon constant ζ are entered using the FIRE SPECIFICATION, ADDITIONAL COMBUSTION PARAMETERS menu item shown in Figure 46.

Option 2: Manual input of pre/post-flashover soot yields

This option allows the user to manually specify a constant soot yield (g/g) for each of the pre-flashover and post-flashover stages of the fire. The switch between pre-flashover and post-flashover is based on either an upper layer temperature of 500°C or an incident radiant flux on the floor, as selected by the user (see section 6.14.1).

When running in VM2 mode, this option is used with a pre-flashover yield of 0.07 g/g, a post-flashover yield of 0.14 g/g and a flashover criterion of 500°C for the upper layer temperature. In VM2 mode, post-flashover yields will also be used upon reaching the ventilation limit.

6.7 Carbon monoxide production

There are two options available for specifying carbon monoxide yields using the FIRE SPECIFICATION, CO/SOOT yield file menu item as shown in Figure 47.

Option 1: Auto (based on GER and object)

This option does not require the user to specify the carbon monoxide yield. The carbon monoxide yield (kg CO per kg fuel mass loss) is determined using the linear piecewise algorithm shown in Figure 48 as a conservative fit to experimental data. Also shown is a comparison with the experimental data from Gottuk et al. (Gottuk, 1992; Gottuk et al., 1992) The relationship used depends on the global equivalence ratio, ϕ_e as given in equation (35).

Option 2: Manual input of pre/post-flashover CO yields

This option allows the user to manually specify a constant carbon monoxide yield (g/g) for each of the pre-flashover and post-flashover stages of the fire. The switch between pre-flashover and post-flashover is based on either an upper layer temperature of 500°C or an incident radiant flux on the floor, as selected by the user (see section 6.14.1).

When running in VM2 mode, this option is used with a pre-flashover yield of 0.04 g/g, a post-flashover yield of 0.40 g/g and a flashover criterion of 500°C for the upper layer temperature.

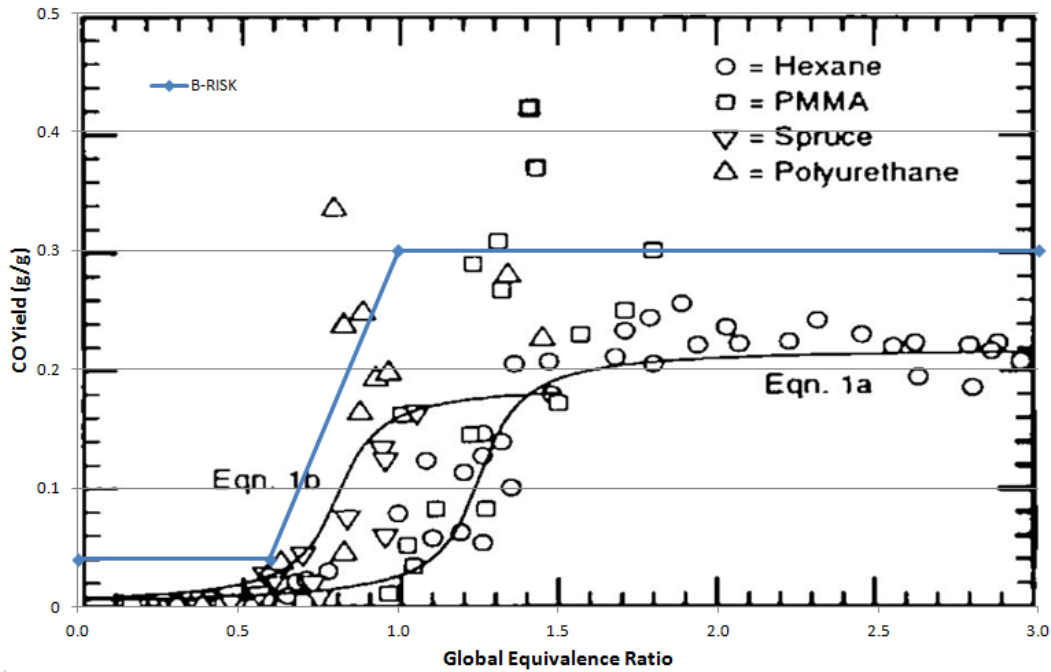


Figure 48. Carbon monoxide yields versus equivalence ratio [Adapted from (Gottuk et al., 1992)].

6.8 Burning rate enhancement

The program allows the option of enhancing the burning rate of the fire based on the level of incident radiant flux received at the floor due to heat transfer from the gas layers and the room surfaces. This option can be turned on using the MISC SETTINGS, COMPARTMENT EFFECTS file menu item as shown in Figure 49.

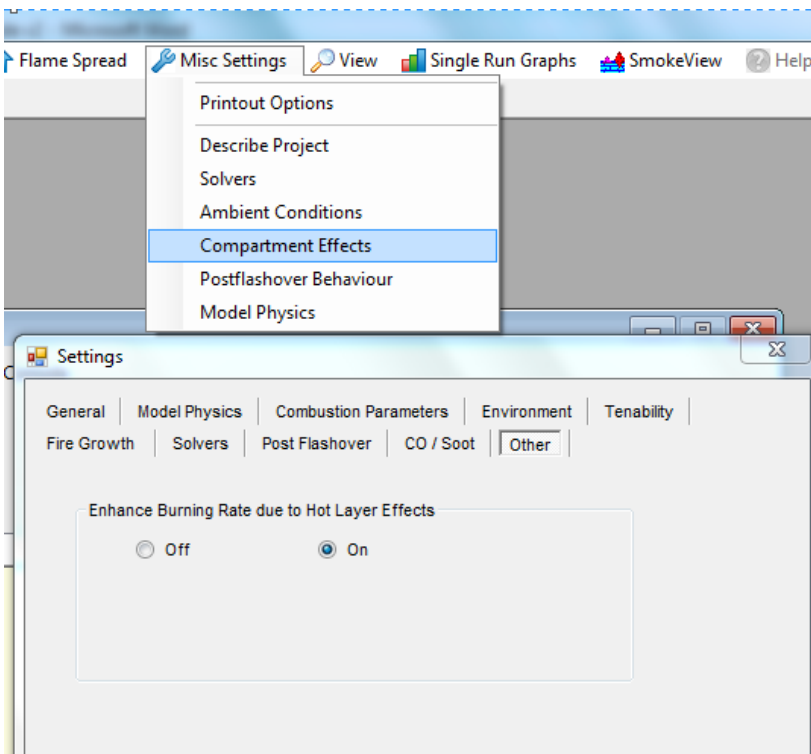


Figure 49. Burning rate enhancement.

The additional heat release from the fuel ΔQ , due to the externally applied radiant heat from the gas layers and the room surfaces \dot{q}_e'' , is then estimated from equation (42), where L_g is heat of gasification of the fuel (averaged over all fuel items) and ΔQ is added to the (free-burning) heat release rate for use in the energy balance calculations.

This calculation is done for each burning item and the total summed to determine the total unconstrained rate of heat release for the fire.

$$\Delta Q = \frac{\Delta H_c A \dot{q}_e''}{L_g} \quad (42)$$

An estimate of the surface area (A in m^2) is calculated in one of two ways.

Firstly, if the heat release rate per unit area (HRRPUA in kW/m^2) parameter for the item/object is non-zero, the following equation applies where \dot{Q}_f is the heat release rate of the free-burning fuel item (kW):

$$A = \frac{\dot{Q}_f}{\text{HRRPUA}} \quad (43)$$

Secondly, if the HRRPUA parameter for the item/object is zero, the following equation applies where ΔH_c is the heat of combustion of the fuel item:

$$A = \frac{\dot{Q}_f}{\Delta H_c \dot{m}''} \quad (44)$$

A characteristic burning rate per unit area is represented by \dot{m}'' , and this can optionally be defined for an individual item as a linear function of the incident heat flux in the form:

$$\dot{m}'' = A \dot{q}_e'' + B \quad (45)$$

Where A (in g/kJ) and B (in $g/s/m^2$) are constants defined as item properties.

The enhanced burning rate option will not be used when the flame spread sub-model is also selected and should only be used when rate of heat release data for individual objects has been obtained from essentially free-burning well ventilated experiments.

This option is not recommended for use in combination with a power law design fire as used for C/VM2 compliance (see section 4.5).

6.9 Plume entrainment

The strong plume model of Heskestad as described by ISO 16734 (ISO, 2006b) for the buoyant plume is used for entrainment in the far field.

At lower entrainment heights where this plume model is not valid (i.e. near field entrainment), the McCaffrey (1983) correlations are used instead.

6.9.1 Heskestad strong plume

The total mass of air entrained into the buoyant plume between the base of the fire and the smoke layer interface depends on the heat release rate and the height as given by Beyler (1988) in equation (46) derived from classical plume flow theory for a turbulent buoyant point source plume and Heskestad's point source correction (Heskestad, 1983).

Heskestad's correlation (ISO, 2006b) shown in equation (47) is used:

$$m_p \propto \dot{Q}_c^{1/3} (z - z_o)^{5/3} \quad (46)$$

$$m_p = 0.071 \dot{Q}_c^{1/3} (z - z_o)^{5/3} [1 + 0.026 \dot{Q}_c^{2/3} (z - z_o)^{-5/3}] \quad (47)$$

The position of the virtual source (Z_o) from Heskestad (1983) is:

$$z_o = -1.02D + 0.083 \dot{Q}_f^{2/5} \quad (48)$$

For non-circular fire sources, the diameter (D) is calculated on the basis of equivalent area. This assumes that the aspect ratio of the source is close to unity. Since generally only the heat release rate, mass loss rate and effective heat of combustion of the fuel are known, the size (area, diameter) of the fire is estimated based on a specified mass loss rate per unit area for the fuel. The diameter of the fire is determined at each time step either from:

- The fuel mass loss rate (derived from the heat release rate and energy yield inputs) and a characteristic value of the mass loss rate per unit area, which may be input or changed by the user.

$$D = \sqrt{\frac{4A}{\pi}} = \sqrt{\frac{4\dot{m}_f}{\pi\dot{m}_f''}} = \sqrt{\frac{4\dot{Q}_f/\Delta h_c}{\pi\dot{m}_f''}} \quad (49)$$

- The heat release rate and the heat release per unit area provided by the user. This option is always used if a non-zero value for the heat release rate per unit area has been entered.

$$D = \sqrt{\frac{4\dot{Q}_f}{\pi\dot{Q}_f''}} \quad (50)$$

Heskestad's strong plume equation is used when the layer height is above the flame tip, (L), given by Heskestad's correlation (Heskestad, 1984) as follows:

$$L = -1.02D + 0.235 \dot{Q}_f^{2/5} \quad (51)$$

Heskestad's strong plume equation is for fire sources that do not have substantial in-depth combustion (for example, a pool fire rather than a fire in high-racked storage) and when the flame height is no greater than one-half the fire-to-ceiling distance. Outside these limits, the McCaffrey correlations in section 6.9.2 are used.

In the case of the room-corner fire, the plume entrainment is simplified. The total heat release from the burner/source and that part of the wall lining located below the layer interface height are summed together into a single term, and the plume entrainment is calculated on the basis of a single axi-symmetric plume (modified as described in section 4.6.3) originating from the location of the burner.

6.9.2 McCaffrey's correlations

The mass flux entrained into the plume for the continuous flaming, intermittent and buoyant plume regions respectively is given by (McCaffrey, 1983):

$$m_p/\dot{Q}_f = 0.011 \left(\frac{z}{\dot{Q}_f^{2/5}} \right)^{0.566} \quad \text{for } 0 \leq \left(\frac{z}{\dot{Q}_f^{2/5}} \right) < 0.08 \quad (52)$$

$$m_p/\dot{Q}_f = 0.026 \left(\frac{z}{\dot{Q}_f^{2/5}} \right)^{0.909} \quad \text{for } 0.08 \leq \left(\frac{z}{\dot{Q}_f^{2/5}} \right) < 0.20 \quad (53)$$

$$m_p/\dot{Q}_f = 0.124 \left(\frac{z}{\dot{Q}_f^{2/5}} \right)^{1.895} \quad \text{for } 0.20 \leq \left(\frac{z}{\dot{Q}_f^{2/5}} \right) \quad (54)$$

McCaffrey's correlations are empirical, fitted to experimental data and not based on theory. They are, however, an extension of the common point source plume model with a different set of coefficients for each region (Peacock et al., 1993).

The advantage of McCaffrey's correlations is that they are only dependent on the fire size and entrainment height and are not dependent on the fire source diameter.

However, they are also known to over-predict entrainment in high spaces. According to Rockett (1995), they result in a severe over-prediction of plume flows far above the fire (i.e. in tall spaces) but provide good predictions in the immediate over-fire region more relevant for small rooms. Therefore, the Heskestad correlation is used for the buoyant plume under the conditions described in section 6.9.1.

A comparison of the entrainment calculated using the McCaffrey and Heskestad correlations for the buoyant plume region is shown in Figure 50 for a specific fire size and diameter.

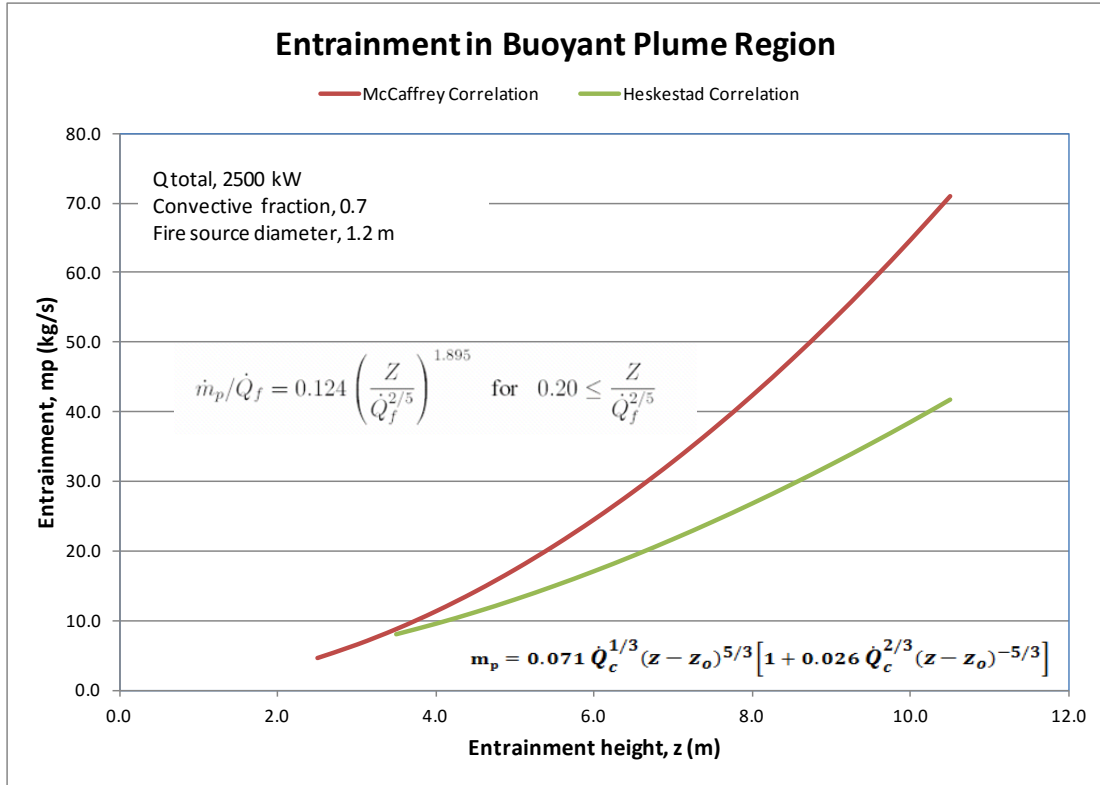


Figure 50. Comparison of plume entrainment using the McCaffrey and Heskestad correlations.

Following the advice of Peacock et al. (1993) there is a constraint on the quantity of gas that can be entrained by a plume arising from a fire. The constraint arises from the physical fact that a plume can rise only so high for a given size of a heat source. This constraint is intended to avoid over-prediction of entrainment early in the fire when the energy flux is small and the entrainment height large.

$$m_p < \frac{\dot{Q}_c}{c_p(T_u - T_l)} \quad (55)$$

6.9.3 Effect of fire location on plume entrainment

The model allows for burning objects to be located in the centre of the room, against a wall or in the corner of the room. For these latter cases, the plume entrainment correlations based on the simple Zukoski equation are used (Karlsson & Quintiere, 1999).

For a corner fire:

$$m_p = 0.028 \dot{Q}_f^{1/3} z^{5/3} \quad (56)$$

For a wall fire:

$$m_p = 0.045 \dot{Q}_f^{1/3} z^{5/3} \quad (57)$$

In the case of the room-corner fire involving burning wall linings, the plume entrainment is simplified by adding together the total heat release from the

burner/source and that part of the wall lining located below the layer interface height. The plume entrainment is calculated on the basis of a single fire source originating at the location of the burner.

6.9.4 Effect of fire plume disturbances on plume entrainment

Fire plume entrainment rates are based on undisturbed axisymmetric plumes. However, it has been shown that fire plumes located near a room opening are affected by the air flow induced through the opening. It is stated that these “wind” effects can increase the rate of entrainment over free plumes by as much as two or three times (Quintiere, Rinkinen & Jones, 1981). In practice, the size of the effect will be influenced by variables such as the distance of the fire plume from the opening, the elevation of the fire and the extent to which it may be baffled by other objects (Quintiere, Rinkinen & Jones, 1981).

An option to consider the impact of a disturbed plume, where the entrained mass flow is twice that for an undisturbed fire plume, is provided when specifying the characteristics of a fire source item. This option can be selected separately for each fire item if desired.

The disturbed plume option is recommended for design of smoke management systems using the Harrison spill plume equations (Harrison, 2009; Harrison, Wade & Spearpoint, 2014) described in section 6.11.

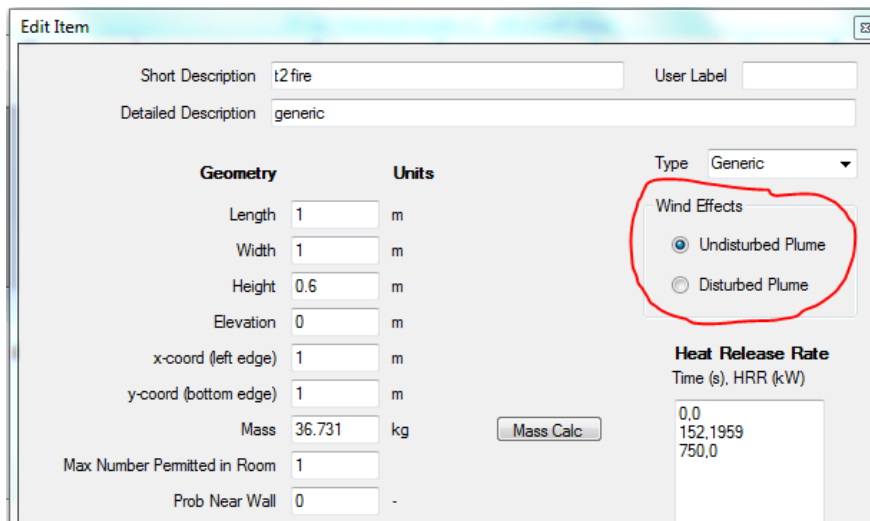


Figure 51. Plume disturbance option.

6.10 Wall vent flows

6.10.1 Natural vent flow

The mass flow of air and hot gases through a wall vent is driven by buoyancy. Bernoulli’s equation can be used to calculate the flows. Derivation and discussion of buoyancy-driven vent flow equations can be found in many places in the literature (Rockett, 1976; Babrauskas & Williamson, 1978; Birk, 1991; Janssens, 1992a; Emmons & Tanaka, 2008).

B-RISK uses natural vent flow routines developed by Cooper and Forney (1990a, b) from a computer code application known as CCFM.VENTS. A complete description of the physical basis can be found in the literature (Cooper & Forney, 1990a, b; Forney &

Cooper, 1990; Forney, Cooper & Moss, 1990), and only a brief description will be included here.

The vent flow calculations are the result of room-to-room cross-vent hydrostatic pressure differences. Only rectangular vents in walls are currently considered.

At each point in time, the vent flow calculation is carried out in three stages. Firstly, the hydrostatic pressure profile over the height of a common wall including a vent is determined. The pressure difference across the vent will drive the room-to-room vent flow. The second stage determines the characteristics of each individual vent, which may involve from one to six horizontal slabs of uniform property, uni-directional flow. The third stage keeps track of the source and destination of each of these slab flows.

CCFM.VENTS includes rules for distributing the vent flow into an adjacent room (upper or lower layer) depending on the relative temperatures of the layers and flow. However, this was modified to use the simpler CFAST rule where flow slabs originating from the upper layer are deposited into the upper layer in the adjacent room and flow slabs originating from the lower layer are deposited in the lower layer in the adjacent room. The temperature of the vent flow is required to be at least 3 K above the temperature in the adjacent room before an upper layer will start to form.

6.10.2 Near-vent mixing

When cool air flows into the room through a wall vent, it is assumed to entrain some of the upper layer gases from the upper layer into the lower layer. The near-vent mixing correlation developed by Utiskul (2007) has been applied where the incoming cold air behaves like a jet entering the vent with a characteristic velocity and diffusing downward because of buoyancy (Quintiere & McCaffrey, 1980). While the cooler air descends, the surrounding hot gas is entrained with a velocity that is proportional to the incoming flow characteristic velocity. An equation for the ratio of mass entrained to the total incoming mass flow was developed, and single-vent compartment fire experiments were conducted to establish the correlation for the mixing at the quasi-steady state. The correlation exhibited a linear relationship up to an apparent asymptote for the mixing ratio of 1.28.

Utiskul's correlation for the mass flow entrained (\dot{m}_d) in the incoming vent flow (\dot{m}_i) is:

$$\begin{cases} \dot{m}_d = 1.14 \varphi \dot{m}_i & \text{for } \varphi < 1.1 \\ \dot{m}_d = 1.28 \dot{m}_i & \text{for } \varphi \geq 1.1 \end{cases} \quad (58)$$

where,

$$\varphi = \left(\frac{T_o}{T}\right) \left(1 + \frac{N - S}{W_o}\right) \left(\frac{N - z}{N - S}\right)$$

and T_o is the gas temperature of the inflowing gases, T is the gas temperature of the upper layer gases, N is the elevation of the neutral plane above the floor, S is the elevation of the sill above the floor, W_o is the width of the opening and z is the layer height above the floor.

This vent mixing mass flow, taken from upper layer and added to the lower layer, applies both to vents to the exterior and vents to adjacent rooms.

6.10.3 Vent flow entrainment into adjacent spaces

In the case of vents connecting two rooms, there is a mixing phenomenon that occurs where the mass flow out through the vent causes additional air from the lower layer of the adjacent room to be entrained and deposited in the upper layer of the adjacent room. This entrainment flow is assumed to only occur when the layer height in the source room is lower than the layer height in the destination room.

The flow is determined using equations given by Peacock et al. (1993) for the CFAST model, and this entrainment is modelled as a "standard" vent type. Alternative vent types can be assigned to model various forms of spill plumes as described in section 6.11.

A virtual point source is used to model the flow in the vent with the enthalpy in the vent flow given by:

$$\dot{Q}_{eq} = \dot{c}_p(T_{u,1} - T_{u,2})\dot{m}_{1-2} \quad (59)$$

The mass flow in the vent from the upper layer of the source room to the upper layer of the destination room is \dot{m}_{1-2} , and $T_{u,1}$ and $T_{u,2}$ are the upper layer temperatures in the source and destination rooms respectively.

The height of the plume z_p is given by:

$$z_p = \frac{z_{1-2}}{2/5} + v_p \quad (60)$$

The difference in elevation between the layer interface position in each room is z_{1-2} . The virtual source point v_p is defined by inverting McCaffrey's plume equations.

$$v_p = \left(\frac{90.9\dot{m}}{\dot{Q}_{eq}} \right)^{1.76} \quad \text{if } 0 < v_p < 0.08 \quad (61)$$

$$v_p = \left(\frac{38.5\dot{m}}{\dot{Q}_{eq}} \right)^{1.001} \quad \text{if } 0.08 < v_p \leq 0.2 \quad (62)$$

$$v_p = \left(\frac{8.10\dot{m}}{\dot{Q}_{eq}} \right)^{0.528} \quad \text{if } 0.2 < v_p \quad (63)$$

To determine the entrained flow z_p , which is then used in McCaffrey's plume equations (section 6.9.2) in place of $z/Q_f^{2/5}$.

6.11 Spill plumes

6.11.1 General

Spill plumes occur when the flow of gases leaving a fire compartment opening rotate around and vertically rise from the spill edge into the adjacent space. The ascending spill plume entrains air as it rises.

The total flow in the spill plume depends on the size of the opening, the convective enthalpy of the gases flowing through the opening, the presence of a balcony, downstand or other construction element that either affect the flow through the opening or the subsequent entrainment into the rising spill plume and the vertical height between the spill edge and the smoke layer interface in the adjacent space. The correlations given in this section are from the research of Harrison (2009) and Harrison and Spearpoint (2007, 2010).

The user assigns a spill plume type to a vent as explained in section 3.6.2. The available spill plume types are two-dimensional adhered, three-dimensional adhered, two-dimensional balcony, three-dimensional balcony (unchannelled) and three-dimensional balcony (channelled).

If a spill plume type is not assigned to a vent, the default standard entrainment for vent flow into an adjacent space is used (see section 6.10.3).

When modelling spill plumes in B-RISK, the fire compartment is connected to the adjacent room (e.g. atrium) with a vent representing the compartment opening. The projecting balcony or soffit (if one exists) that extends from the compartment opening to the spill edge is not part of the physical B-RISK model, nor are any channelling screens that might be required beneath the balcony projection. However, both these elements are assumed to be present in the B-RISK calculations depending on the spill plume type that is selected for the vent (or compartment opening).

6.11.2 Adhered spill plumes

Adhered spill plumes are applicable where there is a wall or solid construction directly above the spill edge, preventing entrainment from one side and leading to the plume adhering to the wall. Adhered plumes are also known as single-sided plumes, since entrainment occurring above the spill edge occurs only on one face (see Figure 52).

Adhered spill plumes can be described as two-dimensional or three-dimensional in nature. Two-dimensional adhered spill plumes apply when construction elements prevent entrainment into the side ends of the rising plume. This typically occurs where the compartment opening is the full width of the adjacent space. Three-dimensional adhered spill plumes apply when air can be entrained into the side ends of the rising plumes as well as along one side.

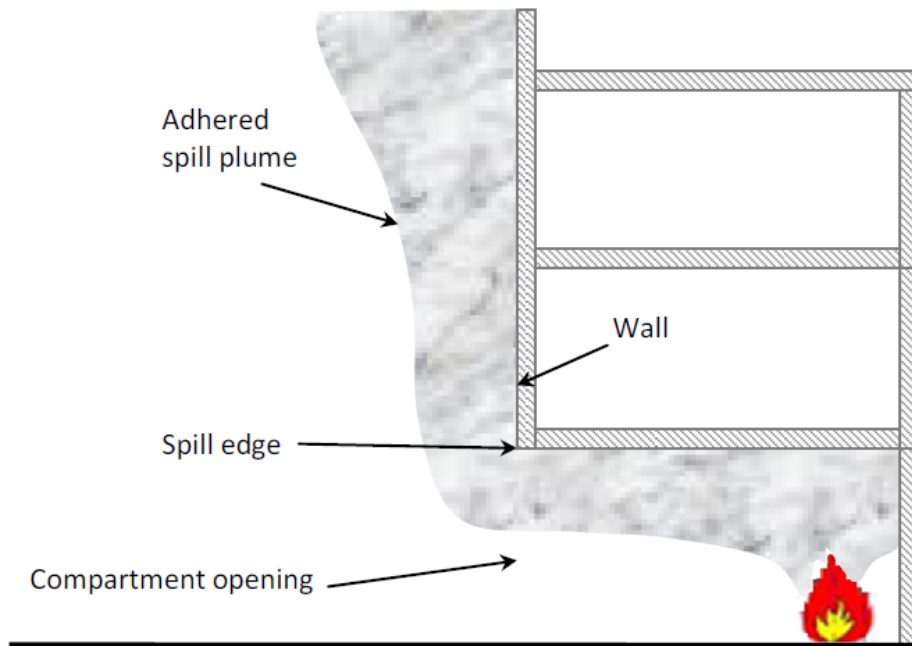


Figure 52. Adhered spill plume without soffit projection [Extracted from Harrison (2009)].

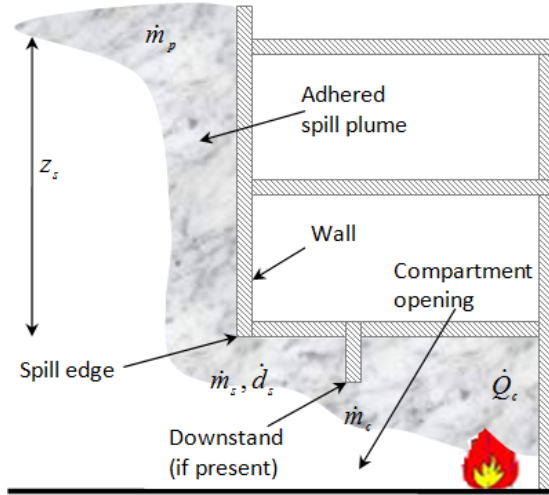
A downstand directly below the spill edge at the compartment opening has little effect on the entrainment above the spill edge, except that, if there is no downstand such that the top of the opening is continuous with the compartment ceiling, a flow coefficient (C_d) of 1.0 for the opening is recommended, otherwise a flow coefficient of 0.6–0.7 is appropriate. The flow coefficient influences the mass flow of gases leaving the compartment opening.

If a horizontal soffit projection exists between the compartment opening and the spill edge as shown in Figure 53, the mass flow at the spill edge (\dot{m}_s) is given by:

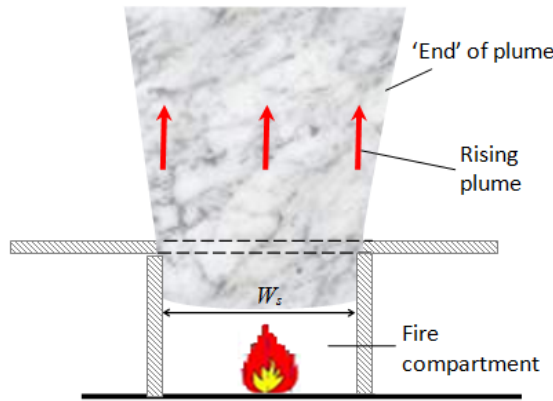
$$\dot{m}_s = 0.89 \left(\frac{h_o}{W_s} \right)^{-0.92} H \frac{\dot{m}_c}{W_s} \quad (64)$$

The soffit projection must be at the same elevation as the compartment ceiling, and the flow between the compartment opening and the spill edge must be channelled with side walls or screens.

In the absence of the projection, $\dot{m}_s = \dot{m}_c$ where \dot{m}_c is the mass flow out the compartment opening.



Section



Front view

Figure 53. Adhered spill plume with soffit projection.

The total flow in a two-dimensional adhered spill plume is given by:

$$\dot{m}_{p,2D} = 0.08\dot{Q}_c^{1/3}W_s^{2/3}z_s + 1.34\dot{m}_s \quad (65)$$

The total flow in a three-dimensional adhered spill plume is determined as:

$$\dot{m}_{p,3D} = 0.3\dot{Q}_c^{1/3}W_s^{1/6}d_s^{1/2}z_s + 1.34\dot{m}_s \text{ where } W_s/d_s \leq 13 \quad (66)$$

Where $W_s/d_s > 13$, the entrainment calculation is treated as a two-dimensional adhered plume as given by equation (65). For large entrainment heights where $z_s > z_{trans}$, the plume flow becomes axi-symmetric in nature and the total mass flow in the three-dimensional adhered spill plume is given by:

$$\dot{m}_{p,3D} = 0.071\dot{Q}_c^{1/3}z_s^{5/3} \quad (67)$$

The transition height z_{trans} is calculated as:

$$z_{trans} = 3.4 \left(W_s^{2/3} + 1.56 d_s^{2/3} \right)^{3/2} \quad (68)$$

6.11.3 Balcony spill plumes

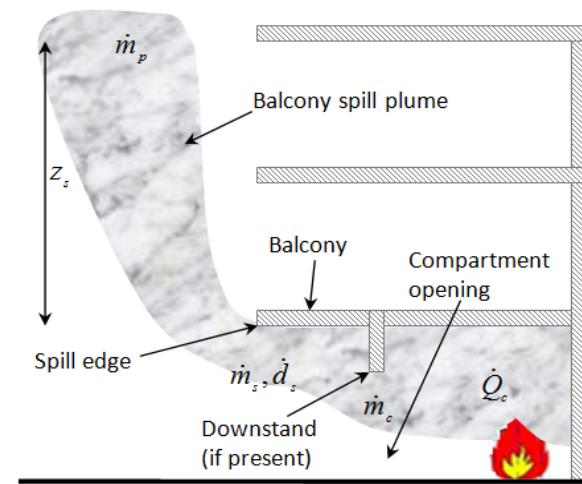
Balcony spill plumes are applicable where a balcony projects beyond the compartment opening and there is no wall or solid construction directly above the spill edge, therefore allowing entrainment to occur from both sides of the rising plume. Balcony plumes are also known as double-sided plumes, since entrainment occurring above the spill edge does so on both faces (see Figure 54).

Balcony spill plumes can also be described as two-dimensional or three-dimensional in nature. Two-dimensional balcony spill plumes apply when construction elements prevent entrainment into the side ends of the rising plume. Three-dimensional balcony spill plumes apply when air can be entrained into the side ends of the rising plumes as well as along both sides above the spill edge.

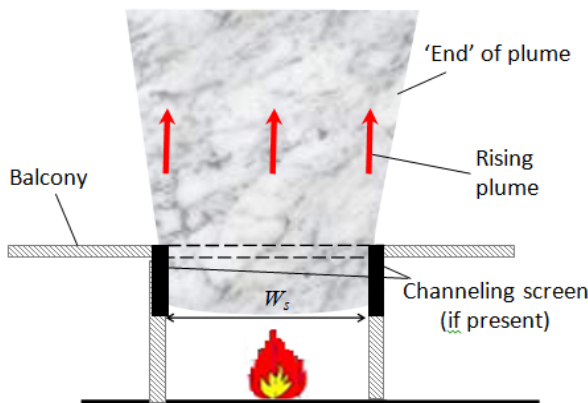
Channelling screens (or side walls) below the level of the spill edge and extending from the compartment opening can be used to reduce the lateral spread of the spill plume, thereby reducing the amount of entrainment above the spill edge.

The total flow in a two-dimensional balcony spill plume is given by:

$$\dot{m}_{p,2D} = 0.16Q_c^{1/3}W_s^{2/3}z_s + 1.34\dot{m}_s \quad (69)$$



Section



Front view

Figure 54. Balcony spill plume with balcony projection.

The total flow in a three-dimensional channelled balcony spill plume is given by:

$$\dot{m}_{p,3D} = 0.16\dot{Q}_c^{1/3}(W_s^{2/3} + 1.56d_s^{2/3})z_s + 1.34\dot{m}_s \quad (70)$$

Where W_s is the width of the compartment opening, z_s is the height of rise from the spill edge to the underside of the smoke layer over which entrainment can occur and d_s is the smoke layer depth in the fire compartment.

Except for large entrainment heights where $z_s > z_{trans}$, the plume flow becomes axisymmetric in nature and the total mass flow in the three-dimensional channelled balcony spill plume is given by equation (67).

If there is no balcony projection present between the compartment opening and the spill edge, the mass flow at the spill edge (\dot{m}_s) is taken as equal to the mass flow leaving the fire compartment opening, i.e. $\dot{m}_s = \dot{m}_c$.

Where a balcony projection is present, the mass flow at the spill edge (\dot{m}_s) is given by equation (64).

The total flow in a three-dimensional unchannelled balcony spill plume is given by:

$$\dot{m}_{p,3D} = 0.16\dot{Q}_c^{1/3}((W_s + b)^{2/3} + 1.56d_s^{2/3})z_s + 1.34\dot{m}_c \quad (71)$$

This equation is limited to cases where $W_s \geq 2b$, where b = length of the horizontal projection. It has not been verified for cases where a downstand exists prior to the spill edge so should not be applied in that situation.

6.12 Natural vent flow through ceilings and floors

The vent flow algorithm VENTCF2A (Cooper, 1997) is used for modelling the gas flows through a ceiling or floor vent. The vent may connect to the outside or it may connect to another room. The flow is driven by cross-vent pressure differences and, when appropriate, combined pressure and buoyancy-driven flows that occur when the density configuration is unstable. This occurs when a dense cooler gas layer is above the vent and a less dense hot gas layer is directly below the vent. For unstable density configurations, VENTCF2A models flow through a circular, shallow (small ratio of depth-to-diameter) horizontal vent. It is expected that it can be used for non-circular vents provided the aspect ratio is not too different from unity (Cooper, 1997).

Vents can be opened and closed during the simulation at the time nominated by the user. This opening/closing is not instantaneous but is assumed to occur over a 2-second period by a linear increase in the area of the vent from fully closed to fully open (and vice versa). Vents can also be automatically opened by the activation of a thermal or smoke detector located within the room immediately below the vent.

These vent flow routines are applicable where the vent area is small compared to the ceiling area. They should not be used to model large openings in floors to accommodate atria etc. In such cases, it is better to model a void as a separate space connected to adjacent rooms with wall vents.

Caution is needed when including vents that connect rooms one above the other, as any additional entrainment into the smoke flow rising to the ceiling of the upper room

is not modelled. Therefore, this type of vent is best used for discharge direct to the outside.

6.13 Oxygen-limited burning

The model takes into account the available air supply and its effect on the heat release rate. The approach taken is to determine the mass flow of oxygen in the plume and compare it to the amount needed for complete combustion of the fuel. Any oxygen present in the upper layer or supplied by the fuel is not used for combustion.

6.13.1 Mass flow of oxygen needed for complete combustion

The mass flow of oxygen in the plume (kg-O₂/s) needed for complete combustion of the fuel is given by:

$$\dot{m}_{\text{oxygen needed}} = \frac{\dot{Q}_f}{13100} \quad (72)$$

This equation is based on the observation that approximately 13,100 kJ of energy is released for every kg of oxygen consumed during the combustion reaction (Huggett, 1980).

6.13.2 Mass flow of oxygen present in the plume

The actual mass flow of oxygen in the plume (kg-O₂/s) is given by:

$$\dot{m}_{\text{oxygen actual}} = \dot{m}_p Y_{O_2,L} C \quad (73)$$

Where C is a coefficient described by Peacock et al. (1993) representing the fraction of fuel that can be burned with the available oxygen and varies between 0 and 1 to provide a smooth cut-off of the burning over a narrow range above the oxygen limit. An oxygen limit of 10% by volume is assumed.

$$C = \frac{\tanh(800(Y_{O_2,L} - Y_{\text{Limit}}) - 4) + 1}{2} \quad (74)$$

$$Y_{\text{Limit}} = \frac{MW_{O_2}}{MW_{LL,avg}} \times 0.1 \quad (75)$$

6.13.3 Oxygen concentration in the upper layer

The oxygen concentration in the upper layer is given by:

$$\%Vol O_2 = Y_{O_2} \times \frac{MW_{UL,avg}}{MW_{O_2}} \times 100 \quad (76)$$

The average molecular weight of the upper layer is determined from the mass fractions of oxygen, carbon dioxide, carbon monoxide and water vapour, with the balance of the layer assumed to be nitrogen as follows:

$$MW_{avg} = Y_{O_2} MW_{O_2} + Y_{CO_2} MW_{CO_2} + Y_{CO} MW_{CO} + Y_{H_2O} MW_{H_2O} + Y_{N_2} MW_{N_2} \quad (77)$$

6.13.4 Minimum oxygen concentration needed for combustion

The minimum oxygen concentration needed for combustion to occur is assumed to vary between 2% and 10% depending on the gas temperature. The method for determining the limiting value is the same as that used in FPETOOL (Nelson, 1990) and is given by:

$$\%Vol O_2 \text{ critical} = \frac{T_{fo} - T_u}{T_{fo} - T_\infty} [O_{L1} - O_{L2}] + O_{L2} \tag{78}$$

Where T_{fo} is a designated flashover temperature (873 K), T_u is the upper layer temperature (K), T_∞ is the ambient temperature (in K), O_{L1} is the minimum oxygen concentration required for combustion near room temperature (10%) and O_{L2} is the minimum oxygen concentration required for combustion near flashover temperatures (2%).

6.14 Post-flashover burning

6.14.1 Flashover criteria

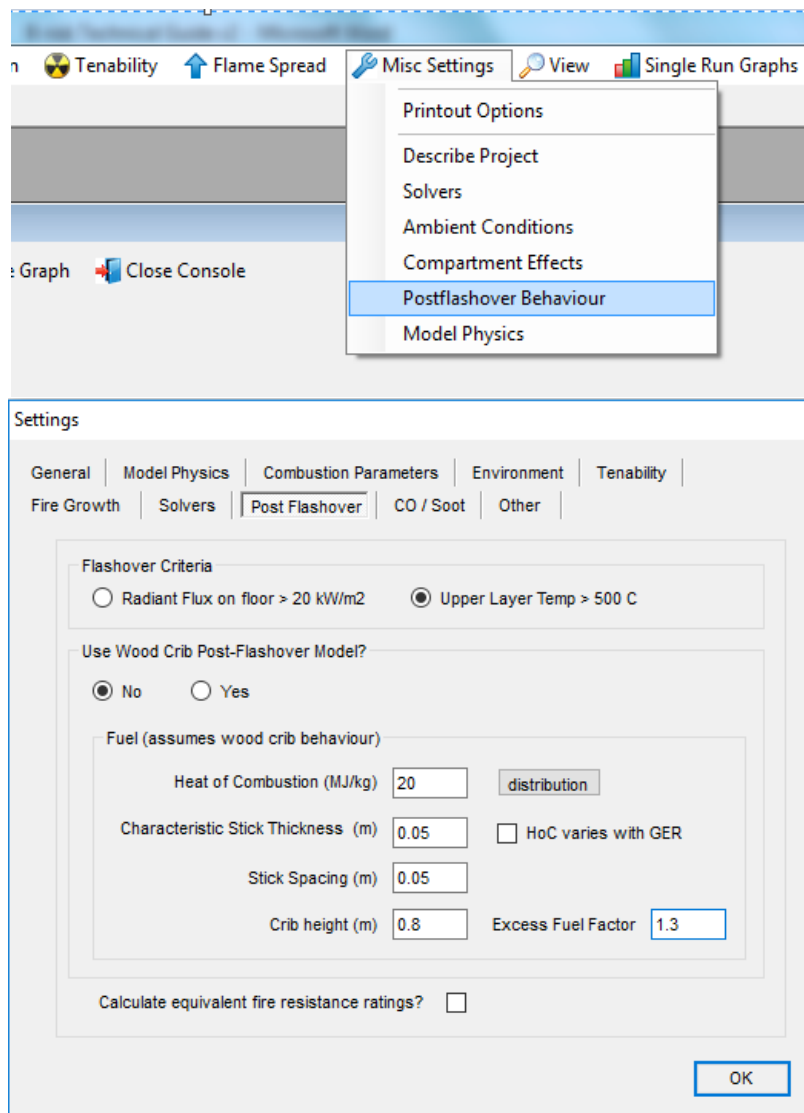


Figure 55. Post-flashover options.

Flashover can be defined by the user to occur either when the radiation heat flux on the floor exceeds 20 kW/m² or when the upper layer temperature reaches 500°C.

This option is set by clicking the MISC SETTINGS, POSTFLASHOVER BEHAVIOUR menu item and selecting the desired flashover criterion as shown in Figure 55.

6.14.2 Ventilation limit and post-flashover behaviour

The ventilation limit is defined here as the time that the HRR first diverges from the specified input HRR due to insufficient oxygen for complete combustion as used in VM2 (MBIE, 2014).

If VM2 user mode has been selected, when the ventilation limit is reached, the maximum theoretical HRR is adjusted to be the lesser of the user-specified HRR at that time or 1.5 times the HRR at the ventilation limit (MBIE, 2014). Since B-RISK determines mass loss rate from the theoretical HRR and heat of combustion, this has the effect of keeping the pyrolysis rate after flashover to a reasonable value.

If VM2 user mode has been selected, when the flashover threshold is reached, the HRR is increased to equal the specified peak value (provided it is greater than the HRR at flashover) over a 15-second interval also in accordance with VM2 (MBIE, 2014).

6.14.3 Post-flashover wood crib sub-model

An optional post-flashover model based on burning wood cribs can be selected as shown in Figure 55.

To use this sub-model, the fire object initially used must have sufficient intensity to generate the flashover threshold in the enclosure. Initially, the pre-flashover model used is based on the heat release and other characteristics of the selected fire item. However, following the attainment of "flashover", a switch to the post-flashover model occurs. The model keeps track of the total amount of fuel consumed during the simulation, and when all the fuel is consumed, the mass loss rate is set equal to zero.

The post-flashover model, based on Babrauskas's COMPF2 model (Babrauskas & Williamson, 1978), requires determination of a ventilation-controlled mass loss rate, a fuel surface area-controlled mass loss rate and crib porosity-controlled mass loss rate, with the lesser of the three rates governing the pyrolysis rate. The post-flashover model assumes behaviour representative of wood cribs (see Figure 56).

Additional input parameters that are required to be specified are:

- an average heat of combustion representative of the total combustible fuel load in the room
- a characteristic stick thickness (d).
- stick spacing (s).
- crib height (h_c).

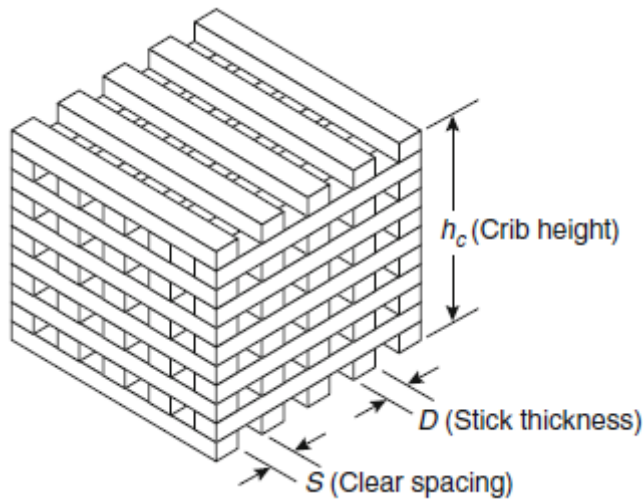


Figure 56. Wood crib parameters.

The mass loss rate for ventilation-controlled burning is given by equation (79) where Ω is a user-defined factor representing an excess fuel fraction where $\Omega = 1$ corresponds to all the fuel-generated burning within the room. It has been observed experimentally that wood cribs do not burn more than 30–40% fuel rich, with Babrauskas (2008) reporting an upper limit of approximately 37% fuel rich ($\Omega = 1.37$) for wood cribs. $\dot{Q}_{f,\text{constrained}}$ is the rate of heat release assuming stoichiometric conditions, and ΔH_c is the heat of combustion of the fuel.

$$\dot{m}_f = \Omega \frac{\dot{Q}_{f,\text{constrained}}}{\Delta H_c} \quad (79)$$

The fuel surface area-controlled mass loss rate is:

$$\dot{m}_f = \frac{4}{d} m_o v_p \sqrt{\frac{m}{m_o}} \quad (80)$$

Where v_p is a surface regression rate for wood and taken as $0.0000022 D^{-0.6}$, m is the mass of fuel remaining and m_o is the original mass of fuel (determined using the specified floor area and fuel load energy per unit floor area).

The crib porosity-controlled mass loss rate is:

$$\dot{m}_f = 0.44 \frac{S}{h_c} \frac{m_o}{D} \quad (81)$$

Where h_c is the crib height. The governing mass loss rate (lesser of the three) is multiplied by the average heat of combustion to give the rate of heat release used in the zone model conservation equations.

6.14.4 Post-flashover plume entrainment

When flashover is deemed to have occurred, a large simplification is necessary for the calculation of plume entrainment, as the pre-flashover models are no longer strictly valid. After flashover, the plume entrainment continues to be calculated using the

McCaffrey “flaming” correlation as follows, where \dot{Q}_{max} is the maximum heat release that can be supported by the available oxygen supply:

$$\frac{\dot{m}_p}{\dot{Q}_{max}} = 0.011 \left(\frac{Z}{\dot{Q}_{max}^{2/5}} \right)^{0.566} \quad (82)$$

During ventilation-limited burning, the total mass flow in the plume effectively corresponds to that required for the oxygen flow in the plume to equal the oxygen flow entering the vents.

6.14.5 Equivalent fire resistance rating

An optional calculation can be made to determine the time in a standard fire resistance test that results in the same cumulative radiant energy exposure (based on the upper layer temperature) at any specified time during the simulation. This approach has been studied by several researchers (Harada et al., 2000; Nyman et al., 2008) as a means of relating the performance of various construction types in a real fire to that in a standard fire resistance test. The equivalence should be treated as indicative only and based on thermal transmission effects. It may not be applicable for other failure mechanisms (e.g. buckling, collapse, formation of fissures/gaps) in fire-rated construction elements.

This equivalence is determined by calculating:

$$Q_{eq}(t) = \int_0^t \frac{\sigma T_u^4}{1000} dt \quad (83)$$

At a specified time, t_{ISO} in the standard fire resistance test, the gas temperature and cumulative radiant energy exposure are given by:

$$T_{ISO} = 345 \log_{10} \left(\frac{8t_{ISO}}{60} + 1 \right) + T_{\infty} \text{ (K)} \quad (84)$$

$$Q_{ISO}(t) = \int_0^t \frac{\sigma T_{ISO}^4}{1000} dt \quad (85)$$

After time t in the fire simulation, the equivalent time in the standard fire resistance test, t_{ISO} can be determined by equating equations (83) and (85), solving for T_{ISO} and then using equation (84) to solve for t_{ISO} .

6.15 Mechanical ventilation

B-RISK allows for mechanical ventilation using fans for supplying or exhausting gases from specified rooms.

Fans can be started manually at the start time entered or automatically on the activation of a smoke detector as described in section 3.6.6. The user specifies the volumetric flow rate in cubic metres per second through each fan and the height of each fan above the floor. The user also specifies if the direction of flow is from the room (extract) or to the room (pressurisation).

The implementation is by adding (pressurisation) or removing (extraction) a specified flow rate (m³/s converted to kg/s) from the layer in which the fan is located (as determined by the specified elevation height of the fan) and including this flow in the mass and energy balance equations described earlier. A fan straddling the layer interface is not considered – the fan is assumed to be either totally within the upper or lower layer.

Optionally, the use of a fan curve can be selected. If this is not done, the program will extract/supply air to the space at the flow rate specified, irrespective of the cross-fan pressure differences. If the fan curve option is selected, the actual flow rate equals the specified flow rate when the cross-fan pressure difference is zero and monotonically reduces to zero as the cross-fan pressure difference reaches the specified pressure limit as described in equations (91) and (92), where \dot{V}' is the actual flow rate through the fan, \dot{V} is the specified flow rate through the fan, ΔP_L is the specified maximum pressure across the fan and ΔP_{cf} is the actual cross-fan pressure difference.

$$\dot{V}' = \dot{V} \left[\frac{\Delta P_L - \Delta P_{cf}}{\Delta P_L} \right]^{1/6} \text{ for } \Delta P_L > \Delta P_{cf} \quad (86)$$

$$\dot{V}' = -\dot{V} \left[\frac{\Delta P_{cf} - \Delta P_L}{\Delta P_L} \right]^{1/6} \text{ for } \Delta P_L < \Delta P_{cf} \quad (87)$$

Following activation of the fan, the flow rate is assumed to linearly increase from zero to the design flow rate over a period of 30 seconds representing a fan start-up delay.

Figure 57 shows a generic fan curve for a user-specified extract rate of 100 m³/s and a cross-fan pressure limit of 50 Pa.

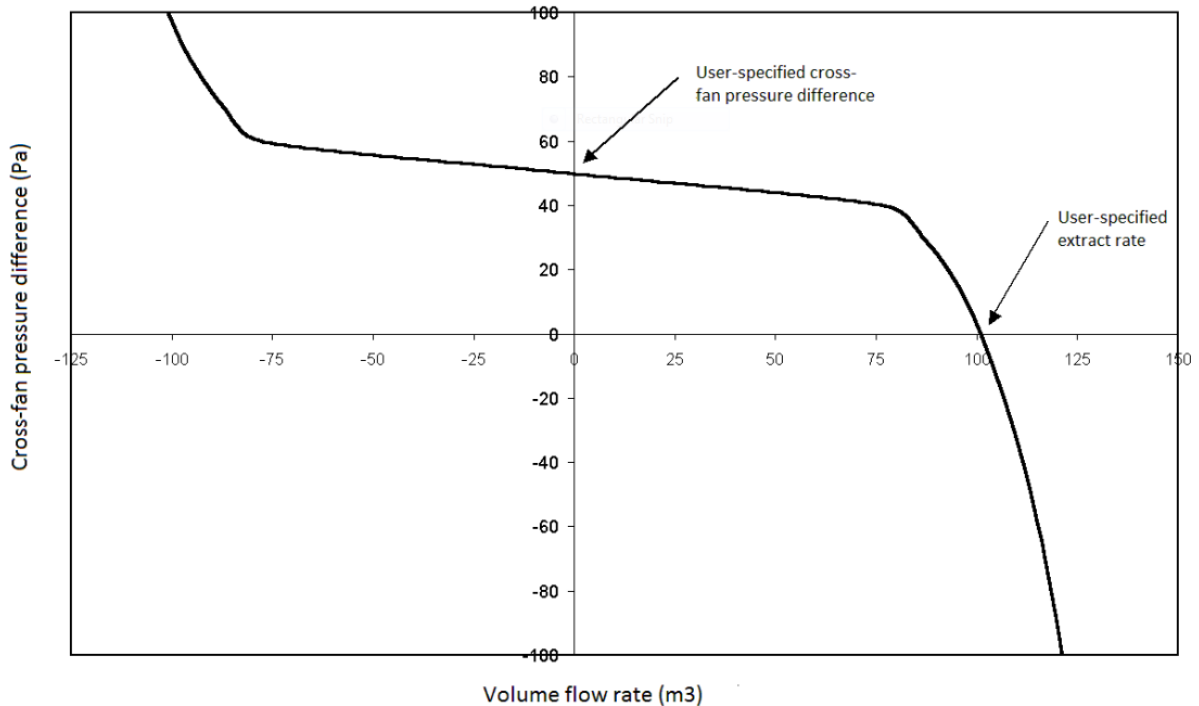


Figure 57. A generic fan curve

The phenomenon of “plug-holing” is incorporated into the calculations. This occurs when the layer is thin and both upper and lower layer gases are drawn through the fan instead of from only the gas layer immediately surrounding the fan.

The maximum mass flow rate through the fan before plug-holing occurs is calculated as (Cooper, 2002):

$$M_{crit} = 1.6\rho_u(H - z)^{5/2} \sqrt{1 - \frac{\rho_u}{\rho_l}} \quad (88)$$

In the event that the specified mass flow through the fan exceeds this critical value, M_{crit} is taken from the upper layer with the balance taken from the lower layer.

6.16 Vent fires

In the event of ventilation-limited burning conditions, there will be insufficient oxygen for complete combustion of the fuel, and therefore it is necessary to account for mass flows of unburned fuel. When the mass flow passes through a vent (to the outside or into another room), it may mix with oxygen and burn in the form of a vent fire, releasing combustion energy into the adjacent space or to the outside.

The criteria used for external burning, i.e. vent fires, is taken from Beyler (2002), where the equivalence ratio at which layer burning begins is:

$$\phi_{ign} = \frac{k}{k - \Delta H_{air} / \Delta H_c - 1} \quad (89)$$

Where:

$$k = \frac{\Delta H_{O_2} Y_{O_2}}{c_p T_{ad} - T_o} \quad (90)$$

And $\Delta H_{O_2} = 13.4$ MJ/kg, Y_{O_2} is the mass fraction of oxygen in the lower layer of the destination room, T_{ad} (=1700 K) is the adiabatic flame temperature of the stoichiometric mixture and T_o is the precombustion temperature resulting from stoichiometric mixing of the air and fuel streams, where the upper layer of the fire room contains the fuel stream and the lower layer of the destination room contains the air stream. T_o is given by equation (91) where r is the stoichiometric fuel to air ratio and Y_f is the mass fraction of unburned fuel in the upper layer.

$$T_o = \frac{T_u + (Y_f/r)T_l}{1 + Y_f/r} \quad (91)$$

6.17 Heat transfer

6.17.1 Radiation exchange model

The model incorporates a four-wall radiation exchange algorithm following the method described by Forney (1994). This algorithm allows the ceiling, upper wall, lower wall and floor to transfer radiation independently between each other. Radiant heating of these surfaces by the flames is also considered by treating the fire as a point source. The emission of radiation by soot particles and absorption by carbon dioxide and water vapour for both layers is also considered. The upper wall comprises those parts of the

wall above the height of the smoke layer interface, while the lower wall comprises those parts below the interface.

The radiation exchange sub-model is required to determine the net radiant heat flux emitted or absorbed by each room surface (i.e. upper and lower walls, ceiling and floor). These radiant fluxes are combined with the convective heat flux and used as the boundary condition for the heat conduction calculations described later. The gas layer absorption due to carbon dioxide and water vapour and emission due to soot particles are required for the energy source terms in the ordinary differential equations of the zone model.

Assumptions

The following assumptions are made in developing the four-wall radiation exchange model (Forney, 1994):

1. Both gas layers and each of the wall, ceiling and floor surfaces are assumed to be at a uniform temperature. This is generally not true where the surfaces meet each other.
2. The surfaces and gas layers are assumed to be in quasi-steady state, remaining constant over the duration of the time step of the associated differential equations.
3. For the purposes of estimating the radiation heat transfer from the fire, the total fire is assumed to radiate uniformly in all directions from a single point source. The point source is located at one-half the flame height but not higher than one-half the distance between the fire surface and the ceiling.
4. The radiation emitted by the room surfaces, gas layers and the fire is assumed to be diffuse and grey (i.e. the radiant flux is assumed independent of direction and wavelength).
5. The room surfaces are assumed to be opaque (i.e. incident radiation is either reflected or absorbed not transmitted), and the gases are assumed to be non-reflective.
6. The room is assumed to be a rectangular box with each surface either perpendicular or parallel to every other surface. Radiation losses through room openings are included.

Heat flux striking a surface

The heat flux striking a room surface may be due to radiation from the flames assuming a point source fire, it may be due to the radiating upper or lower gas layers or it may also be due to radiation from other room surfaces. If the gas layers are transparent, the heat flux striking the k^{th} surface due to the fire is given by Forney (1994) as:

$$q_{f-k} = \frac{\lambda \dot{Q}_f \omega_{f-k}}{4\pi A_k} \quad (92)$$

The fraction of the radiant energy leaving the f^{th} fire and intercepted by the k^{th} surface is given by $\omega_{f-k}/4\pi A_k$ (a configuration factor), and ω_{f-k} is the solid angle between the point source fire and the k^{th} surface. All other symbols are as given in the Nomenclature section.

If the gas layers are not transparent, there are four cases depending on whether the fire is located in the upper or lower layer. In this model, to simplify the situation, the fire is assumed to be located in the lower layer.

The heat flux striking the k^{th} room surface due to an emitting i^{th} gas layer is given as:

$$q_{j-k}^{i, \text{gas}} = \alpha_{j-k}^i \sigma T_i^4 \quad (93)$$

Where $\alpha_{j-k}^i = 1 - \tau_{j-k}^i$, α_{j-k}^i is the absorptivity of the gas and τ_{j-k}^i is the transmissivity of the gas. Table 3 is taken from Forney (1994) and summarises the radiative flux striking the k^{th} room surface due to a point source fire and an emitting gas layer.

Table 3. Radiative heat flux striking the k^{th} room surface.

| Path | Fire | Gas layer | |
|----------------|---|--|--|
| | q_{f-k}^{fire} | $q_{j-k}^{L, \text{gas}}$ | $q_{j-k}^{U, \text{gas}}$ |
| Upper to upper | $\tau_{f-k}^u \frac{\lambda_r \dot{Q}_f \omega_{f-k}}{4\pi A_k}$ | 0 | $F_{k-j} \sigma \alpha_{j-k}^U T_u^4$ |
| Lower to upper | $\tau_{f-k}^u \tau_{f-k}^l \frac{\lambda_r \dot{Q}_f \omega_{f-k}}{4\pi A_k}$ | $F_{k-j} \sigma \alpha_{j-k}^L T_1^4$ | $F_{k-j} \sigma \alpha_{j-k}^U T_u^4 \tau_{j-k}^L$ |
| Upper to lower | $\tau_{f-k}^l \tau_{f-k}^u \frac{\lambda_r \dot{Q}_f \omega_{f-k}}{4\pi A_k}$ | $F_{k-j} \sigma \alpha_{j-k}^L T_1^4 \tau_{j-k}^L$ | $F_{k-j} \sigma \alpha_{j-k}^U T_u^4$ |
| Lower to lower | $\tau_{f-k}^l \frac{\lambda_r \dot{Q}_f \omega_{f-k}}{4\pi A_k}$ | $F_{k-j} \sigma \alpha_{j-k}^L T_1^4$ | 0 |

Solid angles

The fraction of the radiant heat flux from a point source that is intercepted by a wall surface is found using solid angles as described by Forney (1994). For a surface with sides of dimensions x and y and in a plane a distance r from the radiating point source, the solid angle is:

$$\omega(x, y) = \frac{1}{4\pi} \left\{ \sin^{-1} \left(A \frac{y}{\sqrt{y^2 + r^2}} \right) + \sin^{-1} \left(A \frac{x}{\sqrt{x^2 + r^2}} \right) - \frac{\pi}{2} \right\} \quad (94)$$

Where $A = \sqrt{1 + \frac{r^2}{x^2 + y^2}}$

Solid angles for each of the various surfaces are additive, with the relevant geometry shown in Figure 58.

The point source is located at one-half the flame height but not higher than one-half the distance between the fire surface and the ceiling. Flame height uses Heskestad's equation taking the base of the fire corresponding to the first object, the total rate of heat in the room (constrained) and a fire diameter estimated from \dot{Q}_f / \dot{Q}'' .

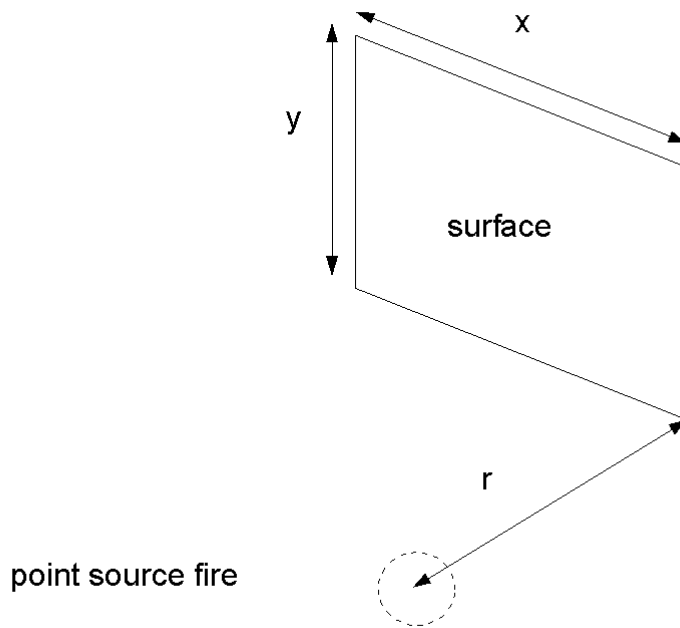


Figure 58. Geometry for determination of solid angles.

Configuration factors

There are a total of 16 configuration factors between the four surfaces to be considered in the room. For the purposes of this section, the four room surfaces will be labelled 1 to 4 as shown in Figure 59. The layer interface is considered to be a "pseudo-surface" labelled "d".

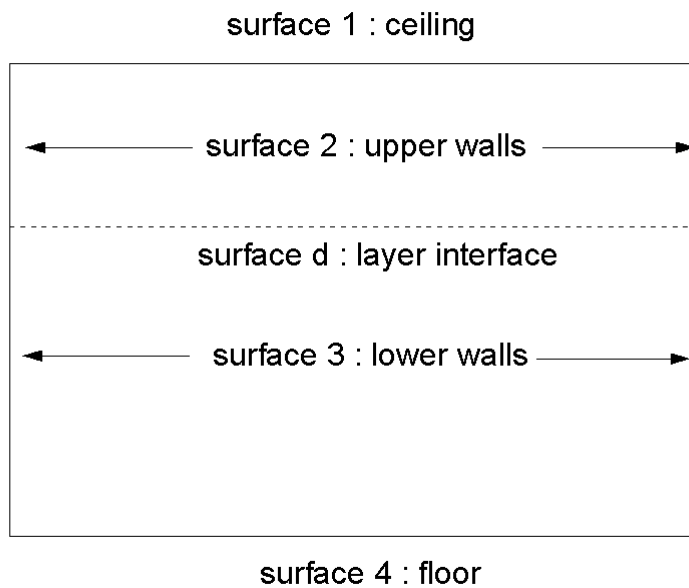


Figure 59. Schematic showing the surfaces considered in the configuration factor formulae.

The configuration factors to be determined are as follows:

$$F_{i-j} \text{ for } i, j = 1, \dots, 4. \quad (95)$$

All the configuration factors can be determined in terms of F_{1-4} , F_{1-d} and F_{4-d} .

There is no change to F_{1-4} during the simulation, and thus it needs only be calculated once for the room. It may be determined from the configuration factor between two parallel rectangular plates, at a distance L apart, as given by Incropera and DeWitt (1990).

$$F_{1-4} = \frac{2}{\pi \bar{X}\bar{Y}} \left\{ \ln \left[\frac{(1 + \bar{X})^2(1 + \bar{Y})^2}{1 + \bar{X}^2 + \bar{Y}^2} \right]^{1/2} + \bar{X}\sqrt{1 + \bar{Y}^2} \tan^{-1} \left(\frac{\bar{X}}{1 + \bar{Y}^2} \right) \right. \\ \left. + \bar{Y}\sqrt{1 + \bar{X}^2} \tan^{-1} \left(\frac{\bar{Y}}{1 + \bar{X}^2} \right) - \bar{X} \tan^{-1} \bar{X} \right. \\ \left. - \bar{Y} \tan^{-1} \bar{Y} \right\} \quad (96)$$

Where $X = X/L$ and $Y = Y/L$ and X and Y are the length and width of the rectangles respectively.

Calculations of F_{1-d} and F_{4-d} can be made in the same way using equation (96), but since the position of the smoke layer interface changes during the fire simulation, they need to be calculated at each time step.

From the reciprocity theorem, $F_{1-4} = F_{4-1}$ since the floor and ceiling areas are assumed to be equal, and the remaining 14 configuration factors can now be determined using simple algebraic formulae by making use of the following configuration factor properties:

$$A_j F_{j-k} = A_k F_{k-j} \quad (97)$$

$$F_{i,j \oplus k} = F_{i-j} + F_{i-k} \quad (98)$$

$$A_{i \oplus j} F_{i \oplus j - k} = A_i F_{i-k} + A_j F_{j-k} \quad (99)$$

$$\sum_{k=1}^N F_{j-k} = 1, j = 1, \dots, N \quad (100)$$

Where $i \oplus j$ denotes the union of two surfaces i and j .

The floor and ceiling are assumed to be flat rectangular surfaces so that:

$$F_{1-1} = F_{4-4} = 0 \quad (101)$$

Since the sum of the configuration factors in an enclosure is 1 and symmetry results in $F_{2-1} = F_{2-d}$, it follows that:

$$F_{1-2} = F_{1-d} = 1 \quad (102)$$

$$F_{2-1} + F_{2-2} + F_{2-d} = 2F_{2-1} + F_{2-2} = 1 \quad (103)$$

It therefore follows that:

$$F_{1-2} = 1 - F_{1-d} \quad (104)$$

$$F_{2-1} = \frac{A_1}{A_2} F_{1-2} \quad (105)$$

$$F_{2-2} = 1 - 2F_{2-1} \quad (106)$$

$$F_{4-3} = 1 - F_{4-d} \quad (107)$$

$$F_{3-4} = \frac{A_4}{A_3} F_{4-3} \quad (108)$$

$$F_{3-3} = 1 - 2F_{3-4} \quad (109)$$

$$F_{1-3} = 1 - F_{1-4} \quad (110)$$

$$F_{3-1} = \frac{A_1}{A_3} F_{1-3} \quad (111)$$

$$F_{3-2} = 1 - F_{3-1} - F_{3-3} - F_{3-4} \quad (112)$$

$$F_{2-3} = \frac{A_3}{A_2} F_{3-2} \quad (113)$$

$$F_{2-4} = 1 - F_{2-1} - F_{2-2} - F_{2-3} \quad (114)$$

$$F_{4-2} = \frac{A_2}{A_4} F_{2-4} \quad (115)$$

Transmission factors

The transmission factor is the fraction of energy that passes unimpeded through the gas. It depends on the absorption coefficient of the soot and on the path length travelled through the gas. The transmission factor is given by:

$$\tau_t = 1 - \alpha_t = 1 - \varepsilon_t \quad (116)$$

Where α_t is the total absorptance and ε_t is the total emissivity of the gas-soot mixture.

The emissivity of a gas-soot mixture is given by Tien, Lee and Stretton (2008) as:

$$\varepsilon_t = (1 - e^{-k_s L}) + \varepsilon_g e^{-k_s L} \quad (117)$$

Where ε_g is the emissivity of the gas alone and k_s is the absorption coefficient of the soot. The absorption coefficient is approximated using the average extinction coefficient for the layer (and neglecting the scattering coefficient), calculated from equation (146) based on the concentration of the soot in the gas layer and the specific extinction coefficient.

The mean path length, L , is determined from an expression for an arbitrarily shaped gas volume given by Tien, Lee and Stretton (2008) as follows:

$$L \approx cL_o \quad (118)$$

Where:

$$L_o = \frac{4V}{A} \quad (119)$$

Where v and A are the volume and area of the boundary surface of the gas body (upper or lower layer) respectively and c is a correction factor equal to 0.9 for arbitrary volumes.

The emissivity of the gas is strongly dependent on absorption by water vapour and carbon dioxide over certain wavelength bands. The emissivity of water vapour ε_{H_2O} and carbon dioxide ε_{CO_2} can be determined from charts if the partial pressure and temperature of each gas is known in addition to the mean beam length. Emissivity data (Incropera & DeWitt, 1990) for these two gas constituents is incorporated into the model, and the gas emissivity is given by:

$$\varepsilon_g = \varepsilon_{H_2O} + 0.5\varepsilon_{CO_2} \quad (120)$$

The partial pressures are determined from the known mass fractions using the ideal gas law as follows:

$$p_i = \frac{m_i RT}{MW_i V} = \frac{Y_i \rho RT}{MW_i} \quad (121)$$

$$\Rightarrow p_i = \frac{Y_i R \rho_\infty T_\infty}{MW_i} \quad (122)$$

Where p_i is the partial pressure of species i , m_i is the mass of species i , R is the universal gas constant, MW_i is the molecular weight of species i , T and V are the temperature and volume of the gas/air layer and ρ_∞ and T_∞ are the reference density and temperature for air.

The mass fractions for the water vapour and carbon dioxide are solved for in the ordinary differential equations (ODE) given in section 6.4.

Solving the net radiation equations

Net radiation refers to the difference between the radiation that is incident on the surface and that which is emitted by the surface. Incoming radiation consists of grey-body surface radiation from the other surfaces, from the radiating fire source and from the upper and lower gas layers. Outgoing radiation consists of grey-body surface radiation and incoming radiation that has been reflected. Forney (1994) gives the net radiation equation to be solved as:

$$\Delta \hat{q}_k'' - \sum_{j=1}^N (1 - \varepsilon_j) \Delta \hat{q}_j'' F_{k-j} \tau_{j-k} = \sigma T_k^4 - \sum_{j=1}^N \sigma T_j^4 F_{k-j} \tau_{j-k} - \frac{c_k}{A_k} \quad (123)$$

The matrix corresponding to this linear set of equations is diagonally dominant and therefore may be solved more easily by iterative methods. Ultimately, the matrix holding the net radiation leaving each surface, $\Delta q_k''$ is required where $k = 1, \dots, 4$. This is related to $\Delta \hat{q}_k''$ by the following expression:

$$\Delta q_k'' = D \Delta \hat{q}_k'' \quad (124)$$

Where matrix D is a scaling matrix holding the emittances of the k^{th} room surface elements as follows:

$$D = \begin{pmatrix} \varepsilon_1 & 0 & 0 \\ 0 & \ddots & 0 \\ 0 & 0 & \varepsilon_N \end{pmatrix} \quad (125)$$

The equation to be solved in matrix form is:

$$\hat{A} \Delta \hat{q}_k'' = A \Delta q_k'' = B E - c_k'' \quad (126)$$

Where:

$$c_k'' = \frac{c_k}{A_k} = \sum_{j=1}^N (q_{j-k}^{u,gas} + q_{j-k}^{l,gas}) + \sum_{j=1}^{N \text{ fire}} q_{j-k}^{fire} \quad (127)$$

Equations $q_{j-k}^{u,gas}$ and $q_{j-k}^{l,gas}$ account for the radiative flux striking the k^{th} surface due to the upper and lower gas layers respectively, and q_{j-k}^{fire} accounts for the radiative flux striking the k^{th} surface due to a point source fire.

Matrix E is a column vector with the k^{th} component as follows:

$$E_k = \sigma T_k^4 \quad (128)$$

The k^{th} and j^{th} components of the $N \times N$ matrix B is:

$$b_{k,j} = \delta_{k,j} - F_{k-j} \tau_{j-k} \quad (129)$$

Where $\delta_{k,j}$ is the Kronecker delta function.

The components of the $N \times N$ matrix \hat{A} are as follows:

$$\hat{a}_{k,j} = a_{k,j}\epsilon_j = \delta_{k,j} - F_{k-j}\tau_{j-k}(1 - \epsilon_j) \quad (130)$$

Equation (126) is solved using a LU decomposition technique (Block, Shakir & Smith, 1993). The matrix \hat{A} is first decomposed according to the LU algorithm. Then, back substitution of the decomposed matrix results in the solution vector. Once the column vector \hat{q}_k is found, q_k , which holds the net radiant heat fluxes for the four room surfaces, can then be found from equation (124). The model output provides a value for "target radiation". This corresponds to the net incident radiation on the surface of the floor.

Energy absorbed by the gas layers

The energy absorbed by a gas layer may be due to radiation from the point source fires, radiation from the surrounding room surfaces or from emission from the other gas layer. The net radiant heat absorbed by the upper and lower layers for the different paths are shown in Table 4 and Table 5 taken from Forney (1994).

Table 4. Radiant heat absorbed by the upper layer.

| Path through the gas | Due to heat emitting surface q_{j-k}^{out} $= A_j F_{j-k} \left(\sigma T_j^4 - \frac{1 - \epsilon_j}{\epsilon_j} \Delta q_j \right)$ | Due to gas layer emission $q_{j-k}^{i, gas}$ $= \alpha_{j-k}^i \sigma T_i^4 A_j F_{j-k}$ | Due to point source fire $q_{f-k}^{fire} = \frac{\lambda_r \dot{Q}_f \omega_{f-k}}{4\pi A_k}$ |
|-------------------------|---|--|--|
| Upper to lower or upper | $q_{j-k}^{out} \alpha_{j-k}^U$ | $-q_{j-k}^{U, gas}$ | $q_{f-k}^{fire} \alpha_{f-k}^U A_k$ |
| Lower to upper | $q_{j-k}^{out} \tau_{j-k}^L \alpha_{j-k}^U$ | $q_{j-k}^{L, gas} \alpha_{j-k}^U - q_{j-k}^{U, gas}$ | $q_{f-k}^{fire} \alpha_{f-k}^U \tau_{j-k}^L A_k$ |
| Lower to lower | 0 | 0 | 0 |

Table 5. Radiant heat absorbed by the lower layer.

| Path through the gas | Due to heat emitting surface q_{j-k}^{out} $= A_j F_{j-k} \left(\sigma T_j^4 - \frac{1 - \epsilon_j}{\epsilon_j} \Delta q_j \right)$ | Due to gas layer emission $q_{j-k}^{i, gas}$ $= \alpha_{j-k}^i \sigma T_i^4 A_j F_{j-k}$ | Due to point source fire $q_{f-k}^{fire} = \frac{\lambda_r \dot{Q}_f \omega_{f-k}}{4\pi A_k}$ |
|-------------------------|---|--|--|
| Lower to lower or upper | $q_{j-k}^{out} \alpha_{j-k}^L$ | $-q_{j-k}^{L, gas}$ | $q_{f-k}^{fire} \alpha_{f-k}^L A_k$ |
| Upper to lower | $q_{j-k}^{out} \tau_{j-k}^U \alpha_{j-k}^L$ | $q_{j-k}^{U, gas} \alpha_{j-k}^L - q_{j-k}^{L, gas}$ | $q_{f-k}^{fire} \alpha_{f-k}^L \tau_{j-k}^U A_k$ |
| Upper to upper | 0 | 0 | 0 |

Radiation losses through openings

Heat may be lost from the compartment due to radiation through the room openings. It is assumed that the radiation is always lost to the outside, even if the opening is in fact to another compartment.

The radiation loss reduces the enthalpy of the upper or lower layer as shown below, where $A_{v,u}$ and $A_{v,l}$ are the vent areas located in the upper and lower gas layers respectively:

$$\dot{Q}_{rad,u} = -\varepsilon_{g,u}\sigma(T_u^4 - T_\infty^4)A_{v,u} \quad (131)$$

$$\dot{Q}_{rad,l} = -\varepsilon_{g,l}\sigma(T_l^4 - T_\infty^4)A_{v,l} \quad (132)$$

6.17.2 Heat conduction model

An implicit one-dimensional, finite-difference scheme is used to calculate heat conduction through the ceiling, upper walls, lower walls and floor. This allows the temperature at any node to be calculated by solving a set of simultaneous equations for the unknown nodal temperatures at each time step (Incropera & DeWitt, 1990). The implicit method has the advantage of being unconditionally stable and therefore allows a larger time step to be used in the calculations. The walls and ceiling may be specified as a single layer or as a two-layer system by including a substrate material. The floor is specified as a single layer.

The implicit form of the finite-difference scheme for a surface node is given by Incropera and DeWitt (1990) as:

$$(1 + 2Fo)T_1^{p+1} - 2FoT_2^{p+1} = \frac{2Fo Bi q''}{h} + T_1^p \quad (133)$$

Where the Fourier and Biot numbers are given by:

$$Fo = \frac{\alpha \Delta t}{(\Delta x)^2} \quad (134)$$

$$\alpha = \frac{k}{\rho c} \quad (135)$$

$$Bi = \frac{h}{k} \Delta x \quad (136)$$

The implicit form for an interior node is given as:

$$-Fo T_{m-1}^{p+1} + (1 + 2Fo)T_m^{p+1} - Fo T_{m+1}^{p+1} = T_m^p \quad (137)$$

Writing an equation for each node gives n equations that must be solved simultaneously for each time step. This can be done using the matrix inversion method by expressing the equations in the form $[A][T]=[C]$, where:

$$\begin{bmatrix} 1 + 2Fo & -2Fo & 0 & 0 & \dots & 0 \\ -Fo & 1 + 2Fo & -Fo & 0 & \dots & 0 \\ 0 & -Fo & 1 + 2Fo & -Fo & \dots & 0 \\ \vdots & \vdots & \ddots & \dots & \dots & \vdots \\ 0 & \dots & \dots & 0 & -2Fo & 1 + 2Fo \end{bmatrix} \quad (138)$$

$$[C] = \begin{bmatrix} 2Fo Bi_{int} \frac{\dot{q}''_{int}}{h} + T_1^p \\ T_2^p \\ T_3^p \\ \vdots \\ 2Fo Bi_{ext}(T_{ext} - T_n^p) + T_n^p \end{bmatrix} \quad (139)$$

The total heat flux incident on the interior surface is represented by \dot{q}''_{int} . It includes both radiation (from the four-wall radiation exchange model) and convection.

A table of nodal temperatures is compiled, starting with the prescribed initial conditions. The temperatures at the next time step, [T], are found by multiplying the inverse matrix $[A]^{-1}$ by the column vector [C] (Incropera & DeWitt, 1990) using the method of LU decomposition (Block, Shakir & Smith, 1993).

An alternative method for solving the matrices using Gauss-Jordan elimination (Eagle, 1997) is also available to the user.

6.17.3 Convective heat transfer coefficients

The interior heat transfer coefficient used in the heat transfer calculations between the gas layers and the room surfaces is calculated following the method described by Peacock et al. (1993) for the CFAST model.

The heat transfer coefficient (assuming natural convection) is given by:

$$h_c = \frac{k}{l} C_o (\mathbf{Gr Pr})^{1/3} \quad (140)$$

The characteristic dimension, l , is taken as $\sqrt{A_w}$ where A_w is the area of the surface in contact with the layer (upper or lower as applicable).

The Grashof number, Gr , is given as:

$$\mathbf{Gr} = \frac{gl^3 |T_g - T_s|}{\nu^2 T_g} \quad (141)$$

The thermal conductivity, k , of the gases is given by:

$$k = 2.72 \times 10^{-4} \left(\frac{T_g + T_s}{2} \right)^{4/5} \quad (142)$$

The kinematic viscosity, ν of the gases is given by:

$$\nu = 7.18 \times 10^{-10} \left(\frac{T_g + T_s}{2} \right)^{7/4} \quad (143)$$

The temperatures of the gas layer and the wall or ceiling surface are T_g and T_s respectively, Pr is the Prandtl number (=0.72) and C_o is a coefficient that depends on orientation as given in Table 6.

Table 6. Surface coefficients.

| Orientation | Coefficient C_o | Condition |
|-------------|-------------------|-------------|
| Vertical | 0.13 | all |
| Horizontal | 0.21 | $T_g > T_s$ |
| Horizontal | 0.012 | $T_g < T_s$ |

The convective heat flux term is given by:

$$\dot{q}_c'' = h_c(T_g - T_s)A_s \tag{144}$$

6.18 Numerical solution

There are 17 ordinary first-order differential equations that are solved using a stiff differential equation solver. The numerical solution was from that provided in a mathematics library, BNALib (Eagle, 1997). The 17 equations relate to pressure, upper layer volume, upper and lower layer temperature, oxygen, soot, unburned fuel, water vapour, carbon monoxide and carbon dioxide concentrations and finally the sprinkler/detector link temperature.

The recommended initial time step setting is 1 second.

Convergence error control parameters can be specified for the ODE solver and for the vent flow calculations with default values as shown in Figure 60.

The method of solving the heat conduction equations for the room surfaces and the number of nodes used is also shown in Figure 60 with default settings.

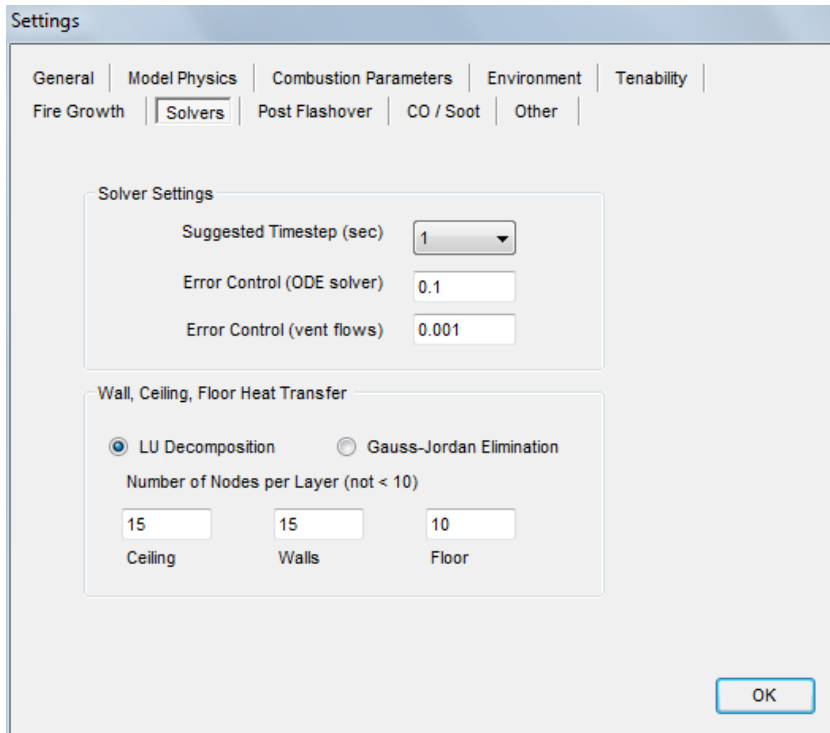


Figure 60. Solver and numerical settings.

7. Life hazard calculations

7.1 Tenability settings

Tenability settings are accessed using the TENABILITY, TENABILITY PARAMETERS file menu as shown in Figure 61.

There is a choice of asphyxiant gas models, and these are described in detail in section 7.3. The activity level influences the occupant respiration rate of combustion products and is used in the FED (CO/CO₂/HCN) asphyxiant gas model.

A monitoring height above the floor can be specified, and species concentrations from either the upper or lower layer will be used in the calculations depending on the position of the layer height relative to the monitoring height. The FED is calculated for the specified egress path.

Tenability end-point criteria can be entered as shown in Figure 61. These do not change the calculations in any way but allow summary results to be reported in relation to the time at which these criteria are reached or exceeded.

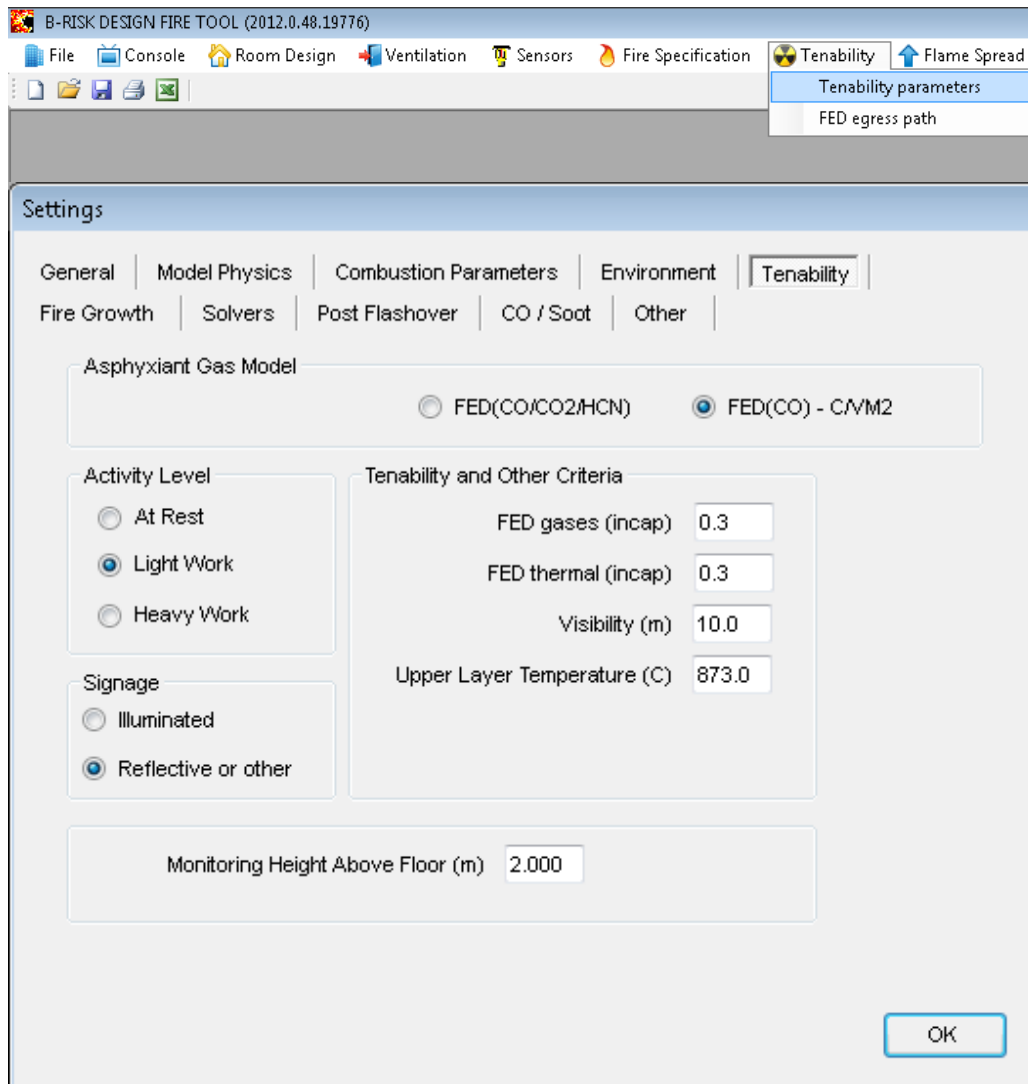


Figure 61. Tenability settings for hazard to life assessment.

Signage can be specified as ILLUMINATED or REFLECTIVE OR OTHER. This influences the visibility calculations as described in section 7.2, with illuminated signage allowing increased visibility through smoke.

7.2 Visibility

The mass fraction of soot in the upper layer is given by solving equations (19) and (20) for species generation at each time step. This requires a value for the soot yield (kg soot per kg of fuel pyrolysed) to be provided by the user. The mass concentration of soot in the upper layer (in kg of soot per m³ of upper layer gas) is then given by:

$$C_{soot} = Y_{soot}\rho_u \quad (145)$$

The average extinction coefficient, k_{avg} (m⁻¹), is given by:

$$k_{avg} = C_{soot}k_m \quad (146)$$

Where k_m is the specific extinction coefficient (m²/kg soot) taken equal to 8790 for flaming combustion (Mulholland & Choi, 1998).

The maximum distance an observer can recognise an object, usually an exit sign, when viewing the object through smoke is defined as the visibility, v , by Beyler (1988).

A study by Jin (1978) found that the product $v.k_{avg}$ is a constant for a given object and lighting condition. The data correlated to a value of 3 for light-reflecting signs and 8 for light-emitting or illuminated signs (Mulholland, 2002). The visibility (m) is therefore given by:

$$V = \frac{3}{k_{avg}} \text{ (reflective signs)} \quad (147)$$

$$V = \frac{8}{k_{avg}} \text{ (illuminated signs)} \quad (148)$$

B-RISK calculates the optical density (OD) of each layer, OD (1/m), as a conversion of the extinction coefficient from natural log to base 10 units.

$$OD = \frac{k_{avg}}{2.3} \quad (149)$$

7.3 Fractional effective dose – asphyxiant gases

Toxicity of asphyxiant products is evaluated using the fractional effective dose (FED) method described by Purser (1988) and ISO 13571 (ISO, 2012). The model evaluates the sum of the FEDs at a specified height (in the upper or lower layer as applicable) for incapacitation due to carbon monoxide, hypoxia (lack of oxygen) accounting for the accelerated breathing rate caused by exposure to carbon dioxide. Optionally, the dose of HCN may also be included. The FED is the ratio between the cumulative dose received after some time to the effective dose needed to cause incapacitation for a person of average susceptibility.

Option 1 – FED(CO/CO₂/HCN)

This option includes the dose effects of CO, HCN, CO₂ and the hypoxic effect of reduced O₂.

The model considers the time-dependent exposure of carbon monoxide in the upper layer by calculating a fraction of an incapacitating dose for CO (see Purser (2008)). RMV is the volume (in litres) of air breathed per minute and varies with the activity level.

$$FED_{CO} = 3.317 \times 10^{-5} \frac{RMV_o}{COHb} \int_0^t VCO_2 \times [CO]^{1.036} dt \quad (150)$$

Where [CO] = carbon monoxide concentration in parts per million (ppm), t = exposure time interval (min), RMV_o = volume of air breathed each minute (L) based on activity level, COHb = exposure dose for incapacitation (% COHb) and VCO₂ = multiplication factor for enhanced uptake of asphyxiant gases, as given below:

$$VCO_2 = \exp\left(\frac{\%CO_2}{5}\right) \quad (151)$$

The user may select an activity level appropriate to their analysis. The model uses values of RMV_o and incapacitation doses of COHb applicable to a 70 kg human, as shown in Table 7 (Purser, 2002).

Table 7. RMV_o and COHb incapacitation dose for different activity levels.

| Activity | RMV _o (l/min) | COHb incapacitation dose (%) |
|------------|--------------------------|------------------------------|
| At rest | 8.5 | 40 |
| Light work | 25 | 30 |
| Heavy work | 50 | 20 |

Similarly, the FED for oxygen hypoxia is determined by evaluating the following integral from Purser (2002) if the oxygen concentration falls below 13%:

$$FED_{O_2} = \int_0^t \frac{1}{\exp(8.13 - 0.54(20.9\% - \%O_2))} dt \quad (152)$$

Similarly, the FED for incapacitation by HCN is determined by evaluating the following integral from Purser (2002) and including CO₂ hyperventilation effects:

For HCN > 80 ppm,

$$FED_{HCN} = \int_0^t \frac{VCO_2}{\exp(5.396 - 0.023[HCN])} dt \quad (153)$$

The model allows the user to select a height within the room at which to evaluate the incapacitation FED. The default is 2 m above the floor, a representative “nose” height for an adult person. The total FED is therefore given by:

$$FED = FED_{CO} + FED_{O_2} + FED_{HCN} \quad (154)$$

The model uses a simple trapezoidal rule to evaluate the integrals using the upper layer species concentrations for the time when the layer interface is below the monitoring height selected by the user and using the lower layer species concentrations for the time when the layer interface is above the monitoring height. The program only evaluates the integrals when the species concentrations are above initial ambient levels (or above 80 ppm in the case of HCN) and below ambient in the case of oxygen.

Option 2 – FED(CO) C/VM2

This option includes the dose effect of CO, the hypoxic effect of reduced O₂ and the hyperventilation effect of CO₂ following the equations used in ISO 13571 (ISO, 2012) and following the requirements of C/VM2 (MBIE, 2014).

The FED(CO) is the fraction of the dose of CO that would render a person of average susceptibility incapable of escape.

Where the CO₂ concentration exceeds 2% by volume, the CO concentration is increased by a factor to allow for the increased rate of CO uptake due to hyperventilation.

This factor is taken as:

$$f = \exp\left(\frac{\%CO_2}{5}\right) \quad (155)$$

According to ISO 13571 (ISO, 2012), this equation is derived from an empirical fit to human hyperventilation, corrected for uptake inefficiencies in the lung, and is accurate to within $\pm 20\%$.

Following ISO 13571, the fractional effective dose is therefore calculated (for %O₂ $\geq 13\%$ by volume and allowing for CO₂ hyperventilation) by summation over the relevant time increments using:

$$FED_{in,CO} = \sum_{t_0}^t \left[\frac{[CO]\Delta t}{35000} \cdot f \right] \quad (156)$$

Where:

[CO] = average CO conc. in parts per million (or $\mu\text{L/L}$) over the time increment Δt

%CO₂ = average % conc. of CO₂ (by volume) over the time increment Δt

Δt = time increment between successive readings of concentration in minutes

t_0 = time at which exposure begins in minutes

t = time at which exposure ends in minutes.

Where the percentage of oxygen is less than 13% by volume, the hypoxic effects of oxygen depletion are also calculated and included in the FED(CO).

$$FED_{in,O_2} = \sum_{t_o}^t \frac{\Delta t}{\exp(8.13 - 0.54(20.9\% - \%O_2))}$$

Where:

$\%O_2$ is the average % concentration of O_2 (by volume) over the time increment Δt

$$FED = FED_{CO} + FED_{O_2} \quad (157)$$

The model uses a simple trapezoidal rule to evaluate the integrals using the upper layer species concentrations for the time when the layer interface is below the monitoring height selected by the user and using the lower layer species concentrations for the time when the layer interface is above the monitoring height. The program only evaluates the integrals when the species concentrations are above initial ambient levels (or above 80 ppm in the case of HCN) and below ambient in the case of oxygen.

7.4 Fractional effective dose – thermal effects

The FED(thermal) is the fraction of the dose of convected and radiated heat that would render a person of average susceptibility incapable of escape. The calculations use equations from ISO 13571 (ISO, 2012) and follow the requirements of C/VM2 (MBIE, 2014).

Calculation of the time to incapacitation under conditions of exposure to convective heat from air containing less than 10% by volume of water vapour can be made assuming the exposed occupant is lightly clothed using:

$$t_{Iconv} = (5 \times 10^7) T^{-3.4} \quad (158)$$

Where:

T = gas temperature expressed in °C

t_{Iconv} = time to incapacitation under conditions of exposure to convective heat, expressed in minutes.

A threshold temperature below which the convective component of the FED thermal does not accumulate has been added. The temperature used is 25°C.

As with toxic gases, an exposed occupant can be considered to accumulate a dose of convected heat over a period of time. The FED of convected heat accumulated per minute is the reciprocal of t_{Iconv} .

The tenability limit for exposure of skin to radiant heat is approximately 2.5 kW/m². Lesser levels of exposure can be tolerated for 30 minutes or more without significantly affecting time available for escape. Calculation of the time to incapacitation under conditions of exposure to radiant heat causing second-degree burning of the skin is given by:

$$t_{Irad} = (6.9) q^{-1.56} \quad (159)$$

Where:

t_{Irad} = time to 2nd degree burns, expressed in minutes

q = radiant heat flux in kW/m².

The radiation incident on the target is assumed to be due to a flat plate source at the layer interface height and at a temperature equal to the upper layer temperature T_u , with emissivity equal to the upper layer emissivity ε_u . The configuration factor F between the layer interface and the target is calculated for a flat surface and a parallel differential element (Tien, Lee & Stretton, 2008).

The incident radiation is given by equation (160):

$$\dot{q}_{rad} = F \varepsilon_u \sigma T_u^4 \quad (160)$$

As with toxic gases, an exposed occupant may be considered to accumulate a dose of radiant heat over a period of time. The FED of radiant heat accumulated per minute is the reciprocal of t_{Irad} .

Following ISO 13571, the FED(thermal) is calculated by summation over the relevant time increments using:

$$FED = \sum_{t_1}^{t_2} \left(\frac{1}{t_{Irad}} + \frac{1}{t_{iconv}} \right) \Delta t \quad (161)$$

Where:

t_1 = time at which exposure begins in minutes

t_2 = time at which exposure ends in minutes.

7.5 Egress path segments

The FED calculations described in sections 7.3 and 7.4 are based on a fixed position (at the monitoring height) in a specified room.

However, ideally the calculation should be attached to an individual as they move from room to room during the evacuation. Therefore, the user has the option to specify up to three egress path segments that define both a room and a time interval over which the FED calculations will be made.

An example is shown in Figure 62.

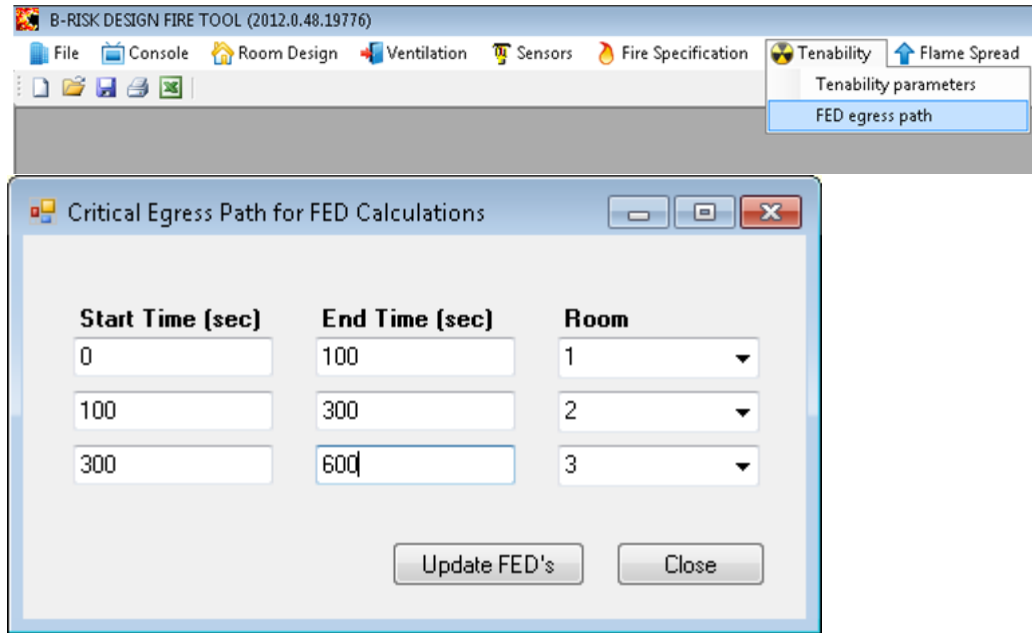


Figure 62. Specifying FED egress path.

8. Sprinklers and thermal detectors

8.1 General

Sprinkler or thermal detector actuation is predicted based on a burning item located within the room of fire origin. Multiple sprinklers can be positioned within the room of fire origin, the response of each sprinkler is determined based on its position relative to the first burning item.

If multiple items are burning in the room, only the characteristics (e.g. rate of heat release) of the first burning item and the ceiling jet it produces are used in the sprinkler or detector response calculation. The contribution from any additional burning item is ignored except to the extent that it contributes to the heating of the hot upper layer within which the sprinkler may be immersed.

Sprinklers or heat detectors may be added, removed, copied or edited using the SENSORS, SPRINKLERS/HEAT DETECTORS menu item as shown in Figure 63. Multiple sensors may be included in a simulation.

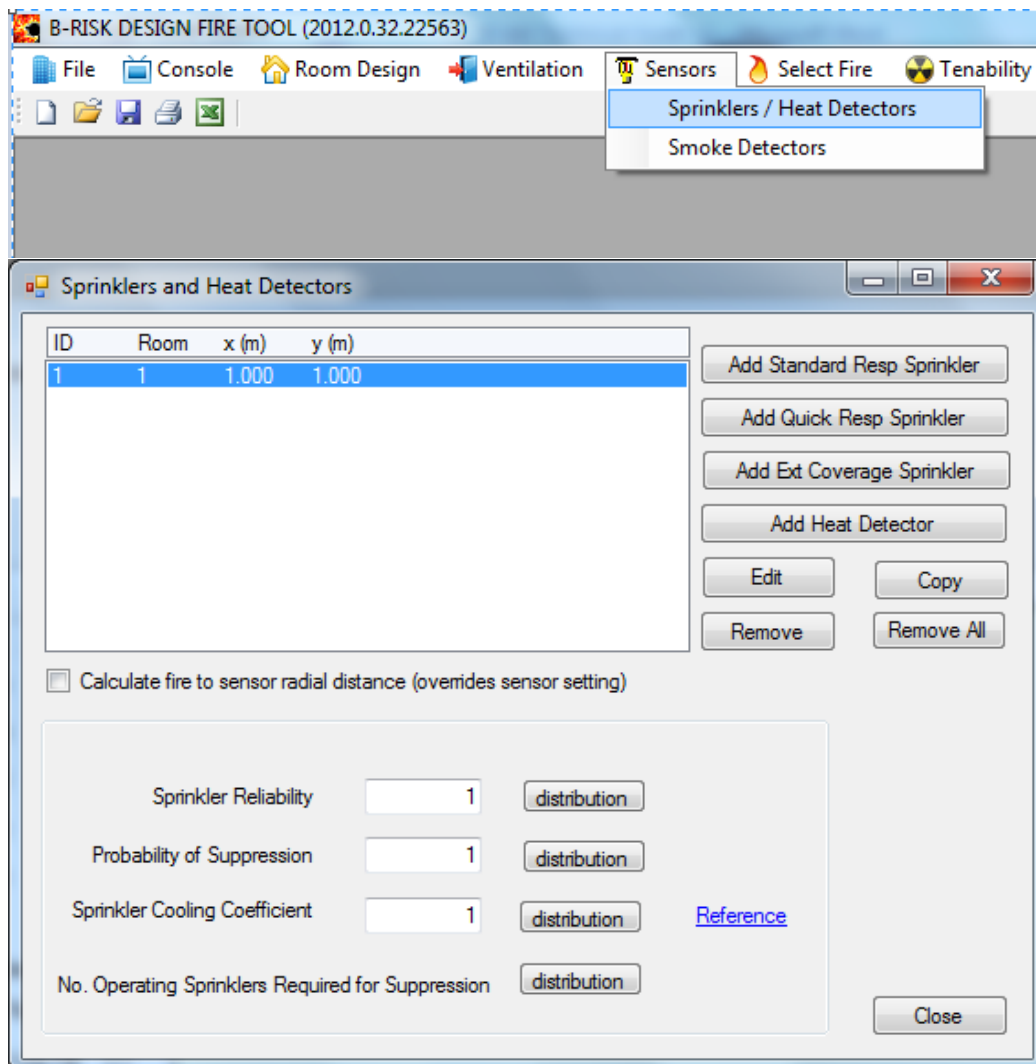


Figure 63. Input form for managing sprinklers or heat detectors.

Standard response, quick response, extended coverage sprinklers or heat detectors can be added using the default sprinkler properties and settings given in VM2 (MBIE, 2014) as shown in Table 8. The properties of these sensors may be subsequently edited if required to suit the needs of the user for non-VM2 use.

Table 8. Default properties assigned to sprinklers and heat detectors following VM2.

| | Standard response sprinkler | Quick response sprinkler | Extended coverage sprinkler | Heat detector |
|---------------------------------|-----------------------------|--------------------------|-----------------------------|---------------|
| RTI (ms) ^{1/2} | 135 | 50 | 50 | 30 |
| C-factor (m/s) ^{1/2} | 0.85 | 0.65 | 0.65 | 0 |
| Activation temp (°C) | 68 | 68 | 68 | 57 |
| Radial distance (m) | 3.25 | 3.25 | 4.3 | 4.2 |
| Distance below ceiling (m) | 0.025 | 0.025 | 0.025 | 0.025 |
| Water application rate (mm/min) | 4.2 | 4.2 | 4.2 | 0 |

Heat detectors are distinguished from sprinklers internally in B-RISK by virtue of having a C-factor and water spray density equal to zero. If either of these two parameters are non-zero, the sensor will be treated as a sprinkler.

Sprinklers or thermal detectors must be located in the room of fire origin to respond.

The required input property data for each sprinkler is shown in Figure 64.

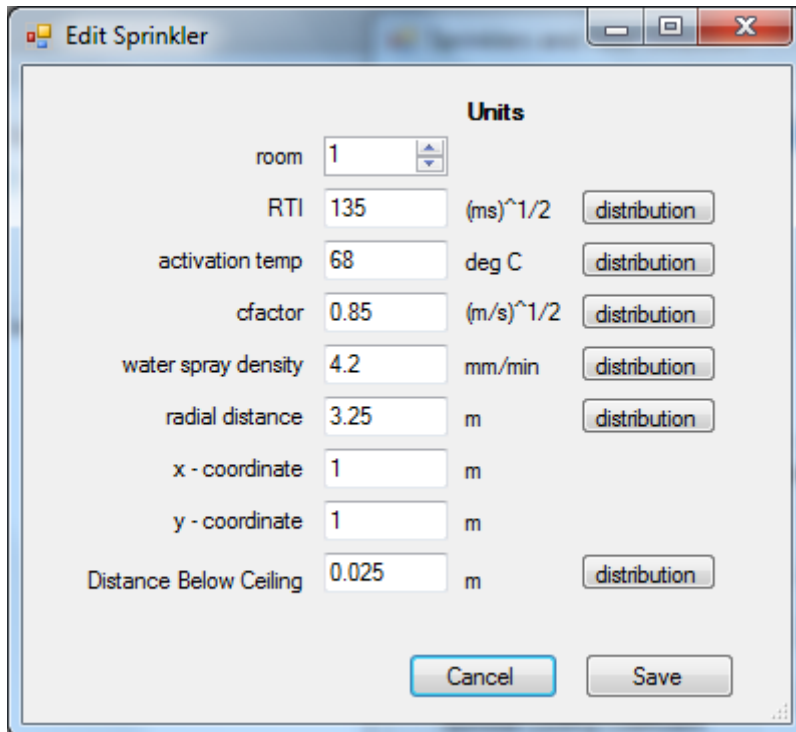


Figure 64. Input form for entering sprinkler or heat detector properties.

Some of the parameters may be assigned statistical distributions. These include the RTI, activation temperature, C-factor, water spray density, radial distance and distance below the ceiling. The available probability distributions are normal, uniform, triangular and lognormal.

The file called "sprinklers.xml" contains the details about each sprinkler and what distributions, if any, have been assigned.

This file will be found in the relevant project folder under the "riskdata" directory (e.g. C:\Users\...\Documents\B-RISK\riskdata\basemodel_default\sprinklers.xml).

If the simulation has the CALC SPRINKLER RADIAL DIST checkbox option selected, the radial distance between the sprinkler and the fire item (i.e. first item ignited only) is calculated based on the position of the first item and each sprinkler in the room. This value of radial distance is saved in the input file for each iteration. If this option is not selected, the radial distance assigned by the user to the sprinkler is used instead. The spatial layout of sprinklers in the room can be viewed in the POPULATE ROOM ITEMS form as shown in Figure 65.

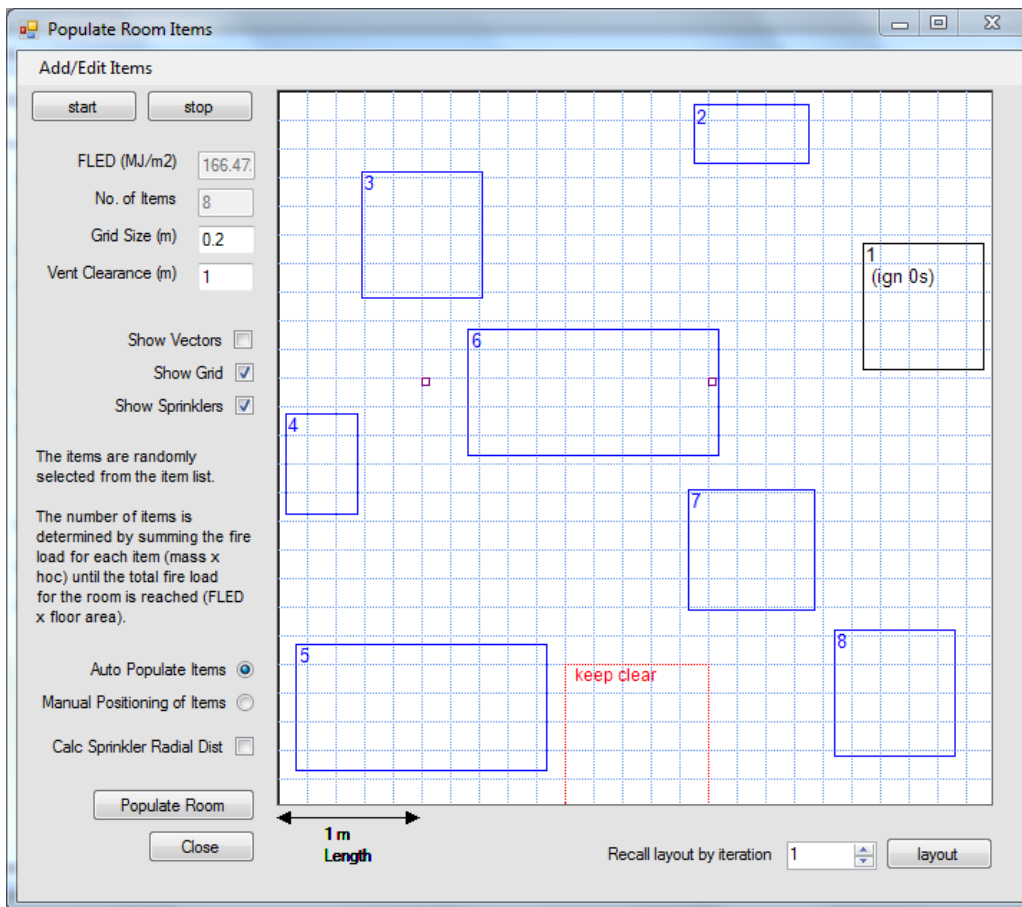


Figure 65. Room layout showing sprinkler locations (small hollow black squares indicate sprinkler location).

8.2 Effect of sprinkler spray on fire-induced doorway flow

Crocker et al. (2010) found that the mass flows exiting a doorway can be predicted during a fire with sprinkler activation by using a cooling coefficient that can be experimentally determined, leading to improved predictions of the fire environment outside the room of origin in sprinklered occupancies. The discharge coefficient for a wall vent opening is modified by multiplying by the sprinkler cooling coefficient. They found that the Tyco LFII sprinkler (TY2234) reduced the mass flow in the doorway by 16% compared to the unsprinklered case, suggesting a sprinkler cooling coefficient of

0.84. Knowledge of the temperature reduction resulting from a sprinkler spray does not need to be known to predict the impact of the sprinkler spray on doorway mass flow rate.

The effect of the sprinkler cooling the plume gases is not accounted for.

The sprinkler cooling coefficient is entered as shown in Figure 63.

8.3 Sprinkler reliability

A sprinkler reliability value or an associated probability distribution can be assigned to the reliability of the sprinkler system. For each iteration, the reliability parameter is sampled from the assigned distribution, and then a uniformly selected random number between 0 and 1 is compared to the sampled reliability value. If the random number exceeds the reliability value, the sprinkler system is deemed ineffective and the operation of the sprinkler system is assumed to have no effect on the rate of heat release for that iteration. If the sampled random number does not exceed the reliability value, the rate of heat release for that iteration will be modified to the probability of suppression or control entered by the user.

The sprinkler reliability is entered as shown in Figure 63.

8.4 Probability of suppression or control

A conditional probability of suppression value (given the sprinkler system is operational) or an associated distribution can be assigned by the user. If the probability of suppression is given as x , then the probability of control is $1-x$. For each iteration, the probability of suppression is sampled from the assigned distribution, and then a uniformly selected random number between 0 and 1 is compared to the sampled probability of suppression value. If the random number is not greater than the probability of suppression value, the sprinkler system operates in suppression mode using the suppression algorithm described in section 8.5. If the random number exceeds the probability of suppression value, the sprinkler system operates in control mode and the rate of heat release for that iteration will be maintained at a constant value following activation of the sprinkler.

The probability of suppression is entered as shown in Figure 63.

8.5 Effect of sprinkler spray on rate of heat release

The two input parameters for sprinkler system reliability and for probability of suppression together result in one of three possibilities for the effect the system has on the rate of heat release of the fire for each iteration.

The effect of the sprinkler on the rate of heat release of the fire may therefore be modelled in one of the following ways:

1. No effect on the rate of heat release of the fire, with the activation time reported only, such as when the system has been compromised and there is no water available. This will occur for all iterations by setting the reliability parameter to zero.
2. Maintain the fire size at a constant heat release rate equal to the fire size at the time of sprinkler activation. This is referred to as "control" and will occur for all iterations by setting the probability of suppression parameter to zero and the

- reliability value to 1. If the total input heat release rate reduces below the rate of heat release at activation, the lesser value applies.
3. Simulate suppression using an algorithm developed by Evans (1994) for unshielded furniture fires where the rate of heat release after activation is given by:

$$\dot{Q}(t - t_{act}) = \dot{Q}(t_{act}) \exp \left[\frac{-(t - t_{act})}{3(\dot{w}'')^{-1.85}} \right] \quad (162)$$

Where \dot{w}'' is the water spray density (mm/s), t_{act} is the sprinkler activation time (s) and $\dot{Q}(t_{act})$ is the heat release rate of the fire at the time of sprinkler activation (kW). This equation applies to sprinkler spray densities not less than 0.07 mm/s.

This option is achieved for all iterations by setting both the probability of suppression and reliability parameters to 1.

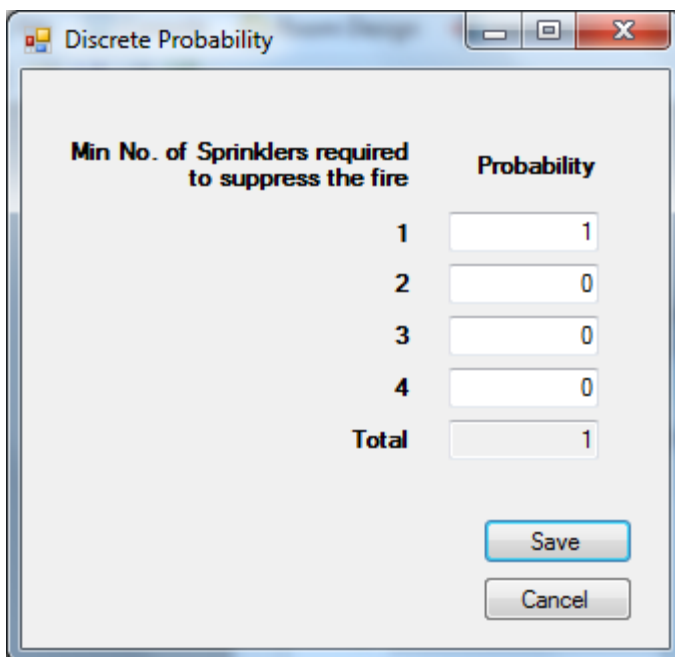
8.6 Minimum number of sprinklers required for suppression or control

The minimum number of operating sprinklers, in the range one to four, required to initiate suppression or control can be specified by the user in the form of a discrete distribution, which is defined such that:

$$p(1-spr) + p(2-spr) + p(3-spr) + p(4-spr) = 1.0 \quad (163)$$

Where $p(x-spr)$ is the probability that x sprinklers are required to suppress or control the fire. The default setting is $p(1spr)=1.0$, $p(2spr)=0$, $p(3spr)=0$, $p(4spr)=0$, i.e. only one sprinkler is required to initiate control or suppression.

The distribution for the minimum number of sprinklers required for suppression or control is entered as shown in Figure 63 and Figure 66.



| Min No. of Sprinklers required to suppress the fire | Probability |
|---|-------------|
| 1 | 1 |
| 2 | 0 |
| 3 | 0 |
| 4 | 0 |
| Total | 1 |

Figure 66. Distribution for minimum number of sprinklers required to suppress or control the fire.

8.7 Ceiling jet algorithms

There are two ceiling jet algorithms available for predicting sprinkler or thermal detector response. One uses Alpert's unconfined ceiling jet correlation (Alpert, 1972, 2008), presented in section 8.7.1, while the other uses the JET algorithm (default) developed at the National Institute of Standards and Technology (NIST) (Davis, 1999) and presented in section 8.7.2. The user selects the ceiling jet model using the MISC SETTINGS, MODEL PHYSICS menu item as shown in Figure 67.

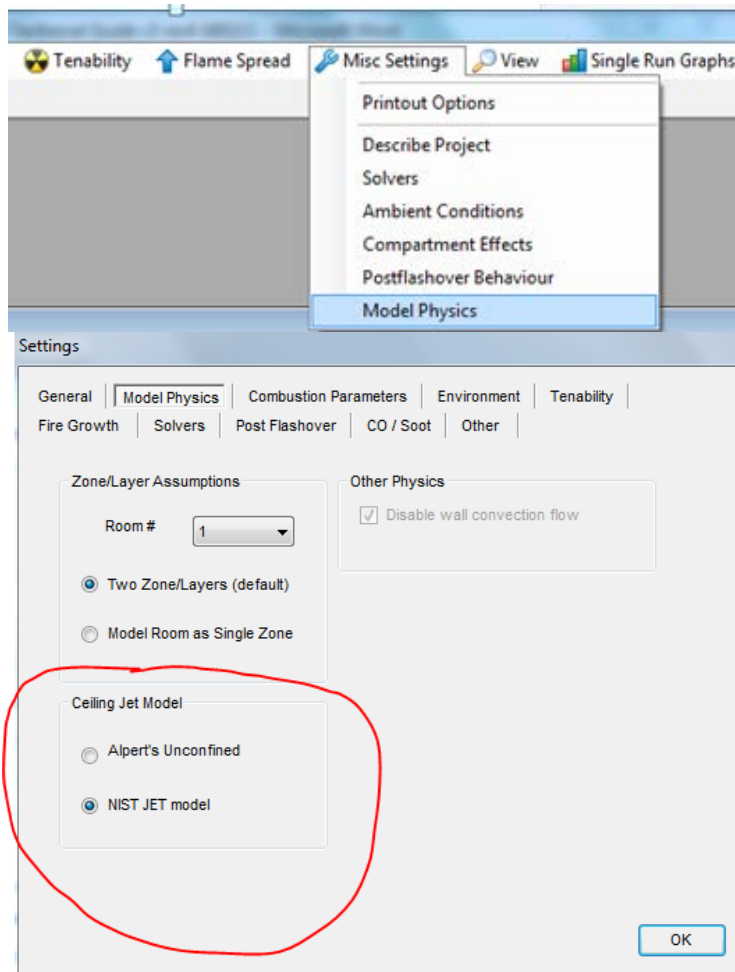


Figure 67. Ceiling jet model selection.

8.7.1 Alpert's correlations

The correlations used for the temperature and velocity of the ceiling jet are those of Alpert (2015) as follows:

$$T_{cj} - T_{int} = \frac{16.9\dot{Q}^{2/3}}{H^{5/3}} \text{ for } \frac{r}{H} \leq 0.18 \quad (164)$$

$$T_{cj} - T_{int} = \frac{5.38\dot{Q}^{2/3}/H^{5/3}}{(r/H)^{2/3}} \text{ for } \frac{r}{H} > 0.18 \quad (165)$$

$$U_{cj} = 0.947 \left(\frac{\dot{Q}}{H} \right)^{1/3} \text{ for } \frac{r}{H} \leq 0.15 \quad (166)$$

$$U_{cj} = 0.197 \frac{(\dot{Q}/H)^{1/3}}{(r/H)^{5/6}} \text{ for } \frac{r}{H} > 0.15 \quad (167)$$

These correlations are for the maximum temperature and velocity in an unconfined ceiling jet, so it is assumed that the detector/sprinkler link is located at the distance below the ceiling at which these maximum values occur.

Equation (169) gives a differential equation describing the temperature of the sensing element.

8.7.2 JET algorithm

The JET algorithm developed at NIST (Davis, 1999) predicts the plume centreline temperature, the ceiling jet temperature and the ceiling jet velocity produced by a single fire plume. The unique feature of this model is that the characteristics of the ceiling jet depend on the depth of the hot layer. The model assumes flames do not touch the ceiling and the fire is located near the centre of the compartment.

Variation of the ceiling jet temperature and velocity with distance below the ceiling is incorporated using the LAVENT method described in NFPA 204 Appendix B (National Fire Protection Association, 1998). The ceiling jet temperature equals the ceiling surface temperature at the ceiling and increases to a maximum value at a certain depth below the ceiling given by:

$$d_{max} = 0.023H \left[\frac{r}{H} \right]^{0.9} \text{ for } r/H > 0.2 \quad (168)$$

Thereafter, the ceiling jet temperature reduces until it equals the upper layer temperature when above the layer interface height.

The differential equation describing the temperature of the sensing element is from Heskestad and Bill (1988), and it incorporates both convective heating of the sensing element and conductive losses to the sprinkler piping. The equation is:

$$\frac{dT_e}{dt} = \frac{\sqrt{U_{cj}}(T_{cj} - T_e)}{RTI} - \frac{C(T_{cj} - T_{int})}{RTI} \text{ for } \frac{r}{H} > 0.2 \quad (169)$$

Based on comparisons with experimental data, the predictions of JET generally agreed with experimental results for compartments with ceiling heights up to 22 m (Davis, 1999).

8.8 Sprinkler output

The input files (inputxxx.xml) created by B-RISK contain the sprinkler data for each iteration. Where parameters have previously been assigned distributions, these files contain the sampled values for each iteration.

```

- <sprinklers NumOperatingSpr="1" spr_cooling_coefficient="1.0000" spr_suppression_prob="0.0000"
  spr_reliability="1.0000" sprink_mode="1">
  - <sprinkler id="1">
    <RTI>95</RTI>
    <c_factor>0.44</c_factor>
    <radial_distance>3.304921</radial_distance>
    <actuation_temp>72</actuation_temp>
    <water_spray_density>0.1</water_spray_density>
    <depth>0.1</depth>
    <x-dim>2.25</x-dim>
    <y-dim>1.5</y-dim>
  </sprinkler>
  - <sprinkler id="2">
    <RTI>95</RTI>
    <c_factor>0.44</c_factor>
    <radial_distance>1.386542</radial_distance>
    <actuation_temp>72</actuation_temp>
    <water_spray_density>0.1</water_spray_density>
    <depth>0.1</depth>
    <x-dim>6.75</x-dim>
    <y-dim>1.5</y-dim>
  </sprinkler>
</sprinklers>

```

The output files (outputxxx.xml) created by B-RISK for each iteration of the model contain the response time for each sprinkler as well as the sprinkler activation time and the number of sprinklers activated.

```

<?xml version="1.0" encoding="UTF-8"?>
<!--Created by BRANZFIRE Version 2012.48-->
- <output>
  - <run num_sprinklers_activated="2" sprinkler_activation_time="131" time_at_VL="0.000" HRR_at_VL="0.000"
    time_at_FO="0.000" HRR_at_FO="0.000" fitted_alpha="0.000" actual_FLED="300.0" sampled_FLED="300.0"
    runtime="8.4" id="input1.xml">
    - <responsetime number="2">
      <sprinkler id="1" units="sec" value="146.0"/>
      <sprinkler id="2" units="sec" value="131.0"/>
    </responsetime>
  </run>
</output>

```

9. Smoke detectors

9.1 General

Smoke detector actuation is predicted based on the smoke concentration at the location of the detector, taking into account the effect and smoke concentration within the ceiling jet if present. Multiple smoke detectors can be positioned within any room.

If multiple items are burning in the room, only the characteristics (e.g. rate of heat release) of the first burning item and its associated ceiling jet are used in the detector response calculation. The contribution from any additional burning item is ignored except for its contribution to the smoke concentration in the hot layer.

Smoke detectors may be added, removed, copied or edited using the SENSORS, SMOKE DETECTORS menu item as shown in Figure 68.

The radial distance between the detector and the fire plume can either be directly specified by the user, or the distance can be calculated based on the coordinates specified for the detector and fire items. For the distance to be calculated, the checkbox shown in Figure 68 must be checked.

If specified smoke detector radial distance from the plume is longer than the length of the room diagonal, the length of the room diagonal is used in the calculations instead of the specified radial distance.

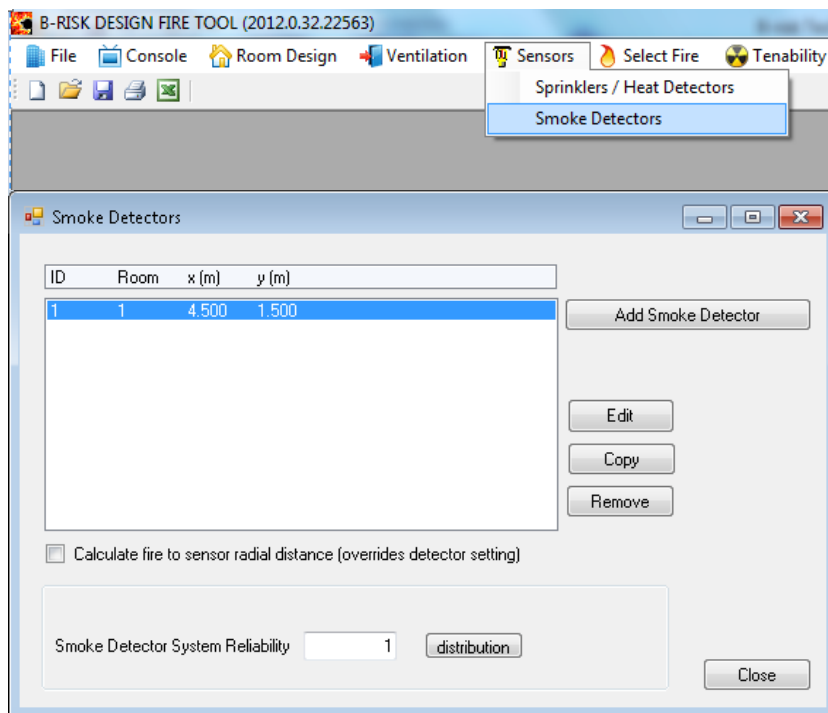


Figure 68. Input form for managing smoke detectors.

The required input property data for each smoke detector is shown in Figure 69.

The user may specify whether the optical density at alarm threshold will apply inside the detector housing or be external to the detector at the specified location. If the checkbox shown in Figure 69 is not checked, the optical density external to the detector will be used.

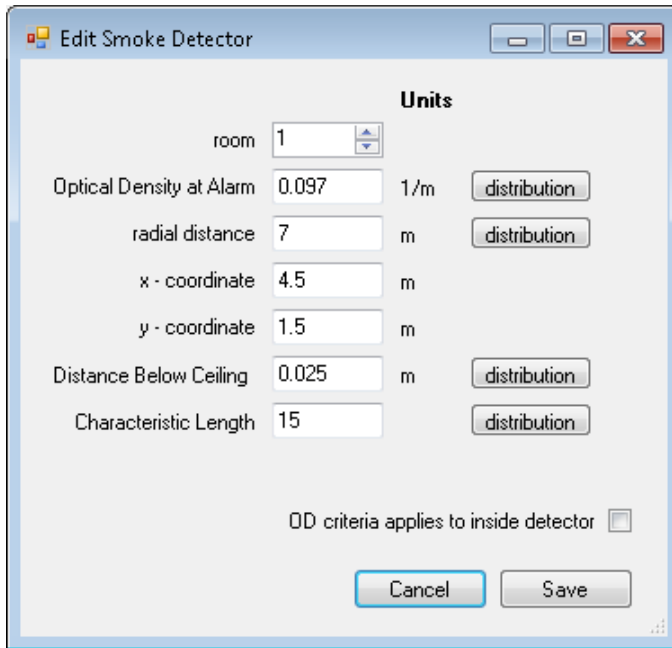


Figure 69. Input form for entering smoke detector properties.

If VM2 user mode is selected, the OD criteria can only be applied to the conditions outside the detector and therefore the characteristic length property will not be used.

Some of the parameters may be assigned statistical distributions. These include the optical density at alarm, radial distance, distance below ceiling and characteristic length. The available probability distributions are normal, uniform, triangular and lognormal.

The file called "smokedets.xml" contains the details about each smoke detector and what distributions, if any, have been assigned.

This file will be found in the relevant project folder under the "riskdata" directory (e.g. C:\Users\...\Documents\B-RISK\riskdata\basemodel_default\smokedets.xml).

9.2 Smoke detection system reliability

A smoke detection system reliability value or an associated probability distribution can be assigned to the reliability of the smoke detection system using the option shown in in Figure 68. For each iteration, the reliability parameter is sampled from the assigned distribution, and then a uniformly selected random number between 0 and 1 is compared to the sampled reliability value. If the random number exceeds the reliability value, the entire smoke detection system is deemed ineffective and will not operate.

9.3 Smoke detector response

Smoke detector response is based on the calculated smoke optical density at the location of the detector. The response time of the detector is calculated using Heskestad's method (1975), while the smoke concentration in the ceiling jet and hence optical density is calculated using a method developed by Davis et al. (2003).

The rate of change of optical density inside the detector housing is given by the following first-order differential equation. This equation is solved at each time step to

determine the time at which the optical density exceeds the threshold value required for the detector to activate:

$$\frac{dD_t}{dt} = \frac{1}{\tau}(D_o - D_i) \quad (170)$$

$$\tau = \frac{l}{u} \quad (171)$$

Where D_o is the optical density outside the detector, D_i is the optical density inside the detector chamber, τ is a time constant for the detector, l is the characteristic length of the detector (which effectively accounts for the time delay for the smoke gases to penetrate the detector housing) and u is the velocity of the ceiling jet at the location of the detector.

Davis et al. (2003) use the concept of a substitute source in the development of a correlation for the smoke concentration in the ceiling jet. The ceiling jet is considered to be submerged within the hot gas layer and thus will be hotter than the case where the hot layer is not present. The substitute source is described by a heat release rate \dot{Q}_2 and location beneath the ceiling H_2 .

\dot{Q}_2 is given by:

$$\dot{Q}_2^* = \left[\frac{D\dot{Q}_1^{*2/3} - C_L(1 + K\dot{Q}_1^{*2/3})}{D + C_LK(1 + K\dot{Q}_1^{*2/3})} \right]^{3/2} \quad (172)$$

$$\dot{Q}_1^* = \frac{\dot{Q}}{\rho_l c_p T_l \sqrt{g(Z - z_o)^{5/2}}} \quad (173)$$

Where $K = 9.1(1 - \lambda_r)^{2/3}$, $C_L = Y_{soot}\rho_u$ is the scalar concentration of smoke in the upper layer and Z is the layer height above the fire while z_o is the location of the virtual point source.

The location of the substitute source Z_2 is given by:

$$\dot{Z}_2 = Z_1 \left[\frac{\dot{Q}_1^*}{\dot{Q}_2^* + \frac{\lambda^2 + 1}{\lambda^2} \frac{C_L}{D} (1 + K\dot{Q}_2^{*2/3}) \dot{Q}_2^{*1/3}} \right]^{2/5} \quad (174)$$

$$D = \frac{Y_s \frac{(\lambda^2 + 1)}{\lambda^2} \rho_l c_p T_l}{3.4 h_c \pi (1 - \lambda_r)^{1/3} (1.201)^2 (0.12)^2} \quad (175)$$

λ is the Gaussian width ratio for the velocity and temperature profiles in the plume where $\lambda^2 = 1.157$.

The maximum concentration at the ceiling on the plume centreline is:

$$C_{spo} = \frac{D\dot{Q}_2^{2/3} \left(\frac{Z_2}{H_2}\right)^{5/3}}{1 + K\dot{Q}_2^{2/3} \left(\frac{Z_2}{H_2}\right)^{5/3}} + C_L \quad (176)$$

The maximum concentration in the ceiling jet at $r = 0.18H$ is:

$$C_{so} = \sqrt{2} \frac{\lambda^2}{\lambda^2 + 1} (C_{spo} - C_L) + C_L \quad (177)$$

Finally, the maximum smoke concentration in the ceiling jet at a radial distance of r from the plume centreline (where $r > 0.18H$) is given by:

$$C_{so}(r) = (C_{so} - C_L) \left(\frac{0.18H}{r}\right)^{0.57} + C_L \quad (178)$$

A more detailed derivation of the above equations is given by Davis et al. (2003).

A further refinement is introduced to account for a variation in the velocity of the ceiling jet with distance below the ceiling. The maximum gas temperature and velocity (and smoke concentration) typically occurs at about 1% of the fire-ceiling height below the ceiling. The ceiling jet velocity affects equation (171) for the time constant and subsequently the rate of change of optical density. Variation of the ceiling jet velocity with distance below the ceiling is incorporated using the LAVENT method described in NFPA 204 Appendix B (National Fire Protection Association, 1998). This modification only affects calculations where the smoke optical density inside the detector is of interest. The calculated optical density outside the detector is a maximum and does not change with distance beneath the ceiling for a given radial distance from the plume centreline.

The optical density limits for actuation are based on AS 1603.2 (Standards Australia, 1989) test limits as described in the Australian Fire Engineering Guidelines (Fire Code Reform Centre, 1996). Three sensitivity classes are given: normal, high and very high, with optical density limits of 0.097, 0.055 and 0.013 m^{-1} respectively. These limits are applicable to photoelectric detectors but are expected to be conservative if applied to ionisation detectors in flaming fires.

Once the time at which the optical density at the detector location exceeds the threshold value (t_{OD}) required for activation, the response time of the smoke detector is calculated including an estimate of the gas transit time for the smoke gases to travel from the fire source to the detector ($t_{transit}$) as given in equations (171) and (172) where H is the vertical distance from the base of the fire to the ceiling, r is the radial distance from the plume to the smoke detector, u_0 is the velocity of the ceiling jet at the ceiling directly above the plume and u_r is the velocity of the ceiling jet at the location of the smoke detector.

$$t_{act,sd} = t_{OD} + t_{transit} \quad (179)$$

$$t_{transit} = \frac{2H}{u_0} + \frac{2r}{(u_0 + u_r)} \quad (180)$$

For smoke detectors located outside the room or fire origin, there is no ceiling jet and therefore no dependence on radial distance. In this case, the average upper layer optical density in the room is compared to the optical density required for response to determine when the detector activates.

In the room of fire origin, the transit time is checked to see if the ceiling jet has reached the detector (a requirement) before the detector is allowed to respond.

For detectors not in the room of fire origin, the detector is not allowed to respond until at least the ceiling jet in the fire room has traversed the length of the fire room diagonal. This transit time is also added to the time at which the optical density criterion is met to give the response time of the detector.

9.4 Smoke detector output

The input files (inputxxx.xml) created by B-RISK contain the sprinkler data for each iteration including the sampled system reliability value and whether the smoke detection system is operational (True) or not (False). Where parameters have previously been assigned distributions, these files contain the sampled values for each iteration.

```
- <smoke_detectors operational_status="True" sys_reliability="1.0000">
  - <smoke_detector id="1" room="1">
    <OD>0.097</OD>
    <radial_distance>7</radial_distance>
    <depth>0.025</depth>
    <x-dim>6</x-dim>
    <y-dim>1.5</y-dim>
    <charlength>15</charlength>
  </smoke_detector>
  - <smoke_detector id="2" room="2">
    <OD>0.097</OD>
    <radial_distance>7</radial_distance>
    <depth>0.025</depth>
    <x-dim>4.5</x-dim>
    <y-dim>1.5</y-dim>
    <charlength>15</charlength>
  </smoke_detector>
</smoke_detectors>
```

The output files (outputxxx.xml) created by B-RISK for each iteration of the model contain the response time for each smoke detector.

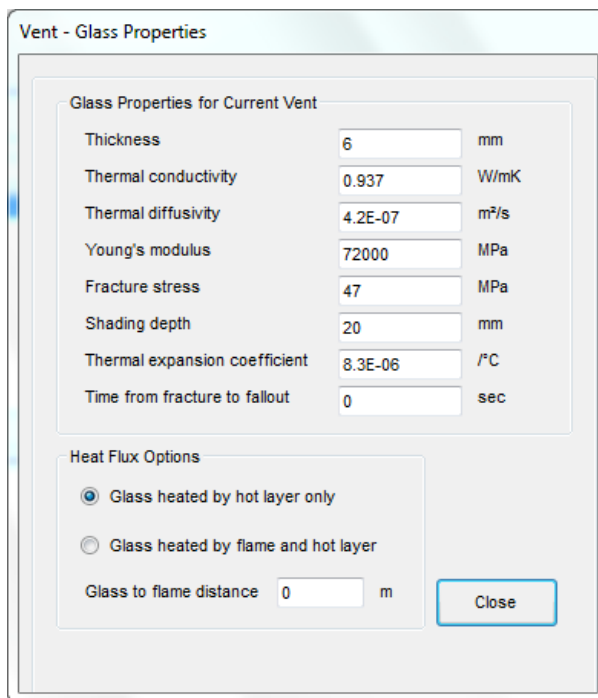
```
<?xml version="1.0" encoding="UTF-8"?>
<!--Created by BRANZFIRE Version 2012.48-->
- <output>
  - <run num_sprinklers_activated="2" sprinkler_activation_time="131" time
    sampled_FLED="300.0" runtime="8.4" id="input1.xml">
    - <responsetime number="2">
      <sprinkler id="1" units="sec" value="146.0"/>
      <sprinkler id="2" units="sec" value="131.0"/>
    </responsetime>
    - <smoke_detectors>
      <smoke_detector id="1" units="sec" responsetime="38.8"/>
      <smoke_detector id="2" units="sec" responsetime="206.0"/>
    </smoke_detectors>
```

10. Glass fracture

An automatic glass fracture model is included based on work by Parry et al. (Parry, 2002; Parry, Wade & Spearpoint, 2003). The model is largely based on the heat transfer model developed by Sincaglia and Barnett (1997) and the fracture criterion of Pagni and Joshi (1991). The finite difference scheme stability criterion was revised from that presented by Sincaglia and Barnett. Routines for assessing flame flux heating have been added. Parry reported predicted fracture times consistent with experimental results from Skelly, Roby and Beyler (1991).

Readers are referred to the publications by Parry et al. (Parry 2002; Parry, Wade & Spearpoint, 2003) for details of how the model has been implemented in B-RISK.

The model does not predict fallout times. This can be specified by the user. A time from fracture to fallout of 0 sec will cause the vent to be opened at the predicted time of glass fracture. The input form for entering glass properties is shown in Figure 70.



Vent - Glass Properties

Glass Properties for Current Vent

| | | |
|-------------------------------|---------|-------------------|
| Thickness | 6 | mm |
| Thermal conductivity | 0.937 | W/mK |
| Thermal diffusivity | 4.2E-07 | m ² /s |
| Young's modulus | 72000 | MPa |
| Fracture stress | 47 | MPa |
| Shading depth | 20 | mm |
| Thermal expansion coefficient | 8.3E-06 | /°C |
| Time from fracture to fallout | 0 | sec |

Heat Flux Options

Glass heated by hot layer only

Glass heated by flame and hot layer

Glass to flame distance m

Close

Figure 70. Input form for vent – glass properties.

11. Fire growth on surface linings

11.1 General

B-RISK includes a flame spread and fire growth model developed principally for the room-corner fire scenario but also generalised to function with distributed room contents using the design fire generator.

The fire growth model is based on the work of Quintiere (1993) and accounts for both wind-aided and opposed flow flame spread. A number of improvements and modifications to the original Quintiere model have been made as described here.

The design fire generator allows individual items in the room to ignite the wall and/or ceiling lining, but this occurs only once each for the wall and ceiling by whichever item is responsible for the earliest ignition event.

The flame spread and fire growth model is not enabled by default and can be selected by the user from the FLAME SPREAD, FLAME SPREAD SETTINGS menu item as shown in Figure 71. The burner is the source of ignition for the surface linings and is represented as a square gas burner. The use of the flame area constant and flame length power are described in section 11.8.

The ignition and flame spread properties of the surface linings are characterised using time to ignition and rate of heat release data from cone calorimeter tests.

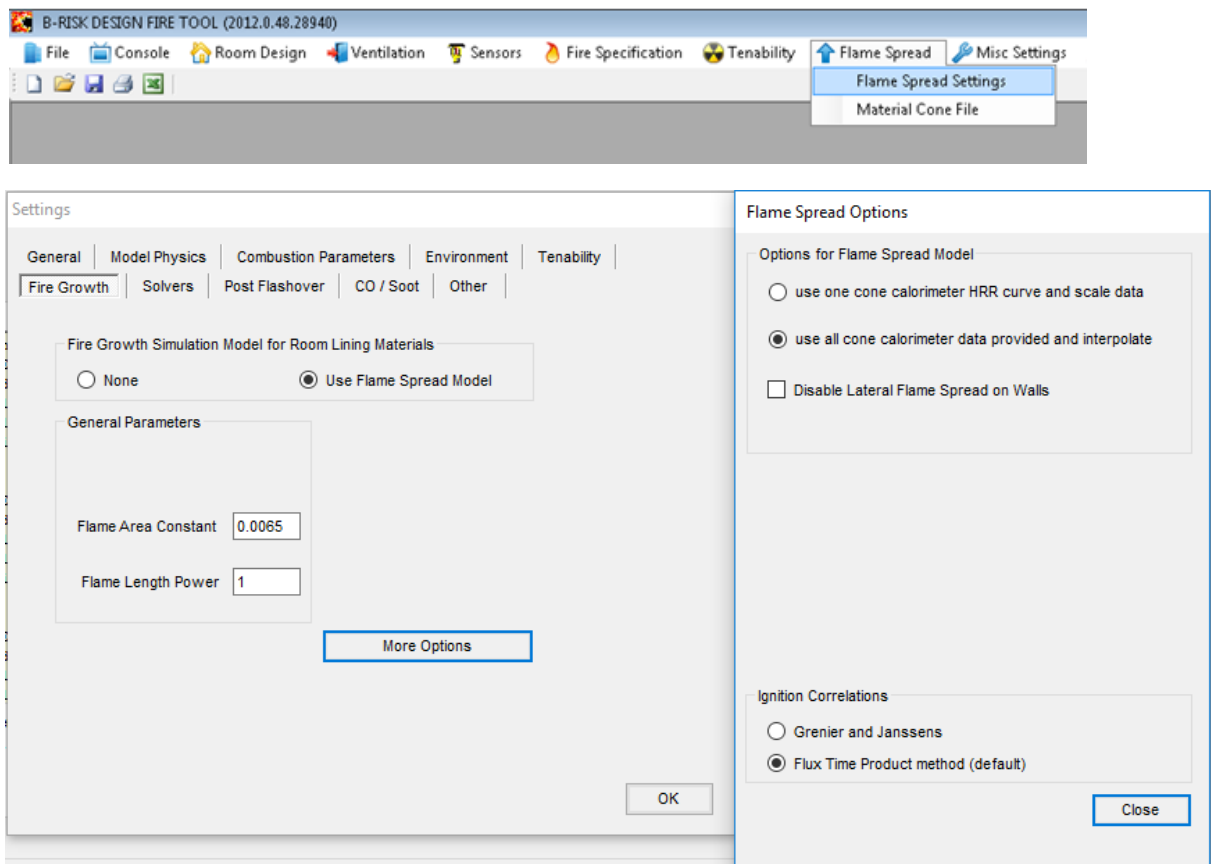


Figure 71. Flame spread settings.

11.2 Quintiere's room-corner model

This flame spread and fire growth model is generally based on previous work by Quintiere (1993). B-RISK predicts ignition, flame spread and the resultant heat released by the wall and ceiling lining material. Two modes of flame spread are considered. Upward flame spread includes fire spread up the wall, beneath the ceiling and along the wall/ceiling intersection on the wall in the region of the ceiling jet. The opposed flow flame spread includes lateral flame spread on the wall originating at the burner location and downward spread on the wall from the ceiling jet region.

While Quintiere's model has been used as the basis of the model described here, a number of significant modifications and changes have been incorporated. These include the following:

- Assuming a non-uniform burning rate based on time-dependent heat release rate data measured in a cone calorimeter.
- Ordinary differential equations for both the upward and lateral pyrolysis fronts are solved. However, only the upward, not lateral, burnout front is solved.
- Estimating the flame flux from a burning object to the wall as described in the next section. Quintiere originally assumed 60 kW/m². The wall region first ignited is assumed to be bounded by the calculated flame height and the side dimensions of the burner.
- Assuming the flame flux in the pyrolysing regions (but outside the burner region) is 35 kW/m² (as discussed later), while the assumed flame flux ahead of the flame front (i.e. regions not yet ignited but subject to preheating) is assumed to be 30 kW/m².
- A new correlation is used to estimate the heat flux from the burner flame to the room surfaces depending on the heat output of the burner.
- Determining the surface temperatures for the wall and ceiling using a finite difference method with the upper layer temperature as a boundary condition. The upper layer temperature is determined from a mass and energy balance for the room. As a result, an upper layer temperature correlation is not used.
- Adding subroutines to account for the direct ignition of the ceiling lining (independent of wall ignition).
- Integration with the design fire generator allows secondary burning items to also ignite wall and/or ceiling linings.

11.3 Characterising the burner

In the ISO 9705 room-corner test (ISO, 1993), the wall is ignited with a propane gas burner of output 100 kW for the first 600 seconds, which is then increased to 300 kW until completion of the test at 1,200 seconds. The burner dimensions are specified using the item length, width and height properties for the item as shown in Figure 27. Dimensions for the standard ISO 9705 gas burner are 0.17 m, 0.17 m and 0.3 m for the length, width and height respectively.

The height of the burner flame, L , in the room-corner test is determined using a correlation from Lattimer (2002).

$$\frac{L}{b_w} = 5.9\sqrt{Q^*} \quad (181)$$

Where $Q^* = Q_b / (1110b_w^{5/2})$ and b_w is the width of one side of a square burner.

To generalise this for the DFG, where the room items comprise rectangular-shaped items, the average plan dimension of the item is used for burner width.

$$b_w = \frac{\text{item length} + \text{item width}}{2} \quad (182)$$

The burner may also be located against a wall or in the centre of the room as well as in a room corner. This has been allowed for by selecting correlations for the burner flame height appropriate to the burner position. The Heskestad correlation for a burner located in the centre of the room is (Heskestad, 1984):

$$L = -1.02D + 0.235\dot{Q}_b^{2/5} \quad (183)$$

The same flame height correlation is also used when the burner is placed against a wall.

When a room is populated with contents, any item within a grid width interval of a wall as shown in the room population screen is assigned a "wall" location, whereas if the item is within a grid interval of two adjacent walls, it is assigned a "corner" location.

Heat flux correlations for a fire in the corner of a room were developed by Lattimer (2002). In a corner situation, the peak heat flux to the wall is given as a function of the burner dimension by:

$$\dot{q}_w'' = 120[1 - e^{-4.0b_w}] \quad (184)$$

The maximum heat flux to the ceiling in the corner (at the point of impingement) is given by:

$$\dot{q}_c'' = 120 \text{ for } (H/L) \leq 0.52 \quad (185)$$

$$\dot{q}_c'' = 13(H/L)^{-3.5} \text{ for } (H/L) > 0.52 \quad (186)$$

The method for determining the heat flux from the burner flame against a flat wall is based on work by Back et al. (1994). They developed a correlation based on square propane burners against a wall. The burners varied in output from 50–500 kW and had edge lengths of 0.28–0.70 m. The maximum heat flux incident to the wall from the burner flame is given by:

$$\dot{q}_w'' = E(1 - e^{-k\dot{Q}_b^{1/3}}) \quad (187)$$

Where $E = 200 \text{ kW/m}^2$ and $k = 0.09 \text{ kW}^{-1/3}$. This heat flux was assumed to be constant over the wall area up to the height of the flame. Above the flame height, the heat flux reduces with height (Z) according to:

$$\dot{q}_w'' = 20(Z/L)^{-5/3} \quad (188)$$

This latter equation is used for estimating the heat flux at ceiling level prior to ignition of the wall, with $Z=H$. The heat flux on the ceiling surface directly above the fire plume, for a fire location away from walls is given by (Lawson & Quintiere, 1985):

$$\dot{q}_c'' = 0.28\dot{Q}_b^{5/6}(H)^{-7/3} \quad (189)$$

This equation assumes the heat flux is mostly convective so may underestimate the total flux.

The heat flux to the wall for a fire location away from walls is based on a point source model, in the same manner as used for the DFG item-to-item fire spread (see section 4.3.2).

$$\dot{q}_w'' = \frac{\lambda_r \dot{Q}_b}{4\pi r^2} \quad (190)$$

11.4 Ignition of the wall lining

There are two methods for determining the ignition time for the wall depending on which ignition data correlation has been selected. When the flux time product (FTP) method (Silcock & Shields, 1995) is used, the time for the wall lining to ignite (t_{ig}) is that time after which the flux time product for the material has exceeded the FTP_n value determined from the correlation of the cone calorimeter ignition data as described in section 11.11.2 and expressed as:

$$FTP_n = \int_0^{t_{ig}} (\dot{q}_e'' - \dot{q}_{cr}'')^n \quad \text{where } \dot{q}_e'' > \dot{q}_{cr}'' \quad (191)$$

The incident heat flux exposing the wall \dot{q}_e'' in the region of the burner flame, \dot{q}_{net}'' , is given by summing the incident heat flux from the flame, \dot{q}_w'' , and the incident heat flux due to the heated gas layers and other room surfaces, \dot{q}_{int}'' as follows:

$$\dot{q}_{net}'' = \dot{q}_w'' + \dot{q}_{int}'' \quad (192)$$

When the Grenier and Janssens (1997) method of correlating the ignition data is selected, a finite difference scheme is used to determine the surface temperature of the wall lining and the wall is ignited when the ignition temperature is reached.

11.5 Energy release rate – Method 1

Two methods are provided for determining the heat released over time by the surface lining materials. The first (Method 1) uses cone calorimeter test data obtained at only a single heat flux, while the second (Method 2) uses cone calorimeter test data obtained using a range of external heat fluxes. Method 2 is recommended to the user whenever possible.

Method 1 estimates the energy release rate from burning room lining materials based on the input of cone calorimeter data at a single heat flux and extrapolates to estimate the energy release at different imposed heat fluxes.

The peak heat release rate per unit area for the lining material is estimated, as generally described by Quintiere, as follows:

$$\dot{Q}_p'' = \frac{\Delta H_c}{L_g} (\dot{q}_w'' + \dot{q}_{int}'' - \epsilon\sigma T_{ig}^4) \quad (193)$$

Where \dot{q}_w'' is the applicable flame heat flux over the pyrolysis region, \dot{q}_{int}'' is the heat flux from the hot gas layer and other room surfaces (excluding the reradiation term)

and T_{ig} is the assumed temperature of the pyrolysing surface being equal to the ignition temperature of the surface or the surface temperature determined from the zone model, whichever is the higher. The effective heat of combustion from the cone calorimeter is represented by $\Delta H_{c,r}$ and L_g is the heat of gasification determined by the model from a correlation of the peak heat release rate data from cone calorimeter experiments.

The model separately considers the pyrolysing region outside the burner flame region from that impinged on by the burner flame. While the burner flame heat flux is calculated as described above, the flame flux to the material outside the burner region is taken as 35 kW/m².

The model normalises the input heat release rate curve (from the cone calorimeter) by dividing by the peak heat release rate ($\dot{Q}_{p, cone}''$, from the cone test) at each time step. The value of the peak rate of heat release determined by equation (193) is then multiplied by the normalised ratio given that the elapsed time from ignition is known.

$$\dot{Q}''(t) = \frac{\dot{Q}_c''(t)}{\dot{Q}_{p, cone}''} \dot{Q}_p'' \quad (194)$$

The model also makes a transformation of the new heat release rate curve by scaling the time axis so that the total area under the curve (total energy available) remains the same as that measured in the cone calorimeter test as illustrated in Figure 72.

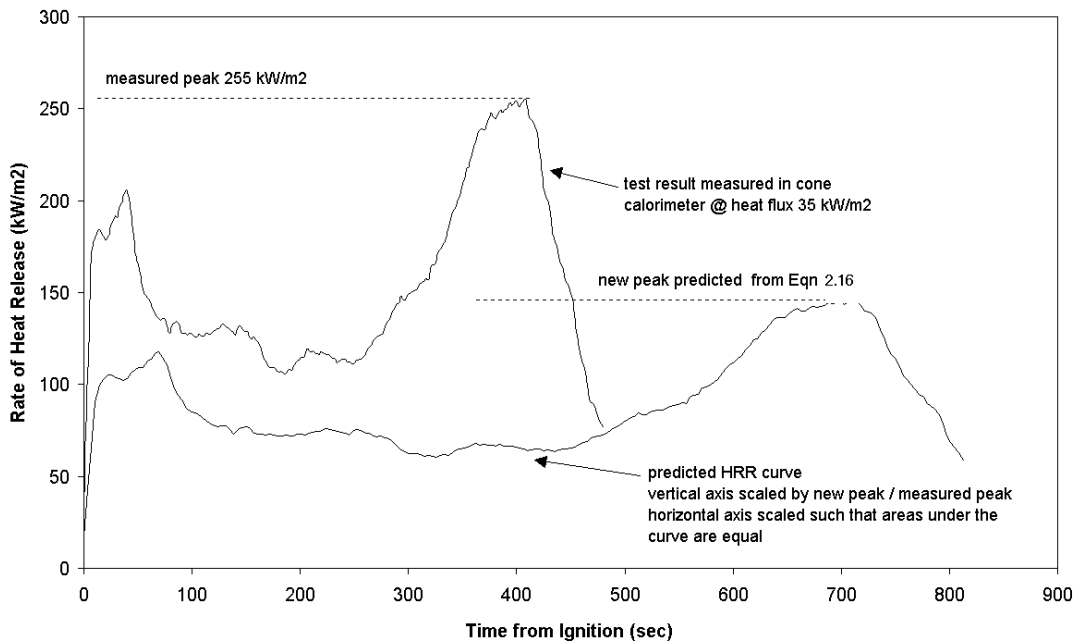


Figure 72. Transformation of the heat release rate curve.

The total energy released is the sum of that from the burner, the walls and the ceiling, and this is given by:

$$\dot{Q}(t) = \dot{Q}_b + \sum (\dot{Q}''(t) \Delta A_p(t)) \quad (195)$$

Where \dot{Q}_b is the heat release rate of the burner, $\dot{Q}''(t)$ is the heat release rate per unit area from the lining material at time t and ΔA_p is the incremental pyrolysis area. At each time step, the pyrolysis area is calculated as described below and the time step at which each incremental area first ignited is therefore known. The total heat release rate is the sum of the incremental pyrolysis areas multiplied by the time-dependent heat release rate for each incremental area.

11.6 Energy release rate – Method 2

This method estimates the energy release rate from burning room lining materials based on the input of cone calorimeter data at multiple heat fluxes and interpolates the data to estimate the energy release at a specified imposed heat flux based on the elapsed time since ignition.

The total energy released is the sum of that from the burner, the walls and the ceiling, and this is given by:

$$\dot{Q}(t) = \dot{Q}_b + \sum (\dot{Q}''(t) \Delta A_p(t)) \quad (196)$$

Where \dot{Q}'' is the energy release per unit area for each incremental area and depends on the elapsed time of burning for each incremental area. This is determined from the available set of cone calorimeter heat release rate curves for the material determined for a range of external heat fluxes. The data set is interpolated using a cubic spline technique (Eagle, 1997) to determine the applicable energy release rate given the elapsed time from ignition and the imposed heat flux to the wall. Data is extrapolated so that, where the imposed heat flux is outside the range bounded by the cone calorimeter tests, the energy release rate is estimated by multiplying the data from the nearest curve by the ratio of the predicted incident flux to the cone curve external flux. The heat release rate of the burner is represented by \dot{Q}_b , and ΔA_p is the incremental pyrolysis area. At each time step, the pyrolysis area is calculated as described below and the time step at which each incremental area first ignited is therefore known. The total heat release rate is the sum of the incremental pyrolysis areas multiplied by the time-dependent heat release rate for each incremental area.

This method relies on the availability of time-dependent cone calorimeter heat release rate data for a range of different heat fluxes (typically ranging from 25 to 75 kW/m²) and is the preferred method.

11.7 Determining the pyrolysis area

There are two cases to consider. The first is when the pyrolysis front has not yet reached the ceiling, and the second is when it has. The area calculations are the same as those described by Quintiere (1993). In the first case, the wall adjacent to the burner has ignited and is pyrolysing, while the pyrolysis front has not yet reached the ceiling, as shown in Figure 73. The region initially adjacent to the burner is defined by $(x_{p,0}, y_{p,0})$. On ignition of the wall, $x_{p,0} = b_w$ m and $y_{p,0} = 0.4L$ m, where $y_{p,0}$ represents the height of the ignited region above the burner, L is the flame height and $x_{p,0}$ represents the width of the burner.

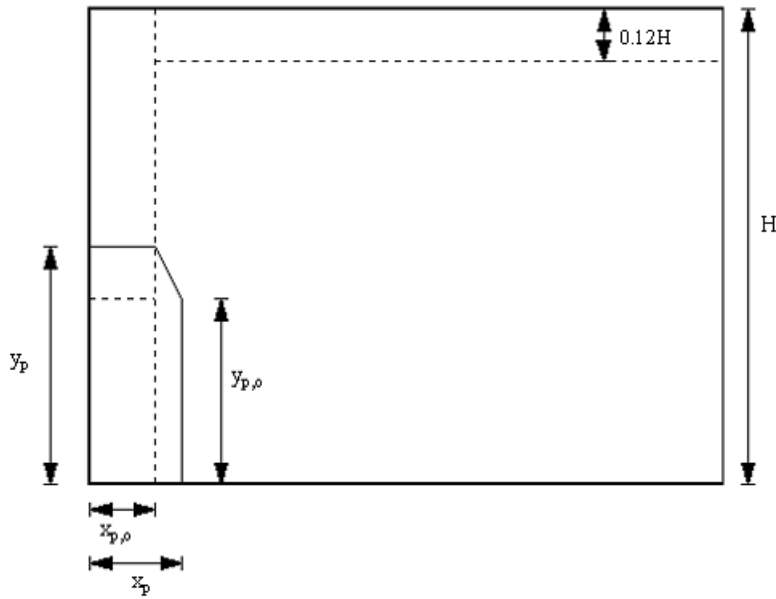


Figure 73. Wall ignited – pyrolysis front has not reached the ceiling.

The pyrolysis area is given by:

$$A_p = 2[y_p x_{p0} + (x_p - x_{p0})y_{p0} + 0.5(y_p - y_{p0})(x_p - x_{p0})] \quad (197)$$

In the second case, the wall adjacent to the burner has ignited and is pyrolysing, and the pyrolysis front has reached the ceiling, as shown in Figure 74.

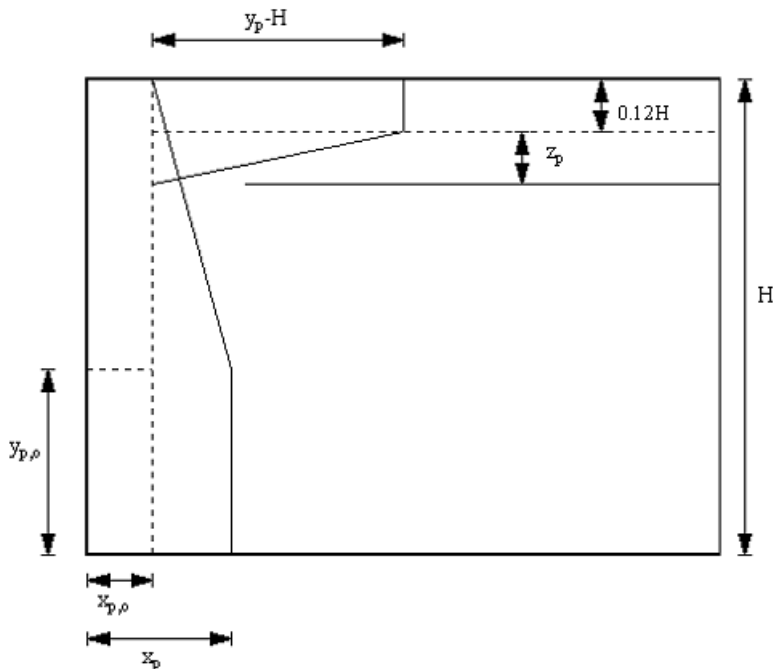


Figure 74. Wall ignited – pyrolysis front has reached the ceiling.

The total pyrolysis area will be the sum of three areas – the wall area A_{p1} , the ceiling jet area A_{pj1} and the ceiling area A_{pc1} .

The required equations are:

$$A_{p1} = 2[Hx_{po} + (x_p - x_{po})y_{po} + 0.5(x_p - x_{po})(H - y_{po})] \quad (198)$$

$$z_p = x_p - x_p(t_H) \quad (199)$$

Where t_H is the time when the γ -pyrolysis front reaches the ceiling.

And for $z_p = 0$,

$$A_{pj1} = 2(y_p - H)(0.12H) \quad (200)$$

And for $z_p > 0$,

$$A_{pj1} = 2 \left[(y_p - H)(0.12H) + 0.5z_p(y_p - H) - 0.5(0.12H + z_p)^2 \left[\frac{x_p - x_{po}}{H - y_{po}} \right] \right] \quad (201)$$

$$A_{pc1} = \text{the lesser of the ceiling area or } \frac{\pi}{4(y_p - H)^2} \quad (202)$$

$$A_p = A_{p1} + A_{pj1} + A_{pc1} \quad (203)$$

The depth of the ceiling jet is taken as 12% of the ceiling height above the burner surface, being an upper end rule-of-thumb estimate from Evans (1988).

11.8 Upward flame spread

The governing equation for upward flame spread is given by Quintiere as:

$$\frac{dy_p}{dt} = \frac{y_f - y_p}{t_{ig}} \quad (204)$$

Where, for thermally thick materials, t_{ig} is given by:

$$t_{ig} = \frac{\pi}{4} k\rho c \left[\frac{T_{ig} - T_s}{\dot{q}_{ff}''} \right]^2 \quad (205)$$

The heat flux ahead of the flame, \dot{q}_{ff}'' , is assumed to be 30 kW/m², while T_s is the lining surface temperature and $k\rho c$ is determined as described in section 11.11.1. The position of the upward pyrolysis front is represented by y_p , and y_f is the flame length in the upward direction.

Alternatively, where the FTP method (Silcock & Shields, 1995) is used to correlate the ignition data, the time to ignition expression used is:

$$t_{ig} = FTP_n (\dot{q}_{ff}'' - \dot{q}_{cr}'')^{-1/p} \quad (206)$$

For the case where the flame from the wall or ceiling material is contiguous with the burner flame, the flame length y_f is given by equations (181) or (183) depending on the location of the burner and with Q taken as the heat release from both the burner and lining material.

The upward burnout front is also modelled to determine the case where the burner flame and wall-ceiling flame are not contiguous or have separated as:

$$\frac{dy_b}{dt} = \frac{y_p - y_b}{t_b} \quad (207)$$

Where y_b is the position of the upward burnout front, t_b is a burnout time (s) and is equal to the area under the heat release rate curve (kJ/m^2) divided by the applicable heat release rate for the lining material (kW/m^2) at a particular time (from the small-scale cone calorimeter data).

When $y_b >$ burner flame length, the burner flame and the wall-ceiling flame are assumed to be non-contiguous or separate. In this case, the position of the flame front is given by:

$$y_f = y_b + K (\dot{Q}_p'' - (y_p - y_b))^n \quad (208)$$

Where K is the flame area constant ($=0.0065$), n is the flame length power ($=1$) (Kokkala, Baroudi & Parker, 1997) and \dot{Q}_p'' is the heat release rate per unit area for the lining material. When Method 1 (section 11.5) for determining the energy release rate is used, \dot{Q}_p'' is determined from equation (193). When Method 2 (section 11.6) for determining the energy release rate is used, \dot{Q}_p'' is determined by interpolation of the peak heat release rates from the cone calorimeter data provided.

In addition, the model allows for the height of the burner above the floor and takes this into account in the calculations, although this is not shown in equations (207) and (208). This height is typically 0.3 m for the ISO 9705 burner.

Although the model allows for different lining materials to be specified for the wall and ceiling lining respectively, only one governing upward flame spread rate is calculated. Since the flame spread rate could be influenced by the ceiling material or by that wall material in the ceiling jet region beneath the ceiling, B-RISK uses the worst case and thus the material with the lower ignition temperature in equations (204) and (207).

11.9 Independent ignition of the ceiling lining

B-RISK also allows for separate materials to be specified as the wall and ceiling lining, and therefore there may be instances where the ceiling lining is ignited directly by the fire plume, instead of progressive flame spread originating from the wall lining material. It may also be that a non-combustible or inert material is used for the wall lining so that it would never ignite, thus the possibility of direct ceiling ignition has been considered.

For a corner fire, the incident heat flux on the ceiling is determined using equations (184) to (186) depending on the position of the flame tip in relation to the ceiling. Additional heating by the gas layers and other room surfaces are also added.

For a wall fire, the incident heat flux on the ceiling is determined using equation (187) if the flame is touching the ceiling or from equation (188) if the burner flame is not touching the ceiling. Additional heating by the gas layers and other room surfaces are also added.

$$\dot{Q}_{ceiling}'' = \dot{q}_w'' + \dot{q}_{int}'' \quad (209)$$

Following ignition of the ceiling, the pyrolysis area and heat release is determined at each time step. The area first ignited is assumed to be a quarter-circle for a fire in a corner, a semi-circle for a fire against a wall and a full circle for a fire in the centre of the room with a radius of $y_p - H$ in each case (where y_p is measured from the floor and H is the floor to ceiling height).

When the fire is located in the corner or against a wall, the pyrolysis area on the ceiling is compared to the area determined in the previous case involving progressive spread from the wall to the ceiling, and the greater of the two areas is used.

11.10 Lateral and downward flame spread

The lateral pyrolysis front is given by:

$$\frac{dx_p}{dt} = \frac{\Phi}{k\rho c(T_{ig} - T_s)^2} \quad (210)$$

Where Φ is a flame spread parameter. Equation (210) is only applicable for $T_s > T_{s,min}$ where $T_{s,min}$ is the minimum surface temperature for spread, noting that T_s and $T_{s,min}$ are determined from the LIFT test (American Society for Testing Materials, 1990).

11.11 Material property data

11.11.1 Method of Grenier and Janssens

Input of data for the wall/ceiling materials

The user supplies information about the lining material from cone calorimeter tests. The test heat flux, the time to ignition and the peak heat release rate achieved are required. The model will then correlate the ignition data to estimate the ignition temperature and effective thermal inertia and will correlate the peak heat release rate to estimate the heat of gasification. Data measured at a minimum of three external heat fluxes is required, although a greater number of external heat fluxes are preferred. The method used is described in the following subsections.

Ignition temperature and thermal inertia

The procedure for determining the surface temperature for ignition T_{ig} and the effective thermal inertia $k\rho c$ from cone calorimeter measurements is taken from Grenier and Janssens (1997) and Janssens (1991, 1992b):

1. Samples are tested at a range of different irradiance levels (at least three). Ideally, there should be replicates tested at each irradiance. The average time to ignition, t_{ig} , for each heat flux is determined. Taking the time to ignition, t_{ig} as the time for the heat release rate to reach 30 kW/m² agreed reasonably well with the observed ignition times.

2. Correlate the ignition times by plotting $(1/t_{ig})^n$ on the Y-axis versus \dot{q}_e'' on the X-axis. Determine the value of n that results in the highest coefficient of determination (R^2), allowing n to be in the range 0.547 to 1.
3. Determine the X-intercept from a straight line fit through the data. The X-intercept is taken as the critical heat flux for ignition \dot{q}_{cr}'' .
4. Solve (by iteration) the following equation for the surface temperature for ignition, T_{ig} taking the convective heat transfer coefficient $h_c = 0.0135 \text{ kW/m}^2\text{K}$, and surface emissivity at ignition, ϵ as appropriate for the material.

$$\epsilon \dot{q}_{cr}'' = h_c(T_{ig} - T_\infty) + \epsilon \sigma(T_{ig}^4 - T_\infty^4) \quad (211)$$

5. Solve the following equation for the total heat transfer coefficient for the surface at ignition.

$$h_{ig} = \frac{\epsilon \dot{q}_{cr}''}{(T_{ig} - T_\infty)} \quad (212)$$

6. Plot the ignition data again, this time assuming thermally thick behaviour and using $n=0.547$. Include the data point \dot{q}_{cr}'' from above on the X-axis.
7. Determine the slope of a straight line drawn through two points. The \dot{q}_{cr}'' from above on the X-axis and the data point for the highest heat flux. This is a simplification to make the calculation easier.
8. Compute the apparent thermal inertia, $k\rho c$ as:

$$k\rho c = h_{ig}^2 \left[\frac{1}{0.73b\dot{q}_{cr}''} \right]^{1.828} \quad (213)$$

Heat of gasification

The heat of gasification for the material is determined from a correlation of the peak rate of heat release from cone calorimeter tests following the methodology of Quintiere (1993). The cone test results will also provide the effective heat of combustion, ΔH_c (kJ/g). This is required for the following procedure:

1. Correlate the peak heat release rate by plotting \dot{q}_{peak}'' on the Y-axis versus \dot{q}_e'' on the X-axis.
2. Determine the slope of a linear regression line through the data.
3. Calculate the heat of gasification L_g as follows:

$$L_g = \frac{\Delta H_c}{\text{slope}} \quad (214)$$

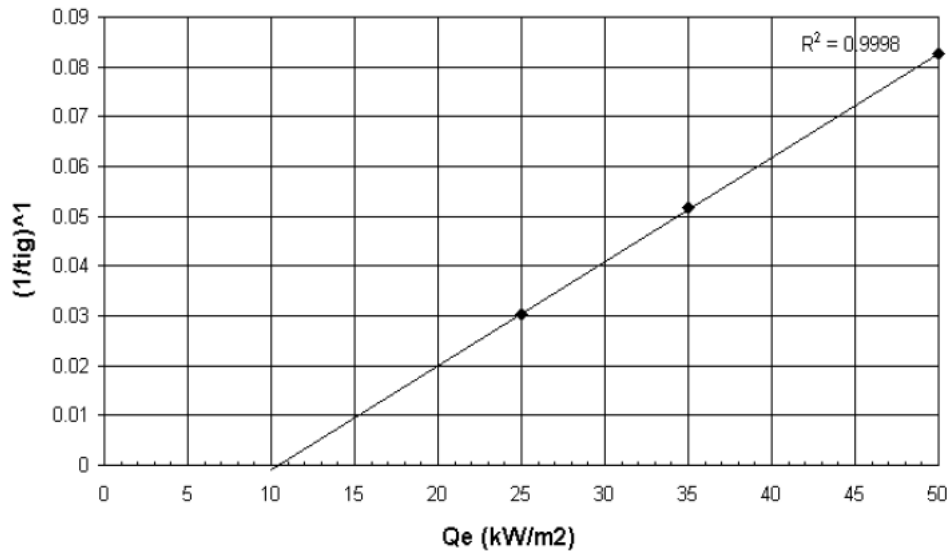
Example

A material has been tested in a cone calorimeter with the results shown in Table 9. The average effective heat of combustion for the material was determined to be 13 kJ/g.

Correlate the ignition times by plotting $(1/t_{ig})^n$ on the Y-axis versus \dot{q}_e'' on the X-axis as shown in Figure 75. By trial and error, the value of n that resulted in the highest coefficient of determination (R^2) and in the range 0.547 to 1 was 1. This indicates thermally thin behaviour.

Table 9. Summary of data from cone calorimeter tests.

| Heat flux (kW/m ²) | Time to ignition (s) | Peak HRR (kW/m ²) |
|--------------------------------|----------------------|-------------------------------|
| 50 | 12 | 137.9 |
| 35 | 19 | 106.7 |
| 25 | 33 | 90.0 |


Figure 75. Correlation of ignition times for best-fit n.

Determine the X-intercept from a straight line fit through the data. The X-intercept is taken as the critical heat flux for ignition \dot{q}_{cr}'' , and here it is determined to be 10.4 kW/m².

Solve (by iteration) the following equation for the surface temperature for ignition, T_{ig} taking the convective heat transfer coefficient $h_c = 0.0135$ kW/m²K, and surface emissivity $\epsilon = 0.88$, $T_\infty = 293$ K and $\dot{q}_{cr}'' = 10.4$ kW/m².

$$\epsilon \dot{q}_{cr}'' = h_c (T_{ig} - T_\infty) + \epsilon \sigma (T_{ig}^4 - T_\infty^4)$$

T_{ig} is determined to be 307°C.

Solve the following equation for the total heat transfer coefficient (kW/m²K) for the surface at ignition:

$$h_{ig} = \frac{\epsilon \dot{q}_{cr}''}{(T_{ig} - T_\infty)} = \frac{0.88 \times 10.4}{(307 - 20)} = 0.032$$

Plot the ignition data again, this time assuming thermally thick behaviour and using $n=0.547$ and including the data point \dot{q}_{cr}'' from above on the X-axis as shown in Figure 76. Determine the slope of the (dashed) line drawn through the highest and lowest points.

$$\text{slope} = \frac{(1/12)^{0.547}}{(50 - 10.4)} = 0.00645$$

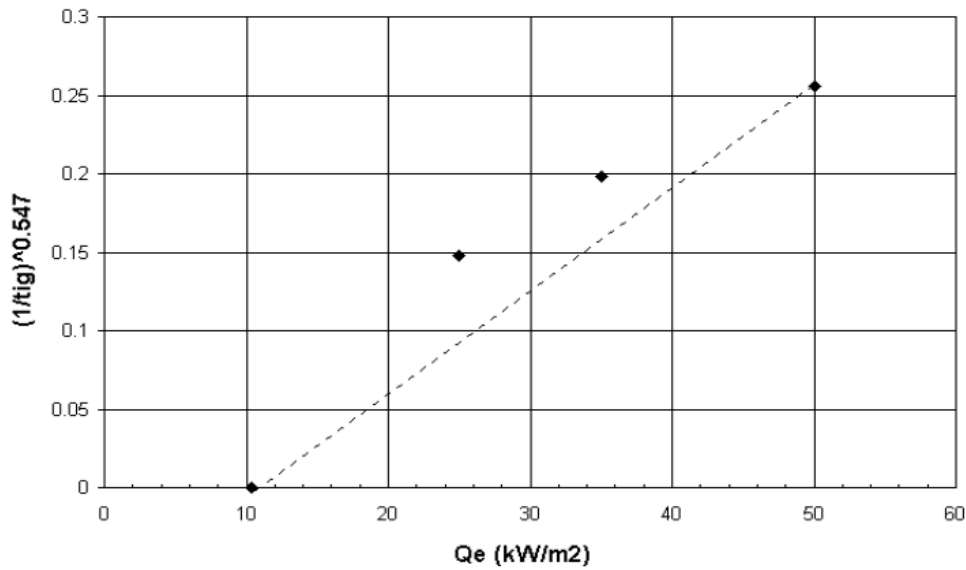


Figure 76. Correlation of ignition times for n=0.547.

Compute the apparent thermal inertia, $k\rho c$ as:

$$k\rho c = h_{ig}^2 \left[\frac{1}{0.73b\dot{q}_{cr}''} \right]^{1.828} = (0.032)^2 \left[\frac{1}{0.73(0.00645)(10.4)} \right]^{1.828} = 0.253$$

Correlate the peak heat release rate by plotting \dot{q}_{peak}'' on the Y-axis versus \dot{q}_e'' on the X-axis as shown in Figure 77. The slope of the linear regression line is found to be 1.93.

Calculate the heat of gasification L_g .

$$L_g = \frac{\Delta H_c}{\text{slope}} = \frac{13}{1.93} = 6.7 \text{ kJ/g}$$

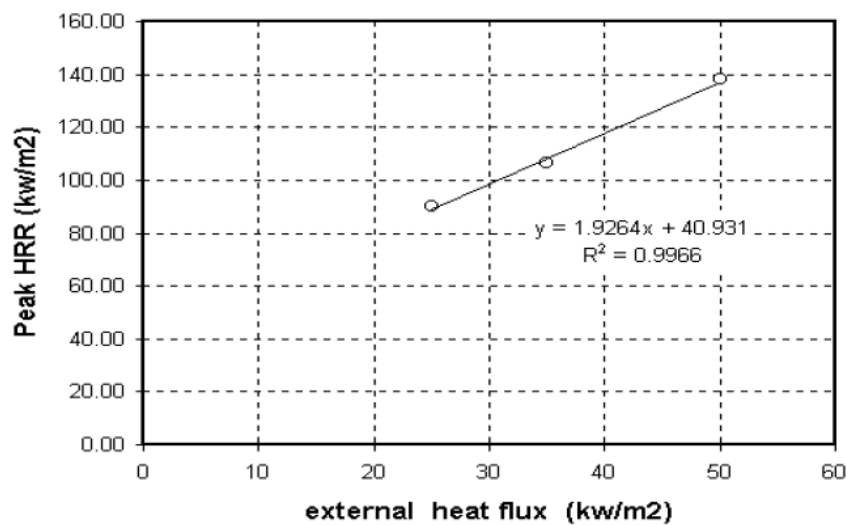


Figure 77. Correlation of peak heat release rates.

11.11.2 Flux time product method

The flux time product (FTP) method is described by Silcock and Shields (1995). They correlated the ignition data assuming a power law expression based on physically consistent dimensionless groups to give the following:

$$(\dot{q}_e'' - \dot{q}_{cr}'')^n t_{ig} = FTP_n \text{ for } n \geq 1 \quad (215)$$

FTP is the flux time product, and n is the flux time product index. Rearranging equation (215) gives:

$$\dot{q}_e'' = \dot{q}_{cr}'' + \frac{FTP_n^{1/n}}{t_{ig}^{1/n}} \quad (216)$$

This represents a straight line by plotting time to ignition raised to the power 1/n against the externally applied heat flux. The value of n resulting in the best fit is determined within the range 1 (thermally thin) to 2 (thermally thick). The FTP_n can then be determined from the slope of the line.

$$FTP_n = (\text{slope})^n \quad (217)$$

Then for any specified external heat flux, the time to ignition is given by rearranging equation (215), and this is equivalent to equation (206) with $n=1/p$.

$$t_{ig} = \frac{FTP_n}{(\dot{q}_e'' - \dot{q}_{cr}'')^n} \quad (218)$$

The flux time product method does not require the effective thermal inertia to be determined.

References

- Alpert, R. L. (1972). Calculation of response time of ceiling-mounted fire detectors. *Fire Technology*, 8, 181–195.
- Alpert, R. L. (2008). Ceiling jet flows. In *SFPE handbook of fire protection engineering* (4th ed.). Quincy, MA: National Fire Protection Association.
- Alpert, R. L. (2015). Ceiling jet flows. In *SFPE handbook of fire protection engineering* (5th ed.). Quincy, MA: National Fire Protection Association.
- American Society for Testing Materials. (1990). ASTM E 1321-90 *Standard test method for determining material ignition and flame spread properties*. Philadelphia, PA: Author.
- Babrauskas, V. (2008). Heat release rates. In *SFPE handbook of fire protection engineering* (4th ed.). Quincy, MA: National Fire Protection Association.
- Babrauskas, V. & Williamson, R. B. (1978). Post-flashover compartment fires: Basis of a theoretical model. *Fire and Materials*, 2(2), 39–53.
- Back, G., Beyler, C., DiNenno, P. & Tatem, P. (1994). Wall incident heat flux distributions resulting from an adjacent fire. In *Fire safety science – proceedings of the fourth international symposium*.
- Baker, G. B., Fleury, R., Spearpoint, M. J., Fleischmann, C. M. & Wade, C. A. (2011). Ignition of secondary objects in a design fire simulation tool. In *Fire safety science – proceedings of the 10th international symposium*. Maryland, USA. 1359–1372.
- Baker, G. B., Spearpoint, M. J., Fleischmann, C. M. & Wade, C. A. (2011a). *Experimental validation for an item-to-item fire spread submodel*. San Francisco, USA.
- Baker, G. B., Spearpoint, M. J., Fleischmann, C. M. & Wade, C. A. (2011b). Selecting an ignition criterion methodology for use in a radiative fire spread submodel. *Fire and Materials*, 35(6), 367–381.
- Beyler, C. (1988). *Fire dynamics and chemistry: An engineering approach* (Draft). Worcester Polytechnic Institute.
- Beyler, C. (2002). Flammability limits of premixed and diffusion flames. In *SFPE handbook of fire protection engineering* (3rd ed.). Quincy, MA: National Fire Protection Association.
- Birk, D. M. (1991). *An introduction to mathematical fire modeling*. Technomic Publishing Company.
- Block, M., Shakir, D. S. & Smith, J. (1993). *ProMath 2.0 and ProMath/VB 2.0 dual version*. Professional BASIC Mathematics Library. TeraTech.

- Cooper, L. Y. (1997). VENTCF2: an algorithm and associated FORTRAN 77 subroutine for calculating flow through a horizontal ceiling/floor vent in a zone-type compartment fire model. *Fire Safety Journal*, 28, 253–287.
- Cooper, L. Y. (2002). Smoke and heat venting. In *SFPE handbook of fire protection engineering* (3rd ed.). Quincy, MA: National Fire Protection Association.
- Cooper, L. Y. & Forney, G. P. (1990a). *The consolidated compartment fire model (CCFM) computer code application CCFM.VENTS – Part I: Physical basis*. (NISTIR 4342). National Institute of Standards and Technology.
- Cooper, L. Y. & Forney, G. P. (1990b). *The consolidated compartment fire model (CCFM) computer code application CCFM.VENTS – Part III: Catalog of algorithms and subroutines*. (NISTIR 4344). National Institute of Standards and Technology.
- Crocker, J. P., Rangwala, A. S., Dembsey, N. A. & Le Blanc, D. J. (2010). The effect of sprinkler spray on fire induced doorway flows: New tools for performance based design. *Fire Technology*, 46(2), 347–362.
- Davis, W. D. (1999). *Zone fire model jet: A model for the prediction of detector activation and gas temperature in the presence of a smoke layer*. (NISTIR 6324). National Institute of Standards and Technology.
- Davis, W. D., Cleary, T. G., Donnelly, M. & Hellerman, S. (2003). *Predicting smoke and carbon monoxide detector response in the ceiling jet in the presence of a smoke layer*. Gaithersburg, MD: National Institute of Standards and Technology.
- Deal, S. (1995). *Technical reference guide for FPEtool version 3.2*. (NISTIR 5486-1). Gaithersburg, MD: National Institute of Standards and Technology.
- Eagle, D. C. J. (1997). *BNALib: A visual basic numerical analysis library for personal computers*.
- Emmons, H. W. & Tanaka, T. (2008). Vent flows. In *SFPE handbook of fire protection engineering* (4th ed.). Quincy, MA: National Fire Protection Association.
- Evans, D. D. (1988). Ceiling jet flows. In *SFPE handbook of fire protection engineering* (1st ed.). Quincy, MA: National Fire Protection Association.
- Evans, D. E. (1994). Sprinkler fire suppression algorithm for HAZARD. In *Proceedings of the 12th joint panel meeting of the UJNR panel on fire research and safety*, Oct 27–Nov 2, 1992.
- Fire Code Reform Centre. (1996). *Fire engineering guidelines*. NSW, Australia: Author.
- Forney, G. P. (1994). Computing radiative heat transfer occurring in a zone model. *Fire Science & Technology*, 14, 31–47.
- Forney, G. P. (2012). *Smokeview (Version 6) – a tool for visualizing fire dynamics simulation data, Volume I: User's guide*. Gaithersburg, MD: US Department of Commerce.

- Forney, G. P. & Cooper, L. Y. (1990). *The consolidated compartment fire model (CCFM) computer code application CCFM.VENTS – Part II: Software reference guide*. (NISTIR 4343). National Institute of Standards and Technology.
- Forney, G. P., Cooper, L. Y. & Moss, W. F. (1990). *The consolidated compartment fire model (CCFM) computer code application CCFM.VENTS – Part IV: User reference guide*. (NISTIR 4345). National Institute of Standards and Technology.
- Gottuk, D. T. (1992). *Generation of carbon monoxide in compartment fires*. (NIST-GCR-92-619). Washington, DC: National Institute of Standards and Technology.
- Gottuk, D. T., Roby, R. J., Peatross, M. J. & Beyler, C. L. (1992). Carbon monoxide production in compartment fires. *Journal of Fire Protection Engineering*, 4(4), 133–150.
- Grenier, A. T. & Janssens, M. L. (1997). An improved method for analyzing ignition data of composites. In *Proceedings of the international conference on fire safety, Vol 23*.
- Harada, K., Kogure, R., Matsuyama, K. & Wakamatsu, T. (2000). Equivalent fire duration based on time-heat flux area. *Proceedings of the fourth Asia-Oceania symposium on fire science and technology* (pp. 513–524).
- Harrison, R. (2009). *Entrainment of air into thermal spill plumes*. (PhD Thesis). University of Canterbury, Department of Civil Engineering. Christchurch, New Zealand.
- Harrison, R. & Spearpoint, M. J. (2007). The balcony spill plume: Entrainment of air into a flow from a compartment opening to a higher projecting balcony. *Fire Technology*, 43, 301–317.
- Harrison, R. & Spearpoint, M. J. (2010). Physical scale modelling of adhered spill plume entrainment. *Fire Safety Journal*, 45, 149–158.
- Harrison, R., Wade, C. A. & Spearpoint, M. (2014). Predicting spill plumes with the fire risk zone model B-RISK. *Fire Technology*, 50, 205–231. DOI: 10.1007/s10694-013-0364-3.
- Heskestad, G. (1975). Generalized characteristics of smoke entry and response for products of combustion detectors. *Proceedings, 7th international conference on problems of automatic fire detection*.
- Heskestad, G. (1983). Virtual origins of fire plumes. *Fire Safety Journal*, 5, 109.
- Heskestad, G. (1984). Engineering relations for fire plumes. *Fire Safety Journal*, 7, 25–32.
- Heskestad, G. & Bill, R. G. (1988). Quantification of thermal responsiveness of automatic sprinklers including conduction effects. *Fire Safety Journal*, 14, 113–125.

- Huggett, C. (1980). Estimation of rate of heat release by means of oxygen consumption measurements. *Fire and Materials*, 4, 61–65.
- Ierardi, J. A. (n.d.). *A guide for specifying combustion chemistry ratios in the CFAST and FASTLite zone models*. Worcester, Massachusetts: Center for Firesafety Studies, Worcester Polytechnic Institute.
- Incropera, F. P. & DeWitt, D. P. (1990). *Fundamentals of heat and mass transfer*. John Wiley and Sons.
- ISO. (1993). ISO 9705 *Fire tests – full-scale room tests for surface products*. Geneva: International Organization for Standardization.
- ISO. (2006a). ISO 16735 *Fire safety engineering – Requirements governing algebraic equations – Smoke layers*. (16735). Geneva: International Organization for Standardization.
- ISO. (2006b.) ISO 16734 *Fire safety engineering – Requirements governing algebraic equations – Fire plumes*. (16734). Geneva: International Organization for Standardization.
- ISO. (2012). ISO 13571 *Life-threatening components of fire – Guidelines for the estimation of time to compromised tenability in fires*. (Standard 13571:2012(E)). Geneva: International Organization for Standardization.
- Janssens, M. (1991). Piloted ignition of wood: A review. *Fire and Materials*, 15, 151–167.
- Janssens, M. (1992a). Room fire models. In V. Babrauskas & S. J. Grayson (Eds.), *Heat release in fires*. Elsevier Applied Science.
- Janssens, M. (1992b). Determining flame spread properties from cone calorimeter measurements. In V. Babrauskas & S. J. Grayson (Eds.), *Heat release in fires*. Elsevier Applied Science.
- Jin, T. (1978). Visibility through fire smoke. *Journal of Fire and Flammability*, 9(2), 135–155.
- Karlekar, B. V. (1983). *Thermodynamics for engineers*. Englewood Cliffs, NJ: Prentice-Hall, Inc.
- Karlsson, B. & Quintiere, J. G. (1999). *Enclosure fire dynamics*. CRC Press.
- Kokkala, M., Baroudi, D. & Parker, W. J. (1997). Upward flame spread on wooden surface products: Experiments and numerical modelling. In *Fire safety science – proceedings of the fifth international symposium*. Melbourne, 3–7 March.
- Lattimer, B. Y. (2002). Heat fluxes from fires to surfaces. In *SFPE handbook of fire protection engineering* (3rd ed.). Quincy, MA: National Fire Protection Association.
- Lawson, J. R. & Quintiere, J. G. (1985). Slide rule estimates of fire growth. *Fire Technology*, 21(4).

- MBIE. (2014). *C/VM2 Verification Method: Framework for fire safety design for New Zealand Building Code clauses C1–C6 Protection from fire*. Wellington, New Zealand: Ministry of Business, Innovation and Employment.
- McCaffrey, B. (1983). Momentum implications for buoyant diffusion flames. *Combustion & Flame*, 52, 149–167. DOI: 10.1016/0010-2180(83)90129-3.
- Modak, A. T. (1977). Thermal radiation from pool fires. *Combustion & Flame*, 29, 177–192.
- Mulholland, G. W. (2002). Smoke production and properties. In *SFPE handbook of fire protection engineering* (3rd ed.). Quincy, MA: National Fire Protection Association.
- Mulholland, G. W. & Choi, M. H. (1998). Measurement of the specific extinction coefficient for acetylene and ethene smoke using the large agglomerate optics facility. In *Twenty-Seventh Symposium (International) on Combustion*. The Combustion Institute. 1515–1522.
- National Fire Protection Association. (1998). *Guide for smoke and heat venting* (NFPA 204). Quincy, MA: Author.
- Nelson, H. E. (1990). *FPETOOL: Fire protection engineering tools for hazard estimation*. (NISTIR 4380). National Institute of Standards and Technology.
- Nyman, J. F., Gerlich, H. J. T., Wade, C. A. & Buchanan, A. H. (2008). Predicting fire resistance performance of drywall construction exposed to parametric design fires – a review. *Journal of Fire Protection Engineering*, 18, 117–139. DOI: 10.1177/1042391507080811.
- Pagni, P. J. & Joshi, A. A. (1991). Glass breaking in fires. In *Fire safety science – proceedings of the third international symposium*.
- Parry, R. (2002). *Implementation of a glass fracture module for the BRANZfire compartment fire zone modelling software*. Christchurch, New Zealand: University of Canterbury, Department of Civil Engineering.
- Parry, R., Wade, C. & Spearpoint, M. (2003). Implementing a glass fracture module in the BRANZFIRE zone model. *Journal of Fire Protection Engineering*, 13, 157–183.
- Peacock, R. D., Forney, G., Reneke, P. A., Portier, R. & Jones, W.W. (1993). *CFAST, the consolidated model of fire and smoke transport*. (NIST Technical Note 1299). National Institute of Standards and Technology.
- Peacock, R. D., Jones, W. W., Reneke, P. A. & Forney, G. P. (2005). *CFAST – consolidated model of fire growth and smoke transport (version 6): User's guide*. (NIST Special Publication 1019 Sixth Edition 1041). Washington, DC: National Institute of Standards and Technology.
- Pitts, W. M. (1994). *The global equivalence ratio concept and the prediction of carbon monoxide formation in enclosure fires*. (NIST Monograph 179). National Institute of Standards and Technology.

- Purser, D. (1988). Toxicity assessment of combustion products. In *SFPE handbook of fire protection engineering* (1st ed.). Quincy, MA: National Fire Protection Association.
- Purser, D. A. (2002). Toxicity assessment of combustion product. In *SFPE handbook of fire protection engineering* (3rd ed.). Quincy, MA: National Fire Protection Association.
- Purser, D. A. (2008). Assessment of hazards to occupants from smoke, toxic gases, and heat. In *SFPE handbook of fire protection engineering* (4th ed.). Quincy, MA: National Fire Protection Association.
- Quintiere, J. G. (1993). A simulation model for fire growth on materials subject to a room-corner test. *Fire Safety Journal*, 20, 313–339.
- Quintiere, J. & McCaffrey, B. (1980). *The burning of wood and plastic cribs in an enclosure: Volume 1*. (NBSIR 80-2054). Washington, DC: National Bureau of Standards.
- Quintiere, J. G., Rinkinen, W. J. & Jones, W. W. (1981). The effect of room openings on fire plume entrainment. *Combustion Science & Technology*, 26, 193–201.
- Rockett, J. A. (1976). Fire induced gas flow in an enclosure. *Combustion Science & Technology*, 12, 165–175.
- Rockett, J. A. (1995). Zone model plume algorithm performance. *Fire Science & Technology*, 15(1&2), 1–15.
- Rogers, G. F. C. & Mayhew, Y. R. (1992). *Thermodynamic and transport properties of fluids SI units* (4th ed.) Blackwell Publishers.
- Silcock, G. W. H. & Shields, T. J. (1995). A protocol for analysis of time-to-ignition data from bench scale tests. *Fire Safety Journal*, 24, 75–95.
- Sincaglia, P. E. & Barnett, J. R. (1997). Development of a glass window fracture model for zone-type computer fire codes. *Journal of Fire Protection Engineering*, 8, 101–118.
- Skelly, M. J., Roby, R. J. & Beyler, C. L. (1991). An experimental investigation of glass breakage in compartment fires. *Journal of Fire Protection Engineering*, 3, 25–34.
- Standards Australia. (1989). *AS 1603 Automatic fire detection and alarm systems – Part 2: Point type smoke detectors*.
- Tewarson, A. (2002). Generation of heat and chemical compounds in fires. In *SFPE handbook of fire protection engineering* (3rd ed.). Quincy, MA: National Fire Protection Association.
- Tewarson, A., Jiang, F. H. & Morikawa, T. (1993). Ventilation controlled combustion of polymers. *Combustion and Flame*, 95, 151–169.

- Tien, C. L., Lee, K. Y. & Stretton, A. J. (2008). Radiation heat transfer. In *SFPE handbook of fire protection engineering* (4th ed.). Quincy, MA: National Fire Protection Association.
- Utiskul, Y. (2007). *Theoretical and experimental study on fully-developed compartment fires*. (PhD). College Park, Maryland: University of Maryland.
- Vose, D. (2000). *Risk analysis – a quantitative guide* (2nd ed.). San Francisco, CA: John Wiley & Sons Ltd.
- Wade, C. (1996). *A room fire model incorporating fire growth on combustibile lining materials*. (Master of Science Thesis, Worcester Polytechnic Institute. Worcester, MA).
- Wade, C. A. (2000). *BRANZFIRE technical reference guide*. BRANZ Study Report SR92. Judgeford, New Zealand: BRANZ Ltd.
- Wade, C. & Barnett, J. (1997). A room-corner model including fire growth on linings and enclosure smoke-filling. *Journal of Fire Protection Engineering*, 8(4), 27–36.
- Wade, C. A., Baker, G. B., Frank, K., Robbins, A. P., Harrison, R., Spearpoint, M. J. & Fleischmann, C. M. (2013). *B-RISK user guide and technical manual*. BRANZ Study Report SR282. Judgeford, New Zealand: BRANZ Ltd. Available: <http://www.b-risk.com>.
- Wyss, G. G. & Jorgensen, K. H. (1998). *A user's guide to LHS: Sandia's Latin hypercube sampling software*. (Report SAND98-0210). Albuquerque: Sandia National Laboratories.

Appendix A. Format of cone data file

An example of a ".txt" file for including the material cone calorimeter data is given here. Note that comments are given in bold. They are not part of the file.

"EUMAT6 material"

"Number of HRR Curves",4

"Heat Flux",25

Input a single heat release rate curve for the material starting from the lowest external heat flux.

"Number of HRR Data Pairs",20

"sec,kw/m²"

The number of data pairs must correspond to the number given above (20).

0,34.4

5,54.7

10,64.5

15,63.7

20,53.1

25,33.1

...

Repeat for next heat flux.

"Heat Flux",35

"Number of HRR Data Pairs",27

"sec,kw/m²"

0,44.4

5,95.3

10,104.7

15,91.6

20,76.4

25,62.1

...

"Heat Flux",50

"Number of HRR Data Pairs",37

"sec,kw/m²"

0,73.1

5,127.4

10,128.5

15,121.2

20,106

25,92

...

"Heat Flux",75

"Number of HRR Data Pairs",34

"sec,kw/m²"

0,36.1

5,73.5

10,75

15,73.7

20,60.4

25,47.8

...

"Ignition Data"

"Number of Pairs",8

"flux kw/m², ignition time sec, peak hrr kw/m²"

Number of entries corresponds to number given above (8). Enter lowest to highest external flux.

25,65,75.2

25,65,64.5

35,35,95.6

35,30,104.7

50,15,151.9

50,10,128.5

75,5,85.4

75,5,75

If number of pairs is set to zero, the user can enter ignition temperature, thermal inertia, heat of gasification, area under the heat release rate curve and critical flux directly as follows.

...

"Number of Pairs", 0

"Ignition Temperature", 740

"Thermal Inertia", 0.366

"Heat of Gasification", 0.72

"Area under Curve", 2359

"Critical Flux", 22

If the area under the curve is entered as zero, the area will be automatically calculated using the rate of heat release curve supplied.

Appendix B. List of model constants

Table 10. Constants used in B-RISK.

| Parameter | Description | Value | Units |
|--------------------------|--|-------------|------------------------------------|
| A | plume entrainment coefficient | 0.076 | |
| C_d | discharge coefficient | 0.68 | |
| c_p | specific heat of air at constant pressure | 1.005 | $\text{kJ kg}^{-1} \text{K}^{-1}$ |
| g | acceleration due to gravity | 9.807 | m sec^{-2} |
| h_{ext} | exterior convective heat transfer coefficient | 5 | $\text{W m}^{-2} \text{K}^{-1}$ |
| M_{air} | molecular weight of air | 29 | |
| M_{CO_2} | molecular weight of carbon dioxide | 44 | |
| M_{CO} | molecular weight of carbon monoxide | 28 | |
| $M_{\text{H}_2\text{O}}$ | molecular weight of water | 18 | |
| M_{O_2} | molecular weight of oxygen | 32 | |
| M_{N_2} | molecular weight of nitrogen | 28 | |
| P | atmospheric pressure | 101.325 | kPa |
| R | Universal Gas Constant | 8314.34 | $\text{J kmol}^{-1} \text{K}^{-1}$ |
| R_{air} | Gas Constant Air | 0.2871 | $\text{kJ kg}^{-1} \text{K}^{-1}$ |
| T_f | flame temperature | 1250 | K |
| T_{∞} | reference temperature of air | 288.15 | K |
| $Y_{\text{O}_2\infty}$ | mass fraction of oxygen in ambient air | 0.2313 | |
| $Y_{\text{CO}_2\infty}$ | mass fraction of carbon dioxide in ambient air | 0.005 | |
| ρ_{∞} | reference density of air | 1.225 | kg m^{-3} |
| π | pi | 3.14159265 | |
| γ | ratio of specific heats | 1.4 | |
| σ | Stefan Boltzmann Constant | 5.66961E-08 | $\text{Wm}^{-2} \text{K}^{-4}$ |
| ΔH_{air} | energy release per mass of air consumed | 3 | kJ g^{-1} |

Appendix C. Troubleshooting

1. Error messages upon opening B-RISK

Files may have become corrupted. Use the `FILE, NEW` command and `SAVE` command to reset the default case. Close and reopen B-RISK.

2. Smokeview crashes with B-RISK

Check Smokeview version. Should be 6.0.x or 6.1.x.

3. Convergence errors

These are sometimes difficult to troubleshoot. Some suggestions:

- Try a smaller error control setting (divide by 10).
- Simplify your model. The more rooms and vents you have, the longer the simulation will take and the more likely there will be convergence errors.
- For European users who normally use the comma as the decimal separator, you may need to switch to using the period as the decimal separator.